METAL CONTACTS TO P-TYPE GALLIUM NITRIDE

LIM WOON CHI, JANIS

NATIONAL UNIVERSITY OF SINGAPORE

2005

ACKNOWLEDGMENTS

I wish to express my most heartfelt thanks to my supervisor, Prof. Chor Eng Fong, for her relentless supervision and generous help over the past three years. Prof Chor, it has been a privilege to work under you and I will always treasure this experience.

To my co-Supervisor, Prof. Tan Leng Seow, for making every meeting value-added with your opinions and for encouragements along the way - thank you.

To Ms. Musni, for the continuous support you have given me in the aspect of administration, from the bottom of my heart - thank you. To Mr. Tan Beng Hwee, for the many times you were around to help me with the technical problems I face while working in the lab - thank you.

To Lip Khoon, for guiding me along when I first started, for the useful discussions we have, for being always approachable and for the friendship - thank you. To Haiting, Chung Foong, Liu Chang, Keyan, Guangxia for contributing to this project in one way or another, and for making my stay in COE an unforgettable one - thank you.

To Chay Hoon (DSI), for all the extra time you put into helping me with the AES - thank you. To Joon Fatt (DSI), Kit Yan (DSI), An Yan (IME), for helping with the various measurements - thank you.

To Dad, Mum, Choon, Ching, for being the very reason I enjoy the love and warmth of family and for your endless prayers and support for me while pursuing my Masters' - thank you.

To Derek, for your constant support and encouragement throughout this project and for being there with me at the mountain tops and in the valleys deep - thank you.

To Jesus, for dying on the cross for me - thank You.

Janis Lim

TABLE OF CONTENTS

SUMMARY

In the first part of this work, the effects of the AQ, Cl_2/N_2 plasma and O_2 plasma treatments on the as-deposited Ni/Au (20/20 nm) contact to p-GaN are studied and found to result in similar I-V characteristics for all, which has been attributed to the small difference observed in their Ga/N and O/Ga ratios.

Next, the effects of N_2 and O_2 annealing (600 ˚C-1 min) on the Ni/Au (20/20 nm) contact to AQ, Cl_2/N_2 plasma and O_2 plasma surface-treated p-GaN are studied. For AQ surface treatment, O_2 annealing gives a better I-V curve than N_2 annealing, attributed to NiO formation and layer-reversal that has taken place upon O_2 annealing and undesirable Ni-Au solid solutions formed upon N_2 annealing. For Cl_2/N_2 plasma treatment, the I-V curve of the N_2-annealed sample is similar to the AQ-treated sample but O_2 annealing resulted in a much worse I-V curve, attributed to the formation of Ni_3N compounds. For O_2 plasma treatment, N_2 and O_2 annealings did not improve its electrical characteristics and both gave comparable I-V curves, attributed to the formation of the N-Ga-O_x and Ga-O_x-C complexes during O_2 plasma treatment which cannot be removed by subsequent AQ.

In the second part, the effects of N_2 and O_2 annealings on the Rh (10 nm), Rh/Ni/Au (10/10/10 nm), Rh/Au (10/10 nm) and Rh/Ni (10/10 nm) contacts are studied. Both N_2 and O_2 annealings are seen to be unlikely to improve the electrical characteristics

of the Rh and Rh/Au contacts. O_2 annealing improves both the Rh/Ni and Rh/Ni/Au contacts while N_2 annealing only slightly improves the Rh/Ni contact, indicating that in general, N_2 annealing is unable to improve Rh-based contacts to p-GaN.

A further study on the O_2-annealed Rh/Ni contact - which achieved the best I-V characteristic - is carried out, where we observe the NiO formation and some in-diffusion of it to the GaN surface, while much of the Rh remains in direct contact with p-GaN, hinting that the final structure of the oxidized Rh/Ni contact might be similar to the oxidized Ni/Au contact except that Rh, known to form gallides, results in a Ga-deficient GaN surface and consequently, a good contact to p-GaN.

LIST OF FIGURES

LIST OF TABLES

LIST OF ABBREVIATIONS AND SYMBOLS

ABBREVIATIONS

AES - Auger Electron Spectroscopy

AQ - Aqua Regia

Au - Gold

Cl_2 - Chlorine

CTLM - Circular Transmission Line Model

DI - Dionised Water

EDX - Energy Dispersive X-ray

Ebeam - Electron Beam

GaN - Gallium Nitride

Ga_2O_3/GaO_x - Gallium Oxide

H_2O - Water

HBT - Heterojunction Bipolar Transistor

HCl - Hydrochloric Acid

HEMT - High Electron Mobility Transistor

HF - Hydroflouric Acid

HNO_3 - Nitric Acid

ICP - Inductively Coupled Plasma

I-V - Current-Voltage

LD - Laser Diode

LED - Light Emitting Diode

MESFET - Metal-Semiconductor Field-Effect Transistor

Mg - Magnesium

MOCVD - Metal Organic Chemical Vapour Deposition

N / N_2 - Nitrogen

Ni - Nickel

NiO - Nickel Oxide

O / O_2 - Oxygen

Pd - Palladium

PR - Photoresist

RIE - Reactive Ion Etching

Rh - Rhodium

TEM - Transmission Electron Microscope

XPS - X-ray Photoelectron Spectroscopy

XRD - X-Ray Diffraction

SYMBOLS

ρ_c - Specific contact resistivity

$q\phi_m$ - Workfunction of Metal

$q\phi_s$ - Workfunction of Semiconductor

$q\phi_o$ - Neutral Energy Level

$q\phi_{Bp}$	-	Schottky barrier height of p-type semiconductor
E_g	-	Bandgap energy of semiconductor
$q\chi$	-	Electron affinity of semiconductor
E_F	-	Fermi energy
i	-	Current across separation *d*
d	-	Distance between inner and outer contact pads
R_s	-	Semiconductor sheet resistance
L_T	-	Transfer length
I_o, I_1, K_o, K_1	-	Modified Bessel Functions
r_i , r_o	-	Inner and Outer radii of circular contact
R_T	-	Total resistance
V_{Ga}**'s**	-	Gallium vacancies
V_N**'s**	-	Nitrogen vacancies

PUBLICATION FROM THE CURRENT WORK

J. Lim, E. F. Chor and L. S. Tan, "*Effects of Chemical and Plasma Surface Treatments on the O_2-annealed Ni/Au Contact to p-GaN*", International Conference on Materials for Advanced Technologies (2005) – *submitted to be published in Thin Solid Films (2005).*

CHAPTER 1

INTRODUCTION

1.1 INTRODUCTION

Research into the properties of Gallium Nitride (GaN) has increased dramatically since the first announcement of the development of blue Light Emitting Diodes (LEDs) using GaN [1]. Subsequent reports have also shown the successful use of GaN in metal-semiconductor field-effect transistors (MESFETs) [2], high electron mobility transistors (HEMTs) [3], laser diodes (LDs) [4], UV photoconductive detectors [5] and heterojunction bipolar transistors (HBTs) [6]. This is due to GaN being a wide bandgap energy material (~3.4 eV at 300 K) compared to Si (1.12 eV) and GaAs (1.42 eV). This property of GaN makes it advantageous for high-temperature operations, since the possibility of valence electrons spontaneously jumping into the conduction band during these operations is much lower.

Large-bandgap semiconductors also generate less noise, which makes GaN a suitable material for the making of highly sensitive detectors in the UV range [5]. In addition, GaN has a high thermal conductivity of 130 W/mK, which is comparable to the thermal conductivity of Si, 149 W/mK. These properties of GaN, along with it being found to be chemically stable at high temperatures, make it excellent for making highly efficient optoelectronic devices, like those mentioned earlier.

1.2 BACKGROUND AND MOTIVATION FOR p-GaN CONTACT WORKS

In light of these recent successes in the development of GaN-based devices, the fabrication of ohmic contacts with low specific contact resistance (ρ_c) is of great technological importance. However, the high ρ_c of the p-type ohmic contact poses one of the major problems in the realization of long-lifetime operation of GaN-based optical devices, like the afore-mentioned laser diode (LD). In short, the high ρ_c of p-GaN limits the efficiency of GaN-based devices.

The two main obstacles faced in the quest for ohmic contacts of low specific contact resistivity to p-GaN were recognised to be the difficulty in:

(i) growing a heavily-doped p-GaN (>10^{18} cm^{-3}) and

(ii) the absence of appropriate metals having workfunction larger than that of p-GaN (~7.5 eV).

These problems have led to several attempts in finding ohmic contacts with low specific contact resistance to p-GaN. A short literature survey on the various metal systems used to achieve a low specific contact resistivity to p-GaN was carried out and will be discussed in the section that follows.

1.2.1 Background: Metal Systems with Low Specific Contact Resistivity

Table 1.1 summarises the specific contact resistances, ρ_c, of metal systems on p-GaN reported in the literature [7-23]. It is tabulated in increasing order of ρ_c and

indicates the conditions under which the ρ_c was obtained: thickness of metal layers used, doping concentration of GaN and annealing conditions.

From the ten metal contacts reporting the lowest ρ_c's to p-GaN in Table 1.1, we observe the following trends:

1. O_2 (or air) annealing is now widely used in p-GaN contact formation, replacing the conventional choice of N_2 annealing because the formation of metal oxides (NiO, RuO_2) has been found to play a significant role in lowering the ρ_c. (Contact works involving the use of O_2 (or air) annealing are highlighted in blue in Table 1.1).
2. Thinner metal layers are used. It is noteworthy that most of the papers reporting the use of thin metal layers also reported the use of O_2 annealing to allow O_2 to penetrate the upper metal layer to react with the under layer, as in the case of Ni/Au, Ir/Ni and Ru/Ni.
3. The use of metals or metals that form oxides with high workfunction, other than Ni, is now prevalent. Examples are Pd (5.11eV), Rh (4.98 eV) and RuO_2 (~5.91eV).

We will now discuss the Ni/Au and Rh-based metal systems to p-GaN in detail. The Ni/Au contact is selected as it has achieved the lowest reported ρ_c to p-GaN with O_2 annealing. The Rh-based contacts are selected as they account for two of the five lowest ρ_c's reported in the literature and having achieved it in the as-deposited state, these contacts show potential to be improved via the common method of annealing.

Table 1.1: Metal contacts with the lowest specific contact resistances (ρ_c) reported in literature [7-23]. The thickness of metal layers, doping concentration of GaN and annealing conditions are indicated. Contacts are arranged in ascending order of ρ_c.

No.	Journal Publication Date	Metal Contacts	Specific contact resistance, ρ_c (Ω cm^2)	Metal Thickness (nm)	Annealing Conditions: Temp/Ambient/Time	Doping conc. of p-GaN (cm^{-3})
1	5/2000 [7]	Pt/Ru	$2.2\ (\pm 2.0)\times10^{-6}$	20/50	600 °C (N_2) 2min	$2\text{-}3\times10^{17}$
2	6/2000 [8]	Ni/Au	4×10^{-6}	5/5	500 °C (O_2) 10min	2×10^{17}
3	7/2003 [9]	Ni/AZO	6.23×10^{-6}	5/450	550 °C (air) 5min	5×10^{17}
4	9/2003 [10]	Rh/Au	9.3×10^{-6}	5/5	As-deposited (i.e., no annealing)	4×10^{17}
5	9/2003 [10]	Rh	1.7×10^{-5}	10	As-deposited (i.e., no annealing)	4×10^{17}
6	11/2002 [11]	Au/Ni/Au	$\sim 10^{-5}$	5/8/4	500 °C (air) 10min	$2\text{-}5\times10^{17}$
7	5/2003 [12]	Ir/Ni	3.4×10^{-5}	5/5	500 °C (O_2) 1min	3×10^{17}
8	6/2000 [13]	Ti/Pt/Au	4.2×10^{-5}	15/50/80	800 °C (N_2) 2min	$\sim2.5\times10^{17}$
9	4/2002 [12], [14]	Ru/Ni	4.5×10^{-5}	5/5	500 °C (O_2) 1min	3×10^{17}
10	9/2001 [15]	Pd/Ni	5.7×10^{-5}	3/7	500 °C (O_2) 1min	3.3×10^{17}
11	9/2003 [10]	Rh/Ni	6×10^{-5}	5/5	As-deposited	4×10^{17}
12	11/2000 [16]	Ni/Pd/Au	1×10^{-4}	20/20/100	500 °C (O_2) 5min	4.1×10^{17}
13	10/1999 [17]	Ni/Au	1×10^{-4}	10/5	500 °C (N_2) 10min	2×10^{17}
14	2000 [18]	Pd/Ni/Au	5.03×10^{-4}	20/30/200	450 °C (N_2) 2min	1.0×10^{18}
15	1/1999 [19]	Pt/Ni/Au	5.1×10^{-4}	20/30/80	350 °C (N_2) 1min	3×10^{17}
16	10/2001 [20]	Ni/ITO	8.6×10^{-4}	10/250	600 °C (air) 2min	$\sim2\times10^{17}$
17	3/2001 [21]	Ni/Au	Low-10^{-3}	10/40	500 °C (O_2/N_2) 5-15min	$6\text{-}7\times10^{17}$
18	1999 [22]	Ni/Zn-Au	3.6×10^{-3}	Unknown	Unknown	4.4×10^{17}
19	1997 [23]	Pt/Au	$2.0\text{-}8.0\times10^{-3}$	50/200	700 °C (before metallization) 15min 750 °C (after)	Unknown
20	3/2001 [21]	Pt/Au	High-10^{-3}	10/40	300-600 °C (O_2/N_2)	$6\text{-}7\times10^{17}$
21	3/2001 [21]	Pt	High-10^{-3}	50	600 °C (O_2/N_2) 5min	$6\text{-}7\times10^{17}$

(a) Ni/Au contact

It has been widely reported that O_2 annealing of the Ni/Au contact to p-GaN has yielded good ohmic contacts [8], [24]-[27]. The specific contact resistance (ρ_c) obtained by the O_2-annealed Ni/Au contacts to p-GaN were as low as 4×10^{-6} Ω cm^2, with hole concentration of 2×10^{17} cm^{-3}, reported by Ho *et. al.* [24] and Chen *et. al.* [25]. This is almost 3 orders of magnitude lower compared to the lowest ρ_c of 2.5×10^{-3} Ω cm^2 (hole concentration of 3.6×10^{17} cm^{-3}) obtained by N_2 annealing of the same contact system [28]. It was also noted by Ho *et. al.* that the lowest ρ_c's were obtained when Ni and Au were of the same thickness. Two mechanisms have been proposed to explain why O_2 anneal is beneficial to the Ni/Au contact to p-GaN. In brief, the two mechanisms are:

(i) O_2 annealing increases the hole concentration at the surface of p-GaN by the re-activation of Mg dopants by breaking the Mg-H bonds [29], [30].

(ii) The formation of NiO, a p-type semiconductor, resulting in a thin Schottky barrier with a small barrier height in contact with p-GaN [24], [25].

The theories behind these mechanisms will now be presented and discussed.

(i) Increase in Hole Concentration

It has been suggested in several reports that the formation of electrically inactive acceptor-hydrogen (Mg – H) complexes during Metal Organic Chemical Vapour Deposition (MOCVD) growth is responsible for the low p-type doping efficiency

in as-grown GaN [31]-[35]. Thus, to electrically activate Mg acceptors in as-grown Mg:GaN, energy is needed to break the (Mg – H) complex bonds.

Koide *et. al.* reported that annealing contacts to p-GaN in an O_2 ambient lowers the ρ_c of the contacts as well as the sheet resistance of the semiconductor [29]. They attributed this to the removal of hydrogen atoms bonded with Mg atoms. Hull *et. al.* verified this claim by performing Secondary Ion Mass Spectroscopy (SIMS) analysis on p-GaN samples activated in 100% N_2 and in O_2(10%)/N_2(90%) [30]. In this experiment, the SIMS depth profiles obtained have shown that the sample annealed in O_2(10%)/N_2(90%) resulted in lower H concentration as compared to the sample annealed in pure N_2. This indicates that the O_2 anneal indeed help in the removal of H atoms, leading to the re-activation of the Mg dopants and subsequently, an increase in the hole concentration of p-GaN.

(ii) NiO Formation

It has also been proposed [24] that ohmic behaviour of O_2-annealed Ni/Au contacts to p-GaN is due to the formation of the final structure Au/p-NiO/p-GaN, where NiO acts as a p-type semiconductor in contact with p-GaN. This p-NiO, with a carrier concentration of 1×10^{16} cm^{-3}, forms a thin Schottky barrier with a small barrier height when in contact with p-GaN. The proposed equilibrium energy band diagram of the Au/thin p-NiO/p-GaN heterostructure [24] is shown in Figure 1.1. A notch (V-shaped cut) for holes is observed in p-NiO close to the

p-GaN surface. This notch is due to the valence band (E_V) being above the Fermi level (E_F), thus trapping a large amount of holes.

During forward bias, holes can easily overcome the barriers by thermionic-field emission to inject from p-NiO into p-GaN. Similarly, during reverse bias, electrons can tunnel through the Au/p-NiO interface barrier and inject into the notch to recombine with the holes. The notch effectively acts as a recombination center for carriers, resulting in a low contact resistance between p-NiO and p-GaN.

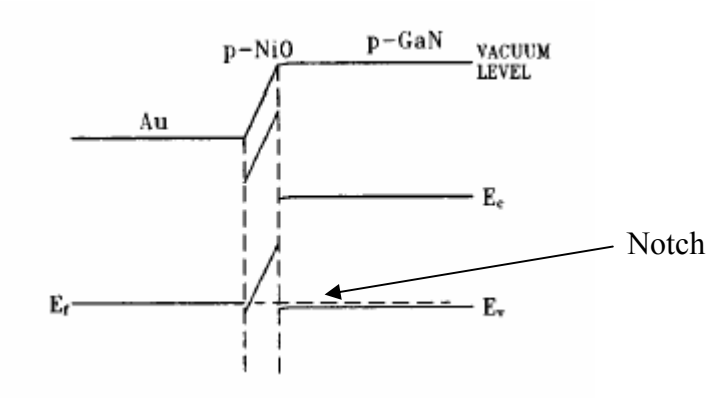

Figure 1.1: Proposed equilibrium energy band diagram of Au/thin p-NiO/p-GaN heterostructure [23].

A good ohmic contact is formed between the Au and p-NiO, since the workfunction of Au (Φ_{Au}= 5.10 eV) is larger than the workfunction of NiO (Φ_{NiO}= 4.9 eV) [24]. However, the good ohmic contact is not due to the large workfunction of Au only, because it has been shown that the use of Pt (with a higher workfunction of Φ_{Pt} = 5.65 eV) in place of Au did not yield positive results for O_2-annealed contact. Thus, it is probably more due to the way in which Au

forms islands which disperse in the NiO matrix, in direct contact with p-GaN. This is depicted in Figure 1.2 [24] by a typical high resolution TEM image that shows the cross-sectional microstructure of oxidized Ni/Au contact to p-GaN.

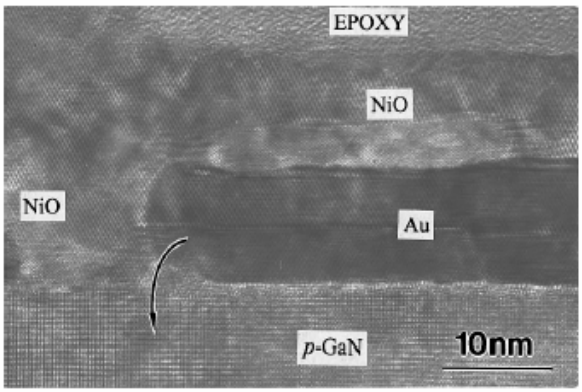

Figure 1.2: High resolution TEM image showing the cross-sectional microstructure of oxidized Ni/Au contact to p-GaN. The sample was heat treated at 500 °C in air for 10 min. The arrow indicates a possible low impedance path for current flow [24].

As seen in Figure 1.2, some NiO is still in contact with p-GaN after O_2 annealing. Au is only found to form discontinuous islands on the surface of p-GaN [8], [24], [25]. This is possible due to the "balling up" of Au at high temperatures, thus resulting in these Au islands on the surface of p-GaN [8]. The inter-diffusion of Ni and Au as well as the in-diffusion of O_2 during O_2 annealing [26] is illustrated in Figure 1.3(a) while the final NiO/Au/p-GaN structure consisting of Au islands and the NiO blanket layer is shown in Figure 1.3 (b).

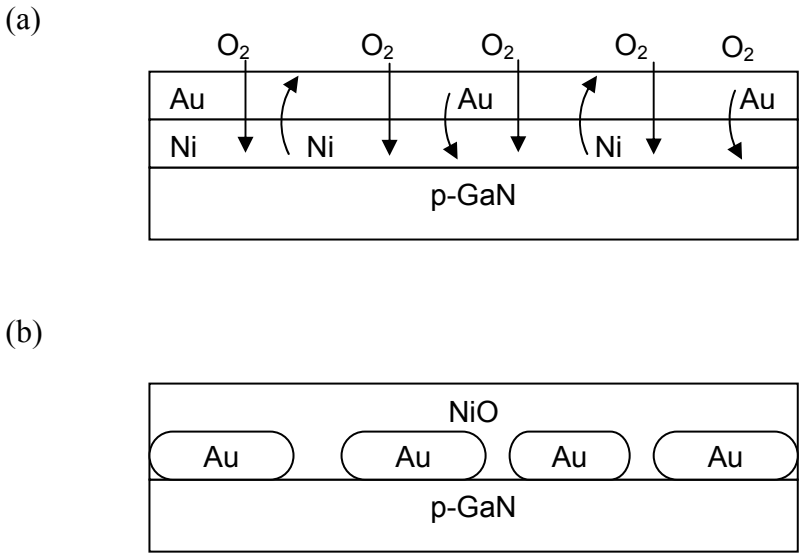

Figure 1.3: Schematics showing (a) the out-diffusion of Ni and in-diffusion of Au during O_2 annealing of the Ni/Au contact to p-GaN, and (b) the final NiO/Au/p-GaN structure after O_2 annealing: Au islands on p-GaN surface with a NiO blanket over the contact.

The existence of Au islands, and not a continuous Au layer, in direct contact with p-GaN is in agreement with early reports that an Au-layer to p-GaN does not result in low-resistance ohmic contacts [36], [37]. This could indicate that the existence of an optimal phase distribution between the NiO and Au upon annealing in O_2, as reported by Ho *et. al.* [24], meaning that the final structure does not consist of a pure Au-layer but an optimal distribution of Au islands in a NiO layer on the surface of p-GaN, as illustrated in Figure 1.3 (b), may be critical to the formation of a good Nu/Au contact to p-GaN.

(b) Rh-based contacts (Rh; Rh/Au; Rh/Ni)

It has been reported by Song *et. al.* that Rh-based contacts to p-GaN resulted in a low ρ_c [10]. In this work, Rh(5 nm)/Ni(5 nm) and Rh(5 nm)/Au(5 nm) contacts

were fabricated, giving ρ_c's of 6×10^{-5} Ω cm^2 and 9.3×10^{-6} Ω cm^2, respectively on p-GaN samples with a hole concentration of 4×10^{17} cm^{-3}. It is noteworthy that these results were obtained without any annealing. Furthermore, an as-deposited pure Rh (10nm) contact yielded a ρ_c of 1.7×10^{-5} Ω cm^2.

Some amount of Ga was found to out-diffuse into the Rh layer and react to form gallides. This is in agreement with earlier works that report the formation of gallide phases by Rh on GaAs [38], [39]. This causes the generation of Ga vacancies (V_{Ga}) in p-GaN which act as acceptors. This in turn increases the carrier concentration and thereby improving the contact to p-GaN.

The mechanism is similar to the mechanisms reported by Pd and Pt contacts to p-GaN [33]. All these metals react with p-GaN to form gallides – beneficial to ohmic contact formation to p-GaN since they generate V_{Ga}. The advantage of using Rh over Pd or Pt is that Rh-gallides form at low temperatures, thus, eliminating the need for post-metal-deposition anneal.

In summary, the low ρ_c's obtained by the Rh-based contacts to p-GaN were attributed to:

(i) Rh having a high workfunction of 4.98 eV and

(ii) Generation of V_{Ga} due to the formation of Rh-gallides.

1.2.2 Motivation for Ni/Au Contact Works to p-GaN

The works reporting a low ρ_c employing the use of O_2 annealing make use of very thin layers of Ni and Au, typically in the range of 5-20nm for each layer [8], [24], [25]. This is to enable the out-diffusion of Ni through the thin Au layer to react with O_2 in order to form NiO – known as the Ni/Au layer-reversal [24], [25], [40] as well as for the Oxygen atoms/species to diffuse through the thin metal layers to the GaN surface for the removal of H from the Mg-H complexes to produce a higher hole concentration near the surface of p-GaN [29], [30].

However, very thin contact layers pose practical problems. As the metal layers are very thin, the percentage error in deposited metal thickness is also high. Thus, high accuracy in the deposition of metal layers is required to ensure consistency and repeatability of results. In addition, micro-probes used in obtaining the I-V characteristics of the contacts must be used with increased care. This is to avoid scratching the ultra-thin layers of metal off the p-GaN surface. Another practical limitation is that of external bonding where a fairly thick layer of metal is required for good and reliable bonding.

Facing the constraint in metal thickness required, other ways to incorporate O_2 into the Ni/Au metal contact system other than annealing in O_2 is explored. One alternative will be to deposit p-NiO prior to Au, since the formation of p-NiO has been recognized as one of the possible mechanisms responsible for the low ρ_c obtained. This was explored by Maeda *et. al.* [41] using sputter deposition of NiO prior to Au deposition. However, the direct deposition of p-NiO did not produce

the same results as annealing the Ni/Au contact in an O_2 ambient. It has been shown that this was because the sputter-deposited NiO was polycrystalline while the NiO layer formed by annealing in O_2 had specific crystalline orientations [8]. This leads us to conclude that the microstructure and orientation of NiO, not just the presence of it, affects the characteristics of the contact.

Another possibility is to deposit the Au layer prior to Ni. This enables Ni at the surface to react with O_2 directly since the out-diffusion of Ni through the upper Au layer takes place during O_2 annealing of the Ni/Au metal system, as reported by Chen *et. al.* [25]. Nonetheless, as was mentioned earlier, O_2 annealing does not result in a pure Au-layer in contact to p-GaN but Au islands dispersed into the NiO matrix on the p-GaN surface [8], [24], [25]. Thus, inverting the layers only ensures NiO formation as the upper layer; it does not ensure that NiO exists in direct contact with p-GaN, which has been recognized to play a fundamental role in the ohmic contact formation of O_2-annealed Ni/Au to p-GaN. In the Ni/Au system, this is ensured by the formation of Au-Ni solid solutions as an intermediary prior to the oxidation of NiO, due to the simultaneous out-diffusion of Ni to the surface and in-diffusion of Au to surface of p-GaN [25]. Thus, the Ni/Au/p-GaN contact system will not be attempted.

In another work, C.L. Lee [42] has shown that the use of Cl_2/N_2 plasma treatment of p-GaN prior to metal contact deposition followed by annealing in an N_2 ambient of the Pd/Ni/Au contact yields good ohmic contacts to p-GaN due to the formation of Ga vacancies (V_{Ga}) – a desirable occurrence for ohmic contact

formation to p-GaN as V_{Ga} effectively contributes hole. We will seek to find out if this applies to the Ni/Au system.

We would also like to explore the effects of O_2 plasma treatment on p-GaN prior to Ni/Au metallization. We hypothesize that the O_2 plasma treatment will cause some N atoms to be "knocked out" from the surface of GaN by the bombardment of the O_2 radicals, which reacts with Ga in the process to form a layer of GaO_x on the surface, as illustrated in Figure 1.4 (b). Subsequent Aqua Regia (AQ) treatment will then strip away this top layer of GaO_x formed, removing some Ga in the process. This possibly leads to a Ga-deficient surface, which is beneficial for the contact formation to p-GaN, since these Ga vacancies (V_{Ga}'s) act as acceptors and help increase the effective hole concentration at the surface of GaN. We will also investigate the effects of annealing on the Ni/Au contact fabricated on the O_2 plasma-treated p-GaN.

1.2.3 Motivation for Rh-based Contact Works to p-GaN

From the work reported on Rh [10], it is observed to react and form gallides with p-GaN in a manner similar to Pd and Pt, except that for the case of Rh, the gallides form at low temperatures. Rh also has a low electrical resistivity of 4.3 μΩ-cm, much lower than most commonly-used materials for contact formation to p-GaN (refer **Appendix I**), indicating its potential to form a good metal contact.

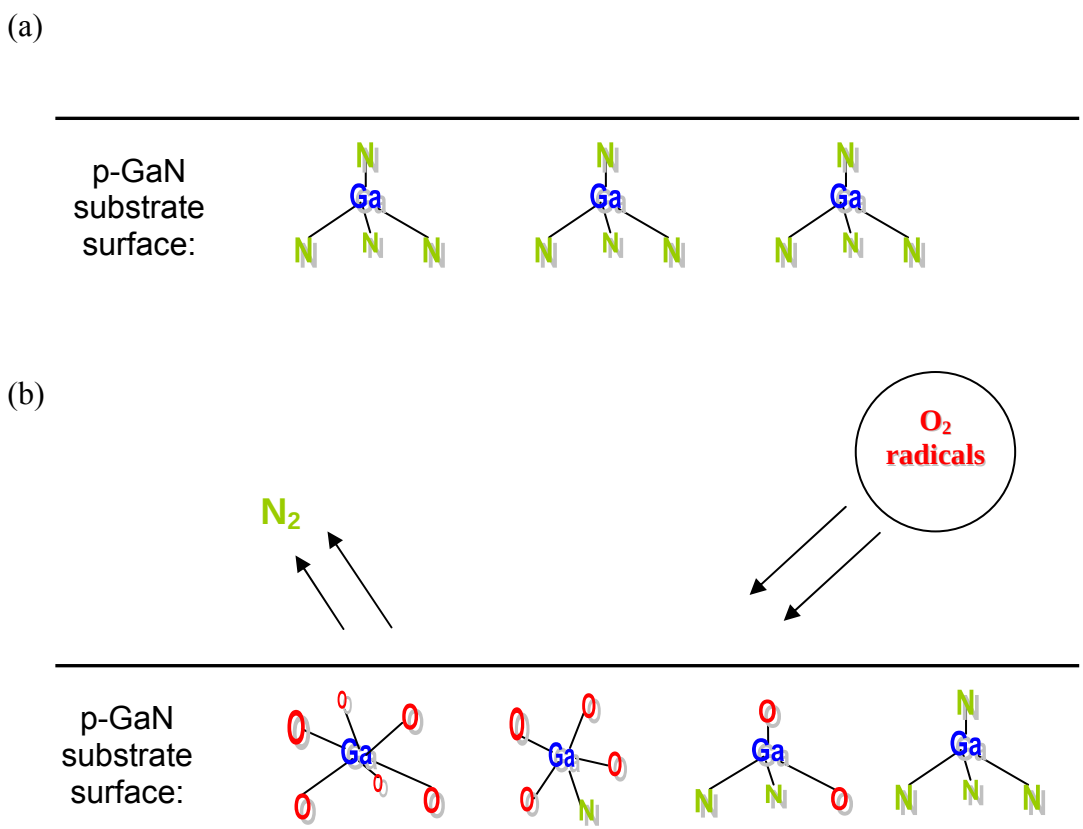

Figure 1.4 Schematics showing (a) the GaN surface prior to O_2 plasma treatment and (b) possible interactions at the GaN surface during O_2 plasma treatment.

In addition, no work has been done in exploring annealed Rh-based contacts to p-GaN thus far. From Table 1.1, we observe that the three Rh-based contacts reported were among the eleven contacts which have been reported with the lowest resistances to p-GaN. Since annealing has been a common and effective method in improving the electrical characteristics obtained by metal contacts to semiconductors, it is worth exploring if annealing can further improve the electrical characteristics of these as-deposited contacts to p-GaN.

1.3 OBJECTIVES

In this project, the main aim is to ascertain the conditions that will lead to contacts with the best electrical characteristics to p-GaN. We will employ the Ni/Au and the Rh-based contact systems for our study.

For the work on the Ni/Au contact to p-GaN, the objectives are:

(a) To study the effects of O_2 annealing on the Ni/Au contact to p-GaN with chemical (Aqua Regia (AQ)) and plasma (Cl_2/N_2 plasma) surface treatments.

(b) To study the effects of O_2 plasma treatment to p-GaN prior to metal deposition on the Ni/Au contact.

For the work on the Rh-based contacts to p-GaN, the objectives are:

(a) To study the effect of annealing, particularly O_2 annealing with N_2 annealing (the more conventional anneal) serving as a basis for comparison, on the electrical characteristics of the following Rh-based contacts to p-GaN: Rh, Rh/Ni, Rh/Au and Rh/Ni/Au.

(b) To find the Rh-based contact with the best I-V characteristics upon annealing and conduct further analyses on it so as to better understand the mechanisms and factors causing the improvement in its electrical characteristics.

1.4 OUTLINE OF THESIS

In this thesis, a theoretical analysis on contacts to p-GaN is first presented, followed by the motivations for the current work. Thereafter, the experimental procedures, results and discussions will be presented. The results and discussions are separated into two chapters for the two contact-based systems studied in this work - the Ni/Au contact and the Rh-based contacts.

In **Chapter One**, a literature search on ohmic contacts to p-GaN as well as the background and motivations for the current work are presented.

Chapter Two gives a brief introduction to the physics of metal-semiconductor contacts and the ohmic contact formation to p-GaN. The Circular Transmission Line Model (CTLM) is also introduced.

Chapter Three presents the experimental procedures that were carried out for the fabrication and measurements of the contacts in this work.

Results and discussions are presented in **Chapters Four** and **Five**. **Chapter Four** presents the study on the effect of annealing on the Ni/Au contact to p-GaN with various surface treatments. **Chapter Five** presents the study on the effects of annealing on the Rh-based contacts to p-GaN.

Chapter Six consists of the conclusions that have been made in this work and suggestions for any future work.

CHAPTER 2

THEORY: PHYSICS OF METAL-SEMICONDUCTOR CONTACT AND CIRCULAR TRANSMISSION LINE MODEL (CTLM)

2.1 INTRODUCTION

In this chapter, the physics of the metal-semiconductor contact, in particular the Schottky-Mott model and the Bardeen model, will be discussed. These models have been recognised to be the foundation of metal-semiconductor contact physics and will provide a better understanding of ohmic contacts to p-GaN. We will also explore the possible ways to improve ohmic contact formation to p-GaN.

The Circular Linear Transmission Line Model (CTLM) will also be presented and discussed. This is a widely-used model for the measurement of the specific contact resistance, ρ_c, which forms the basis for determining a good metal contact system.

2.2 PHYSICS OF METAL-SEMICONDUCTOR CONTACT

2.2.1 Schottky-Mott Model

According to the Schottky-Mott model, a schottky barrier is formed when a metal comes into contact with a semiconductor, which is due to the difference in the work functions of the metal and the semiconductor. This is illustrated in the energy band diagrams shown in Figure 2.1 for p-type semiconductors [43], [44].

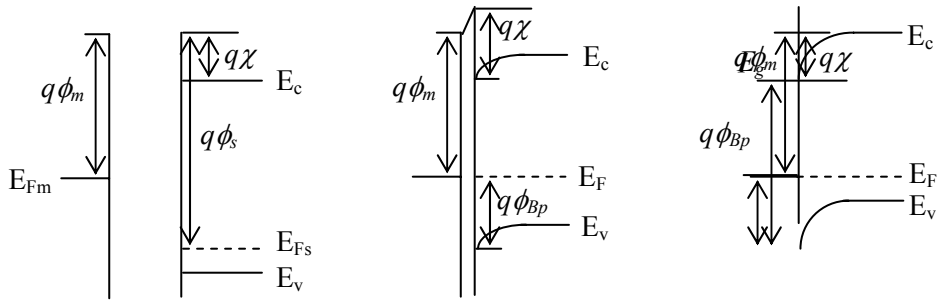

(a) p-type $q\phi_m < q\phi_s$ (rectifying).

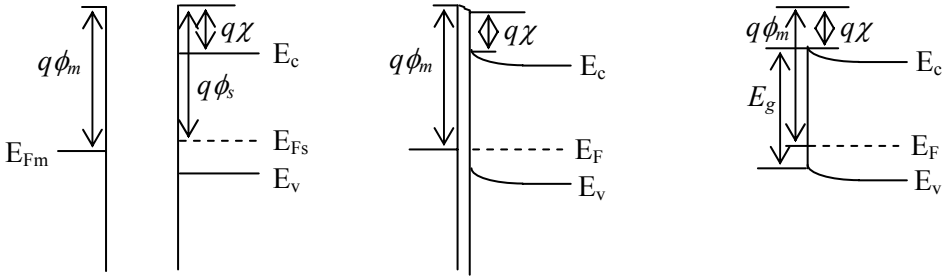

(b) p-type $q\phi_m > q\phi_s$ (ohmic).

Figure 2.1 Energy band diagrams of metal-semiconductor contacts [43], [44].

The height of the Schottky barrier for p-type semiconductor ($q\phi_{Bp}$) measured with respect to the Fermi level is given by [44]:

$$q\phi_{Bp} = E_g - q(\phi_m - \chi) \quad (2.1)$$

where,

E_g = Bandgap energy of semiconductor,

$q\phi_m$ = Workfunction of metal,

$q\phi_s$ = Workfunction of semiconductor,

$q\chi$ = Electron affinity of semiconductor and

$q\phi_{Bp}$ = Schottky barrier height of p-type semiconductor.

The ohmic or rectifying characteristic of the metal contact thus depends on both the workfunction of the metal ($q\phi_m$) and the workfunction of the semiconductor ($q\phi_s$). The conditions for obtaining rectifying or ohmic contacts to p-type semiconductor is summarised in Table 2.1.

From Table 2.1, we see that in order to obtain an ohmic contact to a p-type semiconductor, we need a metal with a workfunction greater than that of the semiconductor, i.e. $q\phi_m > q\phi_s$. However, there is an absence of metals with workfunction greater than that of p-GaN (7.5 eV), which is the main reason for ohmic contact to p-GaN is challenging.

Table 2.1: Summary of the behaviour of contacts on p-type semiconductors under the 2 workfunction conditions: $q\phi_m > q\phi_s$ and $q\phi_m < q\phi_s$.

Workfunction conditions	**Contact on p-type**
$q\phi_m > q\phi_s$	Ohmic
$q\phi_m < q\phi_s$	Rectifying

2.2.2 Bardeen Model

While we see that the Fermi level at the interface shifts when the metal and semiconductor comes into contact for the case of the Scottky-Mott model, the Bardeen model proposes that the Fermi level at the interface is independent of the metal workfunction because of the presence of surface states, which is known as the Bardeen limit [44], [45]. Some experimental results have shown that the strong dependence of the barrier height on $q\phi_m$, as expressed in Equation 2.1, is valid only for ionic semiconductors (such as ZnO, SiC) and semiconductors with an ionic nature, like GaN. On the other hand, for many covalent semiconductors – III-V compounds such as GaAs and InP – experiments have found that the barrier height is a less sensitive function of $q\phi_m$ than predicted by Equation 2.1 in the Schottky-Mott model. It has been claimed in these cases that the barrier height is almost independent of the metal workfunction and is dependent only on the type of semiconductor – a claim made by Bardeen in 1947 [46].

In short, Bardeen proposed that [47]:

i) Surface (localised) states form at free semiconductor surfaces and at a contact,

ii) these states can 'pin' the Fermi level in the centre of the band gap and

iii) a very thin oxide layer (insulator) is present on the semiconductor surface.

Bardeen proposed that the Fermi energy level at the interface is 'pinned' by interface states, which originates from the already present surface states or formed during interfacial reactions.

According to Bardeen, a continuous distribution of surface states present at an insulator (oxide)-semiconductor interface results in an energy level at the surface. When a metal is laid on the semiconductor to form a metal-semiconductor contact, this energy level, known as the neutral energy level $q\phi_o$, will nearly coincide with the Fermi level. Below this energy level, all surface states are filled and hence causing charge neutrality at the surface [46].

The energy band diagrams for the p-type metal-semiconductor contact with surface states is shown in Figure 2.2. When the density of surface states is very large, the deviation of $q\phi_o$ from E_F will be very small [44], where $q\phi_o \approx E_F$. The barrier height for a p-type semiconductor is therefore given by [43], [44]:

$$q\phi_{Bp} = q\phi_o \tag{2.2}$$

where,

$q\phi_{Bp}$ = Barrier height and

$q\phi_o$ = Neutral energy level.

To conclude, Bardeen's model shows that the barrier height is determined by the property of the semiconductor surface and is independent of the workfunction of the metal, as opposed to the Schottky-Mott model.

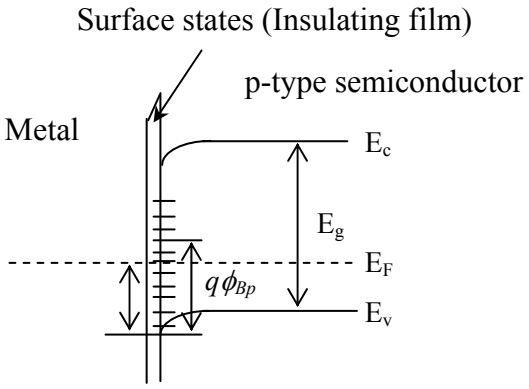

Figure 2.2 p-type metal-semiconductor contacts with surface states.

2.2.3 Ohmic Contact Formation to p-GaN

Although the two above-mentioned models, namely the Schottky-Mott model and the Bardeen model, are oversimplified and represent limiting cases, they aid in the choice of a metal system to be used on the n- or p- type semiconductor. In this case, it is p-type GaN.

Generally,

- **Ionic** semiconductors follow the Schottky model, where the barrier height, ϕ_B, is linearly dependent on the workfunction of the metal, ϕ_m.
- **Covalent** semiconductors follow the Bardeen model, with the Fermi level firmly 'pinned' by the interface states.

Experimental results have shown that GaN does not suffer from Fermi level pinning [48]-[50]. This seems to tally with GaN being a semiconductor with an ionic nature, since the difference in the electronegativity of Ga (1.6 eV) and N (3.0 eV) is reasonably large. Thus, the choice of metal system for p-GaN would

preferably be one with a high workfunction. This condition is based on the Schottky-Mott model, as discussed in Section 2.2.1. However, the workfunction of p-GaN is 7.5 eV while the highest workfunction for a metal (Pt) is only 5.7 eV. Hence, other methods must be employed for ohmic contact formation to p-GaN.

One method, which is also the most common in ohmic contact formation to semiconductors, is to dope the semiconductor heavily at the surface region to enhance field emission [51]. As a result, the depletion width is reduced and the tunneling possibility at the contact is increased. However, as mentioned in Section 1.2, it is known that it is difficult to heavily dope p-GaN due to the large ionization energy of the dopant, Mg.

Another method is to decrease the bandgap of the semiconductor by forming an intermediate semiconducting layer (ISL) at the metal/semiconductor interface, as illustrated in Figure 2.3. By increasing the depletion width and separating the barrier height at the metal/semiconductor interface into the barrier heights at the metal/ISL/semiconductor interfaces, the effective barrier height decreases. While the behavior of the interface is not completely understood at this time, we recall from Section 1.2.1 (a) that the O_2-annealed Ni/Au contact system was reported to form a NiO layer on p-GaN which behaves similarly to an ISL.

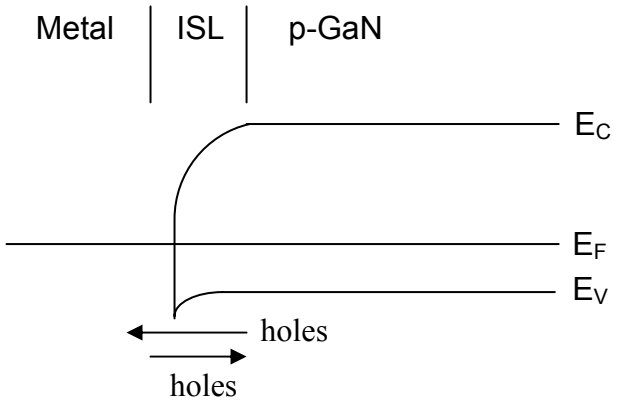

Figure 2.3: The formation of an interfacial semiconductor layer (ISL) to reduce the bandgap of the p-GaN semiconductor at the contact.

The third possible method is to create Ga-vacancies (V_{Ga}'s) at the surface of p-GaN. These V_{Ga}'s, also known as triply charged acceptors, aid in yielding more holes in GaN [52], which is beneficial to the ohmic contact formation to p-GaN. The mechanism can be explained as follows: in the GaN lattice structure, the Ga atom is bonded to 4 N atoms and vice versa, as illustrated in Figure 2.4 (a). When a Ga atom is absent, the N atom is short of one electron to form the stable electronic configuration of 8 outermost electrons, illustrated in Figure 2.4 (b). Thus, this site can be viewed as an acceptor site, as it readily 'accepts' an electron. In the absence of 1 Ga atom, there will be 3 of such acceptor sites, therefore the name 'triply charged acceptors'.

One way by which V_{Ga}'s can be formed is by the employment of plasma surface treatments, where we can purposely form an oxide layer on GaN and then stripping this GaO_x layer and removing some Ga along with it, hence creating some V_{Ga}'s. Another method is by depositing a metal which reacts with Ga to

form gallides. This will result in some out-diffusion of Ga and hence result in some V_{Ga}'s formed at the surface of GaN.

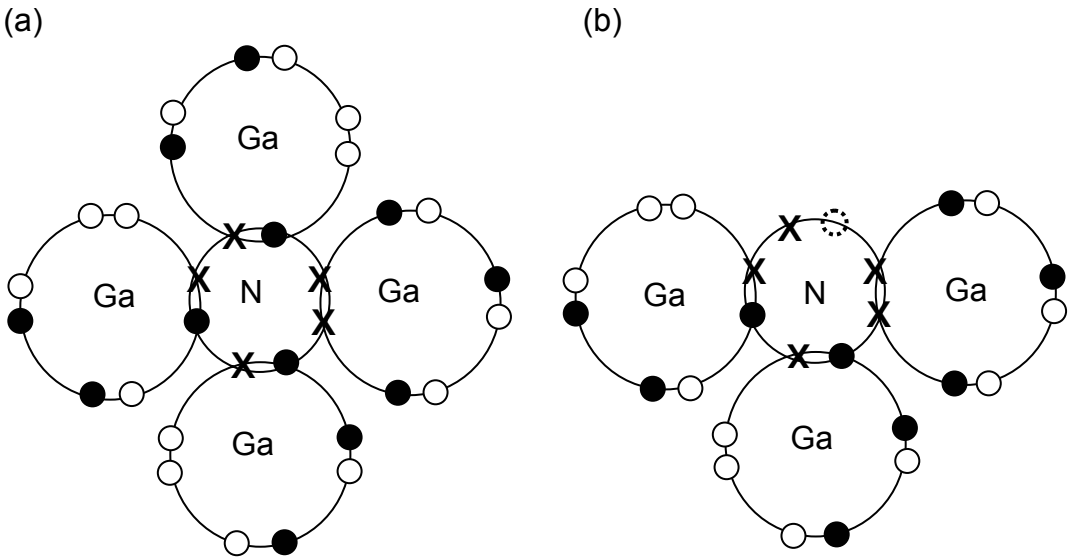

Figure 2.4: Electronic configuration of (a) GaN and (b) GaN with a missing Ga atom [Legend: **X** - electron from N atom; ● - electron from Ga atom; ○ - electron from other N atom (not shown)].

2.3 CIRCULAR TRANSMISSION LINE MODEL (CTLM)

2.3.1 Introduction

The circular transmission line model was employed to measure the specific contact resistance, which is the resistance at the interface between the metal and the semiconductor. The structure is shown in Figure 2.5. The outer radius, r_o, of the circles is 90 μm and the inner radii the circles are 85, 80, 75, 65, 55, 45 μm. The respective gap spacings are 5, 10, 15, 25, 35, and 45 μm.

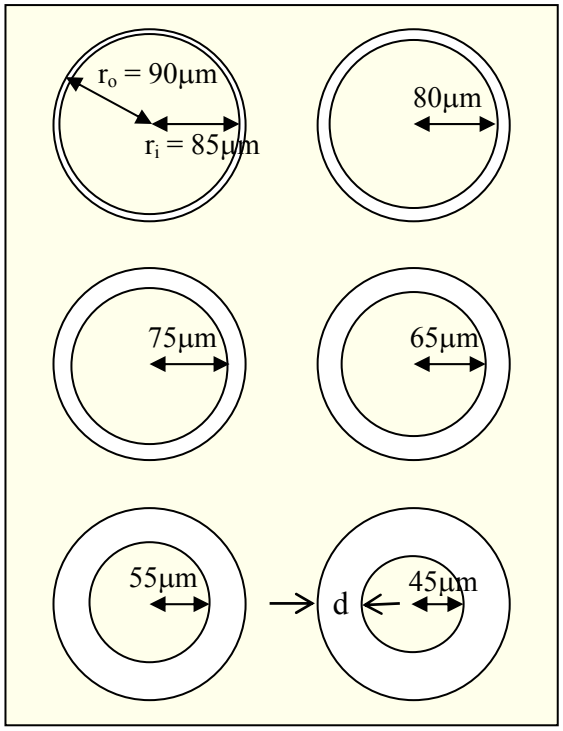

Figure 2.5 Structure of the circular transmission line model for lift-off technique.

2.3.2 Derivation of Specific Contact Resistance

The two-point probe technique is employed in this work. Figure 2.6 illustrates the two-point probe technique being employed on one circular contact pad. A current, *i*, is applied across the inner and outer contact pads using the HP4156 parametric analyzer and the voltage drop, ΔV, across the spacing, *d*, is calculated by [53], [54]:

$$\Delta V = \frac{iR_s}{2\pi}\left[\ln\left(\frac{r_o}{r_i}\right) + \frac{L_T}{r_i}\frac{I_o(r_i/L_T)}{I_1(r_i/L_T)} + \frac{L_T K_o(R_1/L_T)}{r_o K_1(r_o/L_T)}\right] \tag{2.3}$$

where,

i = Current across separation d,

R_s = Semiconductor sheet resistance,

L_T = Transfer length,

I_o, I_1, K_o, K_1 = Modified Bessel Functions and

r_i , r_o = Inner and Outer radii of circular contact.

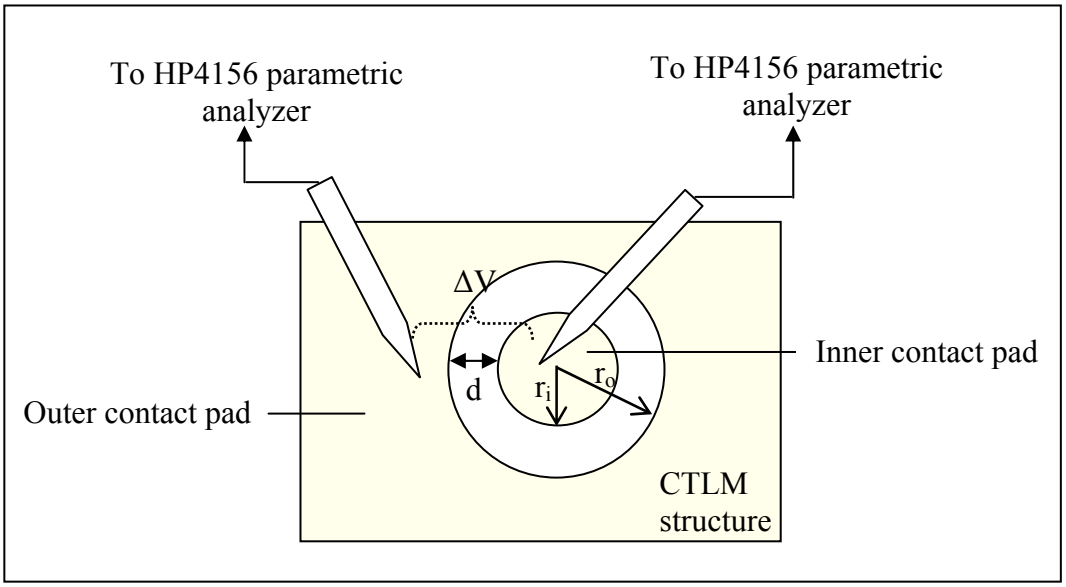

Figure 2.6 Illustration of the two-point probe technique carried out on one CTLM contact pad.

The transfer length, L_T, is related to the specific contact resistance, ρ_c, of the metal/semiconductor contact and the sheet resistance, R_s, of the semiconductor, and is given by:

$$L_T = \sqrt{\left(\frac{\rho_c}{R_s}\right)} \tag{2.4}$$

In cases where r_i and r_o are greater than L_T by a factor of at least 4, both I_o/I_1 and K_o/K_1 approximate to unity [55]. Thus, Equation 2.3 becomes:

$$\Delta V = \frac{iR_S}{2\pi}\left[\ln\left(\frac{r_o}{r_o - d}\right) + L_T\left(\frac{1}{r_o} + \frac{1}{r_o - d}\right)\right] \tag{2.5}$$

The total resistance, R_T, between the contacts is defined as the ratio of the voltage across the separation (ΔV) and the current (i), i.e. $R_T = \Delta V / i$, hence,

$$R_T = \frac{R_S}{2\pi}\left[\ln\left(\frac{r_o}{r_o - d}\right) + L_T\left(\frac{1}{r_o} + \frac{1}{r_o - d}\right)\right] \tag{2.6}$$

And since $2\pi(r_o - d) \gg d$, Equation 2.6 can be simplified to

$$R_T = \frac{R_S}{2\pi r_o}\left[d + 2L_T\right] \tag{2.7}$$

From Equation 2.7, we observed a linear relationship between R_T and the circular contact pad spacing, d. Hence, a graph of R_T versus d can be plotted, as shown in Figure 2.7, in order to determine the value of ρ_c.

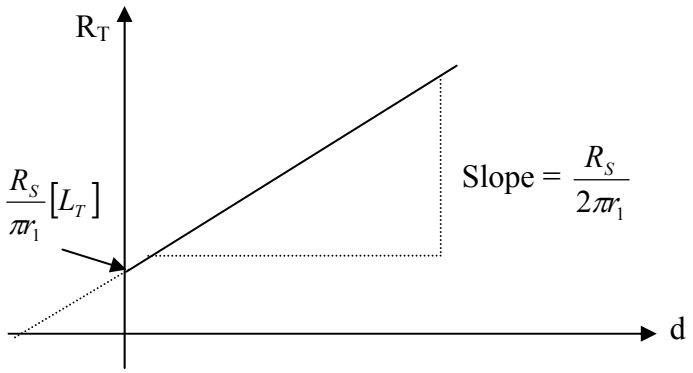

Figure 2.7 Graph of R_T versus d used to calculate specific contact resistance ρ_c of metal contact.

The slope of the graph shown in Figure 2.7 gives the value of $\frac{R_S}{2\pi r_o}$ and the interception with the vertical R_T-axis gives the value of $\frac{R_S}{\pi r_1}[L_T]$. Hence, the value of the transfer length, L_T, can be obtained by dividing the y-interception over the slope:

$$L_T = \text{(y-interception /slope) x 2} \tag{2.8}$$

From Equation 2.4, the value of specific contact resistance, ρ_c, can then be obtained:

$$\rho_{c,} = (L_T)^2 \text{ x } R_s \tag{2.9}$$

The main advantage of the CTLM is that it is not necessary to isolate the diffused or implanted layer like for the Linear Transmission Line Model (LTLM) where current can flow from contact to contact through the region beyond the structure

in the linear arrangement (if it is not isolated). In the circular case, current can only flow from the center to the surrounding contact and no other path is possible.

2.4 SUMMARY

In this chapter, the two most established models of the metal-semiconductor contact were described. GaN, being a semiconductor with an ionic nature, was seen to follow the Schottky-Mott model more closely. We also explored the three possible methods by which we can improve the electrical characteristics of metal contacts to p-GaN since there does not exist any metal or metal compound with a workfunction larger than that of p-GaN's (7.5 eV). The first method, heavily doping the surface of GaN, is not feasible. The second method on forming a ISL will be explored using the O_2-annealed Ni/Au contact, with NiO reportedly forming the ISL. The third method, creation of V_{Ga}'s, will also be explored via plasma surface treatments and Rh, known to react with Ga to form gallides.

The Circular Transmission Line Model (CTLM) and the calculation of the specific contact resistance, ρ_c, were also presented and discussed.

CHAPTER 3

FABRICATION PROCEDURES AND METAL STUDY METHODOLOGY

3.1 INTRODUCTION

The fabrication procedures for the Circular Transmission Line Model (CTLM) contacts to p-GaN and the current-voltage (I-V) measurement technique will be briefly described in this chapter. The parameters that will be studied for the Ni/Au and Rh-based contacts to p-GaN will also be presented.

3.2 EXPERIMENTAL PROCEDURES

The schematic diagram of the layer structure of the p-GaN wafers used in this work is shown in Figure 3.1. It is a single layer, grown by Molecular Beam Epitaxy (MBE) on a sapphire substrate. Two such wafers were used in the course of this work and the hole concentration of these wafers were determined to be 3.38×10^{17} cm^{-3} and 3.52×10^{17} cm^{-3} (refer **Appendix II**). They will be indicated where they are used.

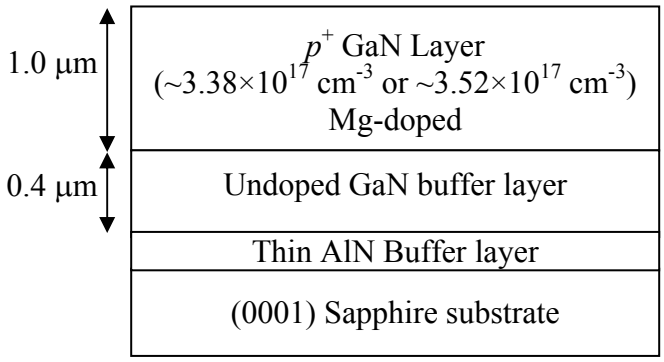

Figure 3.1 Schematic diagram of the layer structure of p-GaN.

3.2.1 Fabrication Procedures

Figure 3.2 summarizes the experimental procedure carried out for the fabrication of the contacts to p-GaN. The two-step surface treatment is employed in this work, where the surface of the sample is cleaned once (using chemical or plasma treatments) prior to lithography and a second time (chemical treatment) prior to metallization. The acids or plasmas used in each experiment will be specified where the samples are discussed. The sample preparation, heat treatment of the contact, and the measurements are described in detail below.

(i) Cleaning

The p-GaN samples were ultrasonically cleaned in acetone followed by methanol for 3 minutes each. The samples were then rinsed in de-ionised (DI) water and then blown dry with N_2. After this, they were dehydrated in an oven at 110˚C for 10 mins.

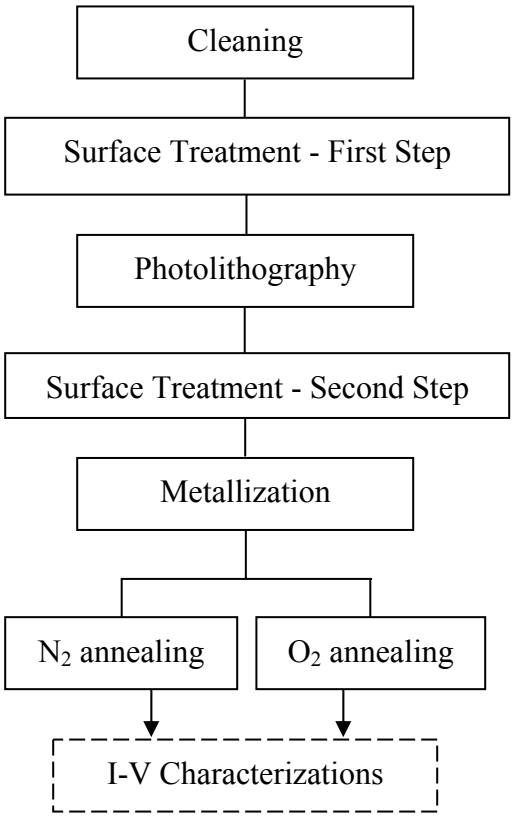

Figure 3.2: Flow Chart summarizing the experimental procedures carried out for the fabrication of contacts to p-GaN.

(ii) Surface Treatment - First Step

Subsequently, the samples were surface-treated with either plasma (Cl_2/N_2 or O_2 plasma) or chemicals (Boiling Aqua Regia – $HCl:HNO_3$ (3:1), $HCl:H_2O$ (1:1) or $HF:HCl:H_2O$ (1:1:2)). The samples undergoing plasma treatment were placed in the Inductively Coupled Plasma (ICP) machine using the ICP parameters summarised in Table 3.1. The RIE power is varied because the effect of RIE power for the Cl_2/N_2

plasma to the Ni/Au contact to p-GaN will be studied. The plasma treatments were followed by 1 min of boiling Aqua Regia (AQ) surface treatment.

Table 3.1: ICP parameters for Cl_2/N_2 and O_2 plasma treatments on p-GaN samples.

Plasma Treatment	**Flow rate of N_2 (sccm)**	**Flow rate of Cl_2 (sccm)**	**Flow rate of O_2 (sccm)**	**RF1 RIE Power (W)**	**RF2 ICP Power (sccm)**	**Chuck Temp (˚C)**	**Chamber Pressure (mTorr)**	**Duration (min)**
Cl_2/N_2	5	25	-	100 / 300	500	25	5	1
O_2	-	-	30	100	500	20	15	1

(iii) Photolithography

The CTLM structures were defined on the samples using standard photolithographic procedures (refer **Section 3.2.2**). AZ 5214, a positive photoresist, was used. The structure consists of six circular patterns, where the radius of the outer circular contacts was 90 μm and the radii of the inner circular contacts were 85, 80, 75, 65, 55, 45 μm. The structure is illustrated in Figure 2.5.

(iv) Surface Treatment - Second Step

The patterned p-GaN samples were then dipped in AQ (15 s), $HCl:H_2O$ (15 s) or $HF:HCl:H_2O$ (quick dip). All the chemicals used in this step are boiled then cooled.

The choice of chemicals for each p-GaN sample follows the chemical which was used in the First Step surface treatment. For the plasma-treated samples, AQ is used.

The samples were then rinsed with DI water and blown dry with N_2.

(v) Metal Deposition

Subsequently, the samples were immediately loaded into the Edwards Electron Beam Evaporator, which was used for metal depositions. The Evaporator was then pumped down to ~1.0×10^{-6} Torr before deposition was carried out. The evaporator was maintained at a pressure of lower than 10^{-5} Torr throughout the deposition.

(vi) Metal Lift-Off

After deposition, metal lift-off was carried out by placing the samples in acetone with ultrasonic bath agitation for 3-5 mins. The samples were then inspected under the microscope to ensure that the metal lift-off was successful throughout the surface of the sample.

(vii) Annealing

Annealing of the samples was carried out in a RC 2442 Annealing Furnace. The samples were annealed in either N_2 or O_2 annealing ambient for temperatures ranging from 300 ˚C to 650 ˚C for various durations which will be specified where the samples are discussed.

3.2.2 Photolithographic Process

The photolithographic process is as follows:

1. Place the sample on the photoresist spinner.
2. Apply two drops of AZ 5214 photoresist (PR) on the sample and spin at 5000 rpm for 30 s.
3. Soft bake at 90 °C for 20 min.
4. Alignment and exposure of the samples were carried out on the Karl Suss mask aligner. The exposure time used was 100 s with constant UV intensity of 1.8 mW/mm.
5. Dip the exposed samples into diluted AZ developer (3 parts AZ Developer and 1 part H_2O) for 75 s followed by rinsing thoroughly with DI water. Examine the sample under a microscope to ensure complete removal of PR.
6. Hard bake at 110 °C for 10 min.
7. Place samples in Aqua Regia, HCl:HNO_3 (3:1) which is boiled then cooled to room temperature for 15 s. Blow dry with N_2.
8. Immediately after, place the samples in the electron-beam machine for metal deposition.

3.2.3 Current-Voltage Measurements

The Current-Voltage (I-V) characteristics were measured for the contacts as-deposited and after each heat treatment by a two-point probe technique using the

Precision Semiconductor Parameter Analyzer HP 4156A and a micro-probe station. The placement of the two probes can be seen in the illustration shown in Figure 2.6. The configurations used for the HP 4156A are summarised in Table 3.2. In the measurement, a current sweep was performed, and the respective voltage was measured. An average of 5 to 10 devices were tested for each surface-treated contact fabricated in this work and the I-V characteristics referred to in the following chapters are typical curves obtained for all the devices tested. After each measurement of I-V curves, the specific contact resistance (ρ_c) can be determined using the CTLM calculations presented in Section 2.3.2.

Table 3.2 Configuration of the HP 4156A analyzer programs.

Parameter	**Configuration for Ni/Au contacts**	**Configuration for Rh-based contacts**
y-axis	Current (I)	Current (I)
x-axis	Voltage (V)	Voltage (V)
Start Current	-5 mA	-5 mA
End Current	5 mA	5 mA
Start Voltage	-10 V	-7 V
End Voltage	10 V	7 V
Step	50 mV	50 mV

3.3 EXPERIMENT PARAMETERS

From **Chapter 1**, we have already established the motivations for the choice of the Ni/Au and Rh-based contact systems to p-GaN in this study. Thereafter, we need to study the effect of factors other than the choice of metal system used on the ohmic contact formation to p-GaN. The factors are identified to be: Thickness of each metal contact layer, type of surface treatment (and parameters used in the case of plasma), annealing ambient, temperature and time.

3.3.1 Ni/Au Contact

For the Ni/Au contact to p-GaN, the effects of the following variables were studied in this work:

(i) Reactive Ion Etching* (RIE) power used for Cl_2/N_2 plasma treatment

(ii) Types of surface treatment: plasma (Cl_2/N_2; O_2) and chemical (AQ; $HCl:H_2O$; $HF:HCl:H_2O$)

(iii) Annealing ambients: N_2 and O_2

(iv) Annealing temperatures: 500 ˚C, 600 ˚C and 650 ˚C for varying durations.

**The RIE power is associated with the physical component of plasma treatments while the ICP power is associated with the chemical component. The RIE power determines the rate of bombardment of the plasma on the surface of p-GaN; the higher the power, the higher the rate of bombardment.*

3.3.2 Rh-based contacts

As for the Rh-based contacts, we will seek to study the electrical characteristics obtained for the Rh, Rh/Ni, Rh/Au and Rh/Ni/Au contacts to p-GaN. For these contacts, we will study the effect of:

(i) Thickness of each metal contact layer,

(ii) Annealing ambients: N_2 and O_2 and

(iii) Annealing temperatures ranging from 300 ˚C to 650 ˚C for varying durations.

3.4 SUMMARY

In this chapter, the CTLM structure fabrication procedure was briefly introduced and the measurement technique employed, the two-point probe method, was briefly explained.

Thereafter, the parameters – variables and constants employed in the experiments for the Ni/Au contact and the Rh-based contacts were defined.

The I-V characteristics that have been obtained from these experiments will be presented and discussed in the chapters that follow.

CHAPTER 4

Ni/Au CONTACT TO p-GaN

4.1 INTRODUCTION

In this chapter, preliminary work such as the choice of chemical surface treatment and the optimization of the ICP parameters (RIE power) of the Cl_2/N_2 and O_2 plasma treatments will first be presented.

The effects of surface treatments (Aqua Regia (AQ), Cl_2/N_2 and O_2 plasma) on the as-deposited Ni/Au contact will also be studied via electrical and Auger Electron Spectroscopy (AES) surface characterizations.

Next, the effects of annealing on the Ni/Au contact to p-GaN with the above-mentioned surface treatments will be studied via electrical characterizations, X-ray Diffraction spectra, AES depth profiles and X-ray Photoelectron Spectroscopy (XPS).

The hole concentration of p-GaN samples used in this work is 3.38×10^{17} cm^{-3}, as determined by Hall measurements except for the samples used for optimization of RIE power for Cl_2/N_2 plasma treatment (**Section 4.3.1**), where the hole concentration is slightly lower at 1.11×10^{17} cm^{-3}. All contacts were fabricated according to the

experimental procedure shown in Figure 3.2 and Ni/Au (20/20 nm) was deposited for all the samples fabricated. Annealing in either N_2 or O_2 ambient was carried out at 600 °C, which has been optimized from a previous work [56].

4.2 CHOICE OF CHEMICAL SURFACE TREATMENT

The following chemical treatments were experimented on the Ni/Au contact to p-GaN: HCl:HNO_3 (3:1) – also known as Aqua Regia (AQ) [57]-[59], HCl:H_2O (1:1) and HF:HCl:H_2O (1:1:2). Although the chemical treatments are intended to remove the native oxide on GaN surface prior to metal deposition, it is reasonable to expect that the degree of their effectiveness in removing oxide may vary. The Ni/Au contacts to p-GaN surface-treated with the afore-mentioned chemicals were fabricated according to the experimental procedure shown in Figure 3.2. The first-step surface treatment refers to boiling the p-GaN samples in one of the 3 chemicals (AQ, HCl:H_2O or HF:HCl:H_2O), as described in **Section 3.2.1 (ii)**. The second step treatment refers to dipping the samples in their respective chemical treatments prior to metallization, as described in **Section 3.2.1 (iv)**.

The resulting I-V characteristics obtained for the N_2- and O_2-annealed Ni/Au contacts are shown in Figure 4.1. The as-deposited I-V curves are also added for comparison.

From Figure 4.1, we observe that for the as-deposited Ni/Au contacts, HCl:H_2O or HF:HCl:H_2O surface treatments have resulted in very similar electrical characteristics, and that the AQ-treated sample has yielded a slightly better I-V curve. Upon N_2 annealing, the HCl:H_2O-treated sample has a slightly better characteristic than the AQ-treated sample, which in turn is slightly better than that of the HF:HCl:H_2O-treated sample.

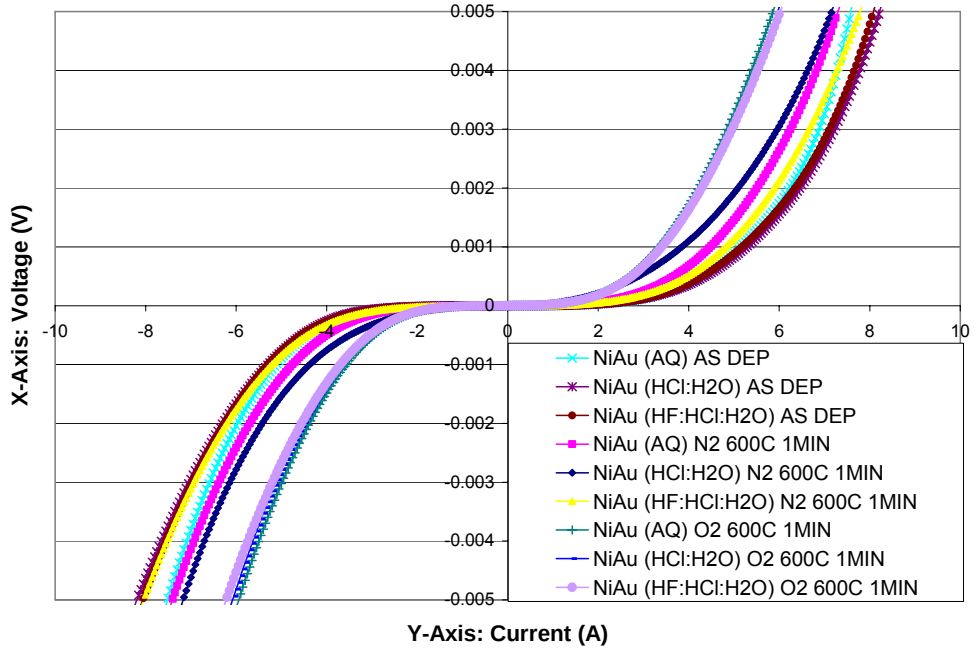

Figure 4.1: I-V characteristics of the as-deposited, N_2-annealed and O_2-annealed Ni/Au contacts to p-GaN with one of the following chemical surface treatments: AQ, HCl:H_2O and HF:HCl:H_2O.

For the O_2 annealed samples, the three chemical surface treatments lead to almost identical I-V characteristics, as shown in Figure 4.1. This could be explained by the

fact that Ni oxidizes to form NiO during the process of O_2 annealing [24]. We postulate that Ni might have reacted with the surface oxides on GaN during the O_2-annealing as well, hence depleting the surface oxides. This claim was also made by Chen *et. al.* [8], where the Ni/Pt contact was shown to improve after O_2 annealing due to the "interfacial reaction" that had taken place between Ni and the surface oxides, hence effectively removing them. As the three chemical surface treatments employed in this experiment may remove surface oxide with varying degrees, we can conclude that the oxidized Ni/Au contact to p-GaN is not sensitive to the amount of residue oxide found on the p-GaN surface, unlike the case for the N_2-annealed contacts that show some sensitivity. This accounts for the negligible difference observed in the I-V characteristics obtained for the various surface-treated samples when annealed in O_2 but not in N_2.

Based on the results presented in Figure 4.1, it is concluded that chemical surface treatments: AQ, HCl:H_2O and HF:HCl:H_2O only lead to slight differences in the I-V characteristics for Ni/Au contact on p-GaN. However, what is more important to note in Figure 4.1 is the positive effect of annealing, with the O_2-annealing being better than the N_2-annealing. The effects of annealing will be further discussed in subsequent sections.

We shall now visually inspect the effect of these chemical treatments on the adhesion of metal contact on p-GaN. Figure 4.2 shows the microscopic (magnification of 100)

pictures of the Ni/Au contact on the AQ, HCl:H_2O and HF:HCl:H_2O surface-treated p-GaN samples after lift-off. Here, we see that the AQ surface treatment results in the best adhesion of the Ni/Au contact on p-GaN. The HCl:H_2O surface treatment causes some peeling off of the metal at the edges while the HF:HCl:H_2O surface treatment results in a much more severe peeling off of the deposited metal. This is consistent with what has been reported by D. Zhang [18] - that AQ surface treatment results in good adhesion of contacts to GaN, as compared to the HCl:H_2O surface treatment. Also taking into account that all three chemical surface treatments do not yield significantly different I-V characteristics, the AQ chemical surface treatment has been selected for this work.

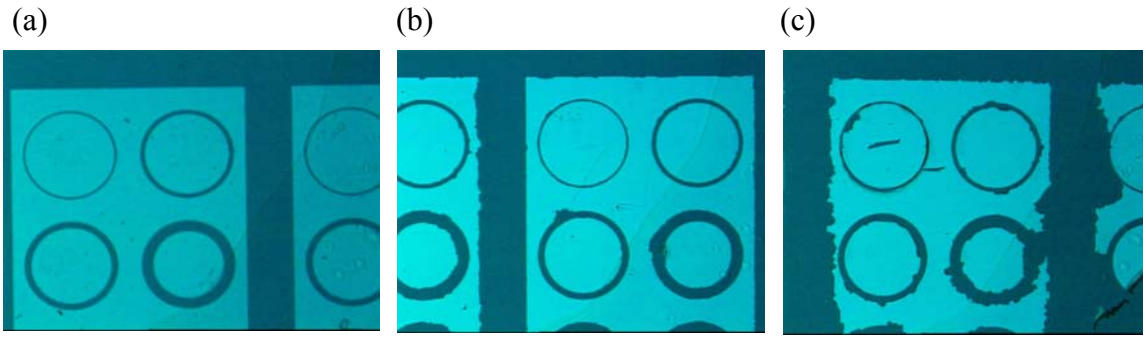

Figure 4.2: Microscopic images (100 times magnification) of Ni/Au contact to p-GaN with the following surface treatments: (a) AQ (b) HCl:H_2O and (c) HF:HCl:H_2O. AQ treated surface results in best adhesion.

4.3 OPTIMIZATION OF ICP PARAMETERS OF PLASMA TREATMENT

We attempt a basic optimization of the RIE powers for the Cl_2/N_2 and O_2 plasma treatments for the Ni/Au contact to p-GaN.

4.3.1 RIE power for Cl_2/N_2 plasma treatment

For the Cl_2/N_2 plasma treatment, six samples were prepared, namely: 100/As_Dep, 100/N, 100/O, 300/As_Dep, 300/N and 300/O according to the experimental procedure shown in Figure 3.2. The numbers 100 and 300 correspond to the RIE powers used: 100 W and 300 W, respectively. As_Dep refers to the as-deposited samples while N and O correspond to the annealing ambient: N_2 and O_2, respectively. The ICP power was kept constant at 500 W. A summary of the RIE power employed and the annealing conditions which gave the best I-V characteristics of each Cl_2/N_2 plasma-treated sample is shown in Table 4.1. The ICP parameters used can be found in Table 3.1.

Figure 4.3 shows the I-V characteristics obtained for the 100/As_Dep, 300/As_Dep and the best I-V characteristics for the 100/N, 300/N, 100/O and 300/O samples. "Best I-V characteristics" in this work refers to the steepest and most linear I-V curve obtained by an annealed sample at a particular annealing temperature (600 °C in this work) and annealing time. From Figure 4.3, it is observed that all the Ni/Au contacts with plasma treatment at RIE power of 300 W yield worse I-V characteristics than those obtained with plasma treatment at RIE power of 100 W. It

is also noted that annealing the contacts surface-treated with a higher RIE power of 300 W worsens their electrical characteristics (with respect to the as-deposited sample).

Table 4.1: RIE power employed and annealing conditions which gave the best I-V characteristics for each of the Cl_2/N_2 plasma-treated samples: 100/As_Dep, 300/As_Dep, 100/N, 300/N, 100/O and 300/O.

Sample	**Plasma Treatment**	**RIE power employed (W)**	**Annealing Ambient**	**Optimum Annealing time (min)**
100/As_Dep	Cl_2/N_2	100	-	-
300/As_Dep	Cl_2/N_2	300	-	-
100/N	Cl_2/N_2	100	N_2	1
300/N	Cl_2/N_2	300	N_2	2
100/O	Cl_2/N_2	100	O_2	1
300/O	Cl_2/N_2	300	O_2	1

Thus, we can conclude that a lower RIE power is better for Cl_2/N_2 plasma treatment used in the Ni/Au contact to p-GaN, which is not unusual since a higher RIE power implies higher bombardment energy on the samples during plasma treatment, which in turn results in more physical damage on the sample surface. This possibly causes a significant amount of defects to form at the p-GaN surface, which eventually hinders or lowers the current flow at the interface. An RIE power of 100 W will henceforth be used for Cl_2/N_2 plasma treatment to p-GaN.

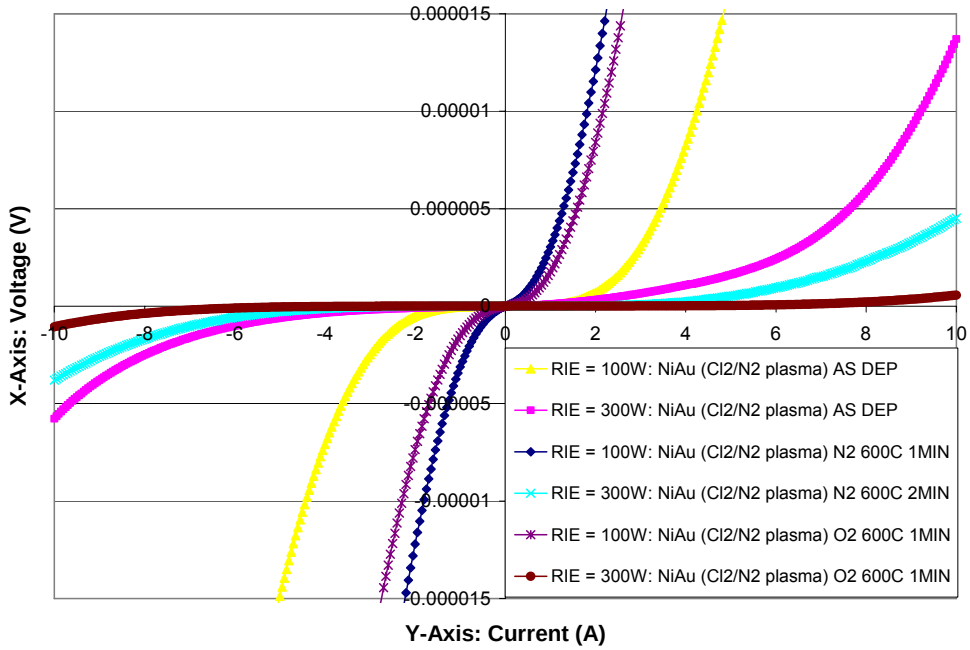

Figure 4.3: I-V characteristics for samples with Cl_2/N_2 plasma treatment at RIE powers of 100 W and 300 W for the as-deposited, N_2-annealed and O_2-annealed contacts.

4.3.2 RIE power for O_2 plasma treatment

For the O_2 plasma treatment, six samples were prepared: 50/As_Dep, 50/N, 50/O, 100/As_Dep, 100/N and 100/O according to the experimental procedure shown in Figure 3.2. The numbers 50 and 100 correspond to the RIE powers used: 50W and 100W, respectively. Here, a lower range of RIE powers is chosen as it has been shown in a previous work [56] that using an RIE power of 100 W is better than 300 W. As_Dep refers to the as-deposited samples while N and O correspond to the annealing ambient: N_2 and O_2, respectively. A summary of the RIE power employed and the annealing conditions which gave the best I-V characteristics of each O_2

plasma-treated sample is shown in Table 4.2. The ICP power was kept constant at 500 W. The ICP parameters used can be found in Table 3.1.

Figure 4.4 shows the I-V characteristics obtained for the 50/As_Dep, 100/As_Dep and the best I-V characteristics for the 50/N, 100/N, 50/O and 100/O samples. From Figure 4.4, it is observed that the Ni/Au contacts with plasma treatments at RIE power of 50 W all yield worse I-V characteristics than those obtained with plasma treatment at RIE power of 100 W. An RIE power of 100 W will henceforth be used for O_2 plasma treatment to p-GaN.

Table 4.2: RIE power employed and annealing conditions which gave the best I-V characteristics for each of the O_2 plasma-treated samples: 50/As_Dep, 100/As_Dep, 50/N, 100/N, 50/O and 100/O.

Sample	**Plasma Treatment**	**RIE power employed (W)**	**Annealing Ambient**	**Optimum Annealing time (min)**
50/As_Dep	O_2	50	-	-
100/As_Dep	O_2	100	-	-
50/N	O_2	50	N_2	0.5
100/N	O_2	100	N_2	1
50/O	O_2	50	O_2	0.5
100/O	O_2	100	O_2	0.5

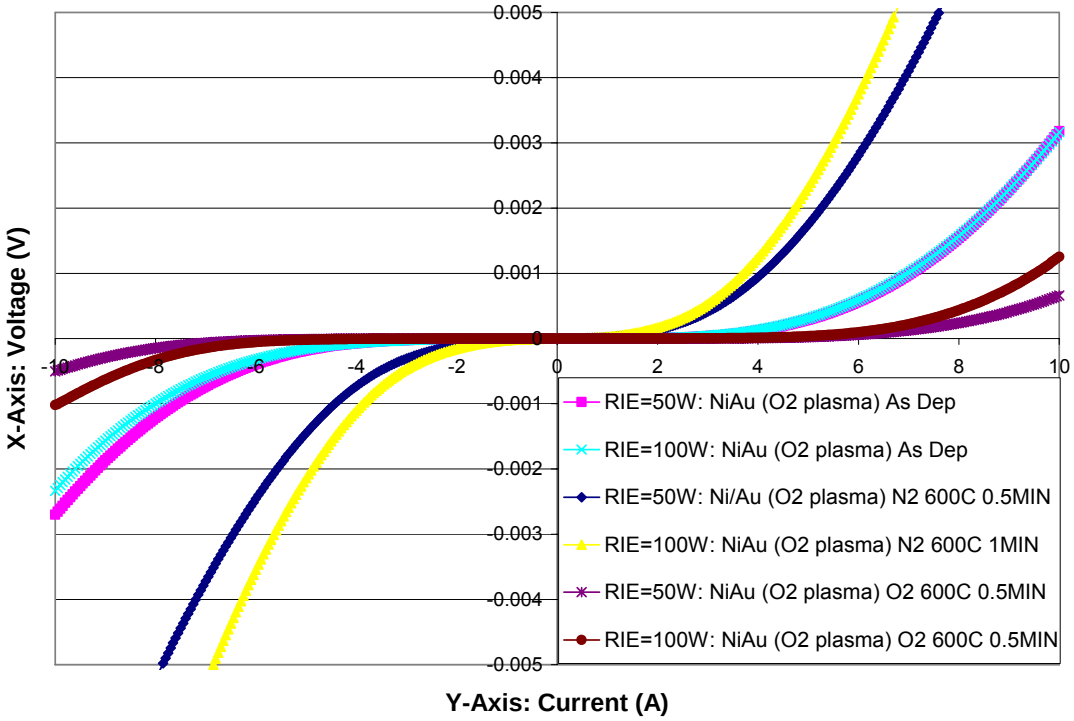

Figure 4.4: I-V characteristics for samples with O_2 plasma treatment at RIE powers of 50 W and 100 W for the as-deposited, N_2-annealed and O_2-annealed contacts.

To conclude, an RIE power of 100 W is observed to be optimal for the Cl_2/N_2 and O_2 plasma treatments. While it has been reported that some damage to the surface resulting in a rougher surface may mean a larger contact surface for contact formation and hence, better I-V characteristics [60], we see here that too much damage results in worse I-V characteristics, which is possibly due to the introduction of too many point defects [61] to the surface of GaN. This explains why too high an RIE power is seen to be detrimental to the p-GaN contacts.

4.4 EFFECTS OF SURFACE TREATMENTS ON THE AS-DEPOSITED Ni/Au CONTACT

4.4.1 Electrical Characterizations

Ni/Au (20/20 nm) contacts to p-GaN are fabricated according to the experimental procedure shown in Figure 3.2 with the following surface treatments: AQ, Cl_2/N_2 plasma and O_2 plasma. Figure 4.5 shows the I-V characteristics of these as-deposited Ni/Au contacts to p-GaN. Here, we see that all three curves are comparable, with the AQ-treated sample giving only a slightly better curve. This means that without annealing, the plasma surface treatments with subsequent AQ have almost the same effect as pure AQ on the Ni/Au contact to p-GaN. We recall from **Section 4.2** that the samples with the AQ, $HCl:H_2O$ and $HF:HCl:H_2O$ chemical surface treatments gave similar I-V characteristics as well. Hence, we can collectively conclude that the electrical characteristics of the as-deposited Ni/Au contacts are reasonably insensitive to the surface treatment, chemical or plasma, employed.

We shall now investigate the surface conditions of the AQ, Cl_2/N_2 and O_2 plasma surface-treated p-GaN via Auger Electron Spectroscopy (AES) and X-ray Photoelectron Spectroscopy (XPS).

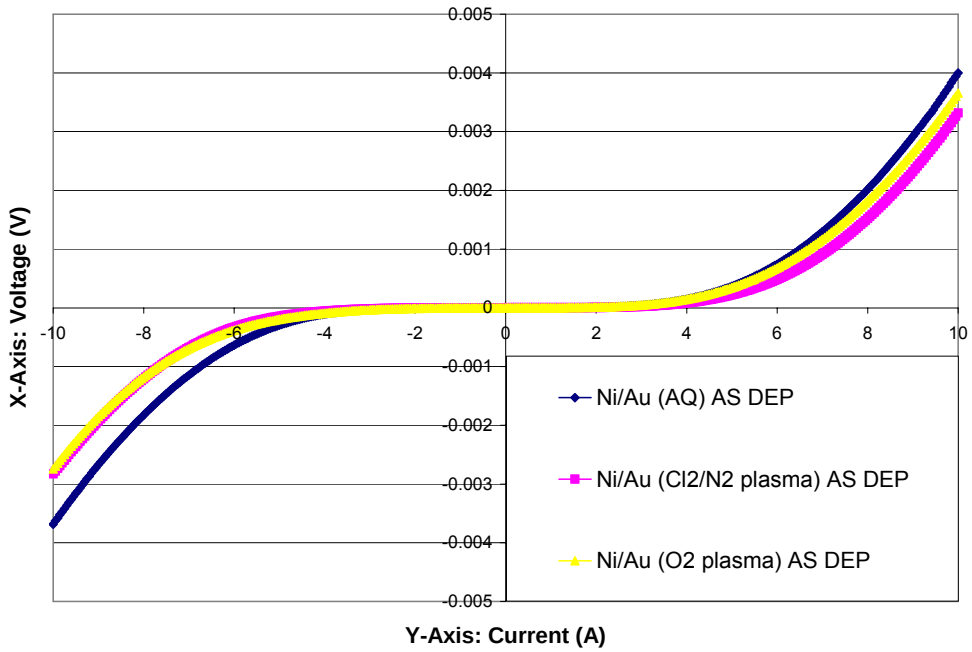

Figure 4.5: I-V characteristics of as-deposited Ni/Au contacts to p-GaN for AQ, Cl_2/N_2 plasma and O_2 plasma surface treatment.

4.4.2 AES Surface Characterizations

In this section, p-GaN samples with the following surface treatments will be referred to by their sample names in brackets: Aqua Regia (Pure_AQ), Cl_2/N_2 plasma (Cl_2/N_2-no_AQ), Cl_2/N_2 plasma + 1 min AQ (Cl_2/N_2 -AQ1), O_2 plasma (O_2-no_AQ), O_2 plasma + 1min AQ (O_2-AQ1) and O_2 plasma + 5min AQ (O_2-AQ5).

Table 4.3 details the surface treatment procedures undergone by the p-GaN samples used in this experiment and summarizes the Ga/N and O/Ga ratios obtained from the AES surface characterizations of these samples. The samples from which electrical characteristics were presented in Figure 4.5 are highlighted in blue. It should be

noted that the AES results should only be viewed qualitatively and not quantitatively due to the large percentage error margin of 20%.

Table 4.3: Details of surface treatment procedures of p-GaN samples and Ga/N and O/Ga ratios obtained by AES and XPS surface characterizations of these samples.

Sample	**Surface Cleaning**	**Surface treatment (First Step)**					**AES results**	
		AQ (boil) 10min	Plasma		AQ (boil)			
			N_2/Cl_2	O_2	1min	5min	**Ga/N**	**O/Ga**
"virgin"	✓						1.599	0.772
Pure_AQ	✓	✓					1.172	0.172
Cl_2/N_2-no_AQ	✓	✓	✓				1.473	0.506
Cl_2/N_2-AQ1	✓	✓	✓		✓		1.217	0.107
O_2-no_AQ	✓	✓		✓			10.767	1.396
O_2-AQ1	✓	✓		✓	✓		1.202	0.340
O_2-AQ5	✓	✓		✓		✓	1.250	0.136

In Table 4.3, the "virgin" (untreated) sample is included as the control sample for comparison. The Ga/N ratio indicates the amount of Ga present in relation to N near the surface of p-GaN. The lower the Ga/N ratio for p-GaN, the better it is for ohmic contact formation, as discussed in **Section 2.2.3**, as this could indicate the presence of more Ga-vacancies. The O/Ga ratio indicates the amount of oxide present on the surface of p-GaN. This oxide is undesirable to the ohmic contact formation to p-GaN, hence as much of it should be removed from the surface of p-GaN (prior to

metal deposition) as possible. The lower the O/Ga ratio, the better is the surface for contact formation.

Studying the trend of the following three samples in particular: Aqua Regia (Pure_AQ), Cl_2/N_2 plasma + 1 min AQ (Cl_2/N_2 -AQ1) and O_2 plasma + 1min AQ (O_2-AQ1), we see that the Cl_2/N_2-AQ1 sample gives the lowest O/Ga ratio (0.107) while the O_2-AQ1 sample yields the highest (0.340), as shown in Table 4.3. Simultaneously, the Cl_2/N_2-AQ1 sample gives the highest Ga/N ratio (1.217) while the Pure_AQ sample gave the lowest (1.172). Considering the small difference between these ratios as well as the trade-off that exists between the Ga/N and O/Ga ratios for each of these three samples, it explains the highly similar I-V characteristics observed in Figure 4.5 for the Ni/Au contact as-deposited on these three samples.

4.5 EFFECTS OF ANNEALING ON NI/AU CONTACT TO SURFACE-TREATED p-GaN

Here, we anneal the as-deposited Ni/Au contacts to AQ, Cl_2/N_2 plasma and O_2 plasma surface-treated p-GaN (presented in **Section 4.3**) in N_2 and O_2 ambient. We will seek to determine if O_2 annealing is indeed better than N_2 annealing for the Ni/Au contact, as reported in the literature [8], [24]-[27]. We will also seek to find out if this is true for the three surface treatments prior to metal evaporation, namely the Aqua Regia (AQ) chemical treatment (the control sample), the Cl_2/N_2 plasma

treatment, and the O_2 plasma treatment. A summary of the surface treatment employed and the annealing conditions which gave the best I-V characteristics of each sample is shown in Table 4.4.

Table 4.4: Summary of surface treatment and annealing conditions which gave the best I-V characteristics for Ni/Au contacts to AQ, Cl_2/N_2 plasma or O_2 plasma surface-treated p-GaN samples: AQ/N, AQ/O, Cl_2N_2/N, Cl_2N_2/O, O_2/N and O_2/O.

Sample Name	**Surface Treatment**	**Annealing Ambient**	**Optimum Annealing time (min)**
AQ/N	AQ	N_2	1
AQ/O	AQ	O_2	1
Cl_2N_2/N	Cl_2/N_2 plasma	N_2	0.5
Cl_2N_2/O	Cl_2/N_2 plasma	O_2	0.5
O_2/N	O_2 plasma	N_2	1
O_2/O	O_2 plasma	O_2	0.5

Henceforth, the samples will be referred to by their sample names as indicated in Table 4.4. The first acronym refers to the surface treatment that was employed and the second acronym refers to the annealing ambient used for a particular sample.

4.5.1 Electrical Characterization

Figure 4.6 shows the best I-V characteristics obtained for the Ni/Au contact to p-GaN with the following surface treatments and annealing ambients: AQ, N_2 anneal;

AQ, O_2 anneal; Cl_2/N_2 plasma, N_2 anneal; Cl_2/N_2 plasma, O_2 anneal; O_2 plasma, N_2 anneal; and O_2 plasma, O_2 anneal. The I-V curve for the AQ surface-treated, as-deposited Ni/Au contact is added for comparison. The I-V curves of the other as-deposited samples are omitted, for the purpose of clarity, since they are similar to that of the AQ-treated sample. Here, we see that N_2 and O_2 annealing result in distinctly different electrical characteristics for these surface-treated contacts, unlike the similar I-V curves that were observed in Figure 4.5 for the as-deposited contacts. We shall now look into the effects of annealing on the Ni/Au contact to the three surface-treated p-GaN samples, namely (a) AQ; (b) Cl_2/N_2 plasma and (c) O_2 plasma individually.

4.5.2 Ni/Au contact to AQ surface-treated p-GaN

Comparing the results for the AQ-treated samples, curves (a) and (b) in Figure 4.6, the O_2-annealed sample clearly gives a better I-V curve than the N_2-annealed one. This confirms what has been reported in the literature [8], [24]-[27] that O_2 annealing improves the Ni/Au contact to p-GaN. It should be noted that since the samples used in this experiment are MBE-grown p-GaN epitaxial wafers and not MOCVD wafers, the theory of O_2 anneal re-activating the passivated Mg dopants and thereby improving Ni/Au contact to p-GaN owing to improved hole concentration may not be relevant here.

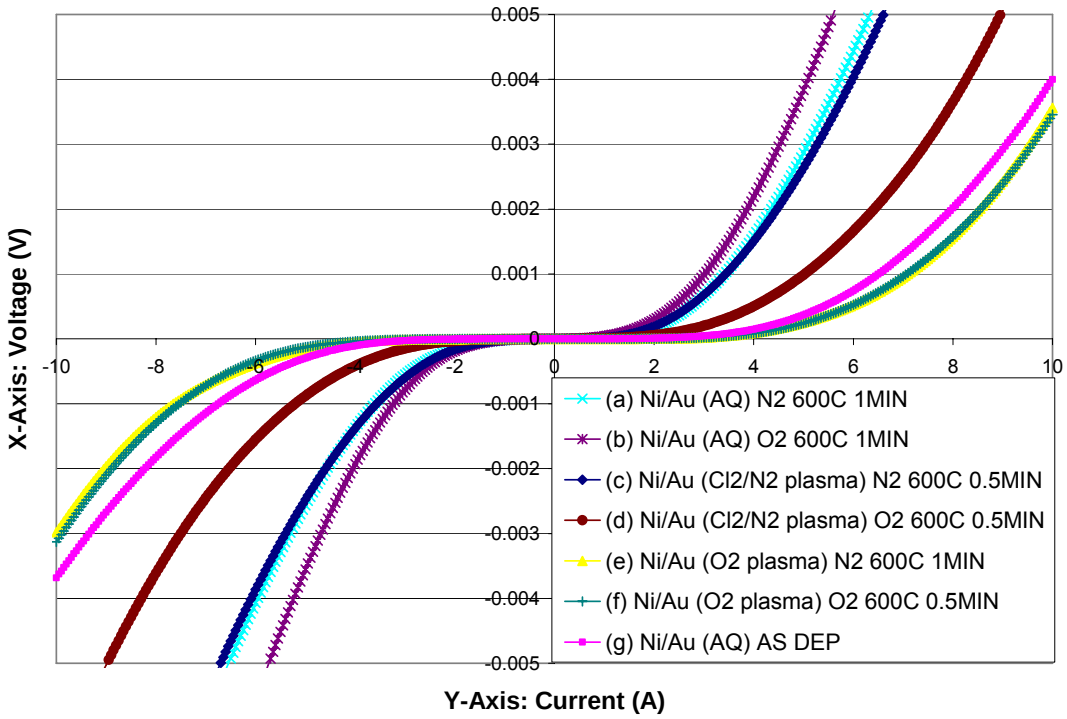

Figure 4.6: Best I-V characteristics of Ni/Au contacts to p-GaN: (a) AQ-treated, N_2 anneal; (b) AQ-treated, O_2 anneal; (c) Cl_2/N_2 plasma-treated, N_2 anneal; (d) Cl_2/N_2 plasma-treated, O_2 anneal; (e) O_2 plasma-treated, N_2 anneal; and (f) O_2 plasma-treated, O_2 anneal. Curve (g) is the I-V characteristic of the as-deposited Ni/Au contact to AQ-treated p-GaN and it is included as a reference for comparison.

The second postulation based on the oxidation of Ni to form NiO seems applicable here as the AQ/O contacts are observed to yield semi-transparent contacts upon annealing, as shown in Figure 4.7, and NiO is known to be transparent in nature. We confirm this with the (X-Ray Diffraction) XRD analyses of the AQ treated samples.

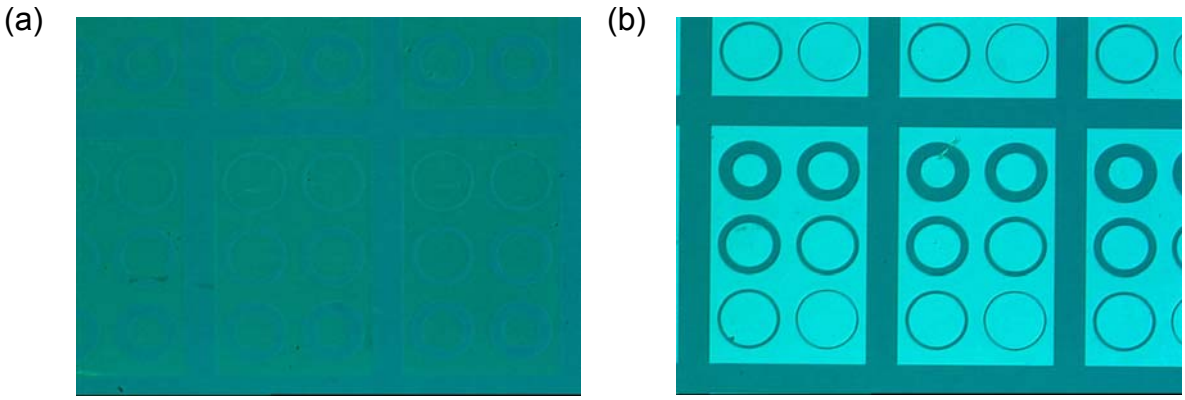

Figure 4.7: Typical microscopic images (50 times magnification) of Ni/Au contacts annealed in (a) O_2 and (b) N_2.

Figure 4.8 (a) and (b) show the XRD profiles of the N_2-annealed and O_2-annealed Ni/Au contacts to AQ surface-treated p-GaN. The N_2 and O_2 annealing were carried out at 600 °C for 1 min – the annealing condition which resulted in the best I-V characteristics for these contacts. From Figure 4.8, we observe that even though NiO is formed for both the N_2- and O_2-annealed contacts, Ni (111) is observed only for the N_2-annealed contact. This indicates the co-existence of Ni with NiO for the N_2 annealed contact in contrast to the complete oxidation of Ni observed for O_2 annealed contact. The other elements detected for these two samples are the same, except that we observe a shift of the Au (111) peak to a slightly higher angle (40.74˚) for the N_2-annealed sample compared to the same peak observed in the other samples (39.68˚). The difference (1.06˚) is exceptionally similar to what has been reported by Jang *et. al.* [27] (1.09˚), where he showed that the right shift for the N_2-annealed sample was due to the formation of Ni-Au solid solutions.

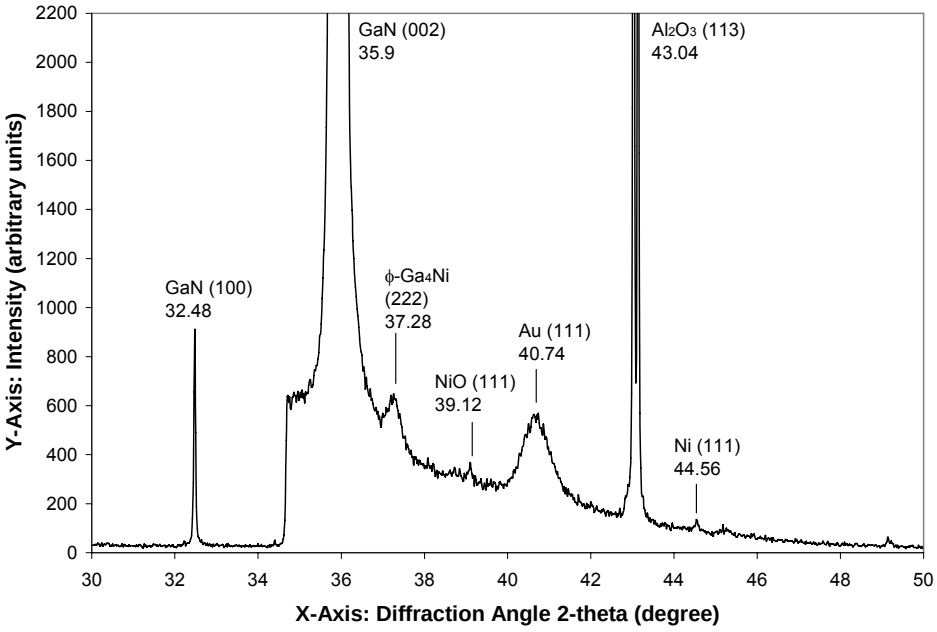

(a) 600 °C-1 min N_2-annealed Ni/Au to AQ surface-treated p-GaN.

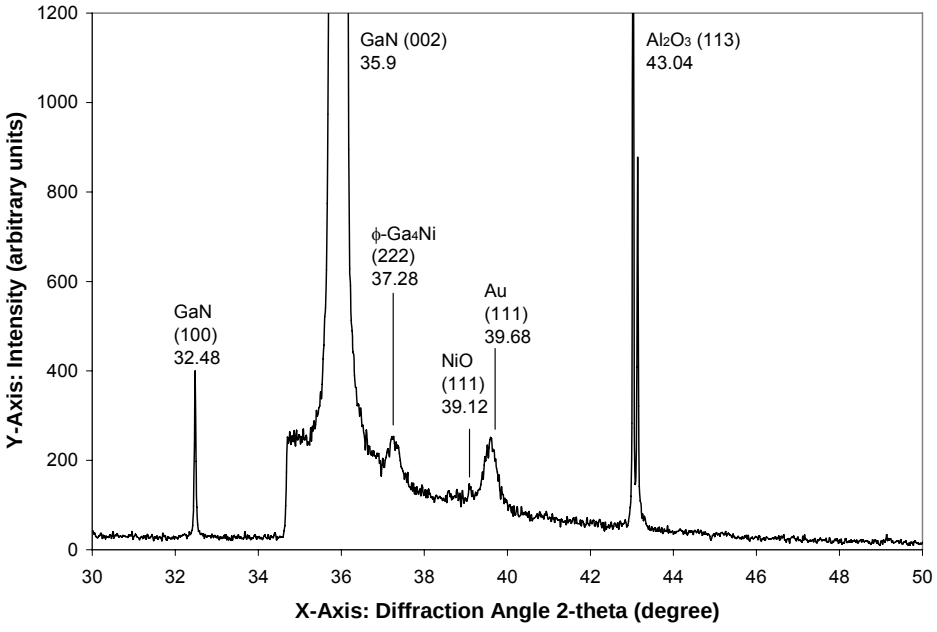

(b) 600 °C-1 min O_2-annealed Ni/Au to AQ surface-treated p-GaN.

Figure 4.8: XRD spectra of the Ni/Au contact to AQ surface-treated p-GaN for (a) N_2 annealing and (b) O_2 annealing. Both annealings were carried out at 600 °C for 1 min.

Figures 4.9 (a) to (c) show the AES depth profiles of the Ni/Au contact to AQ surface-treated p-GaN for as-deposited, N_2 annealing and O_2 annealing. The N_2 and O_2 annealing were carried out at 600 °C for 1 min – the annealing condition which resulted in the best I-V characteristics for these contacts. Comparing the depth profiles for the as-deposited and the N_2-annealed samples shown in Figures 4.9 (a) and (b), we see that a significant amount of Ni and Au inter-diffusion has taken place during N_2 annealing. We also see that a small amount of O has diffused into the surface of the system, which is consistent with the XRD results obtained earlier, which shows partial oxidation of Ni to form NiO. Nevertheless, we see that most of the Ni has not been oxidized and remains at the surface of p-GaN. Instead, we observe that the Au and Ni layers have inter-diffused into each other. This is consistent with the XRD results, which indicate the formation of Ni-Au solid solutions. Here, we see that it is likely that Ni-Au has been formed at the p-GaN surface.

From Figure 4.9 (c), it can be seen that a layer-reversal reaction has taken place during O_2 annealing. The Au peak has shifted to the interface while Ni has diffused out to the surface of the metal system. This is congruent with what has been reported in the literature, that the reversal of the Ni and Au layers take place during O_2 annealing [24], [25]. It is also observed that the O profile coincides with that of Ni,

which agrees with the XRD analysis described earlier on the complete oxidation of Ni to form NiO.

Hence, we can conclude at this point in time that one reason for the O_2-annealed Ni/Au contact giving a better I-V curve than the N_2-annealed contact, as shown in Figure 4.6, is the complete oxidation of Ni that has taken place during O_2 annealing while some crystalline Ni still remain after N_2 annealing. Another possibility is that the Ni-Au solid solution formed may not be desirable to contact formation to p-GaN, since it was formed for N_2 annealing but not O_2 annealing.

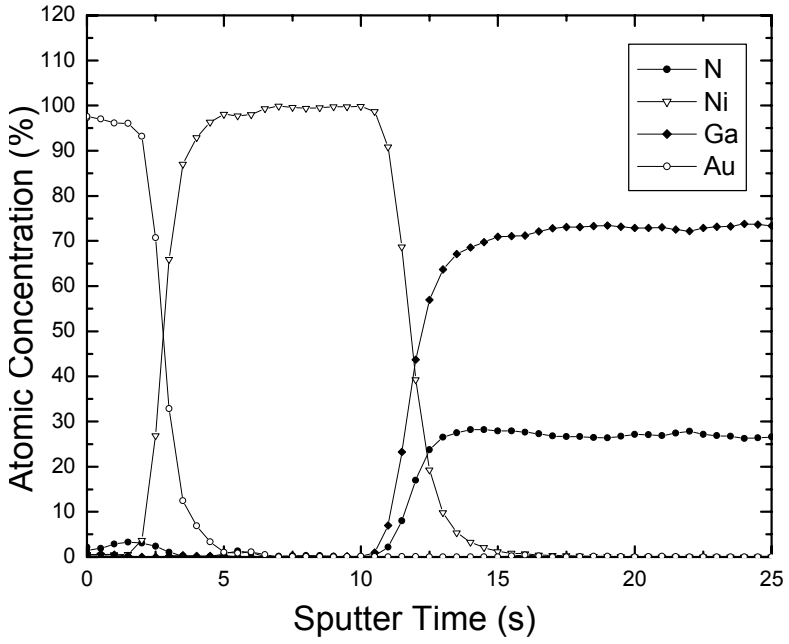

(a) As-deposited Ni/Au to AQ surface-treated p-GaN.

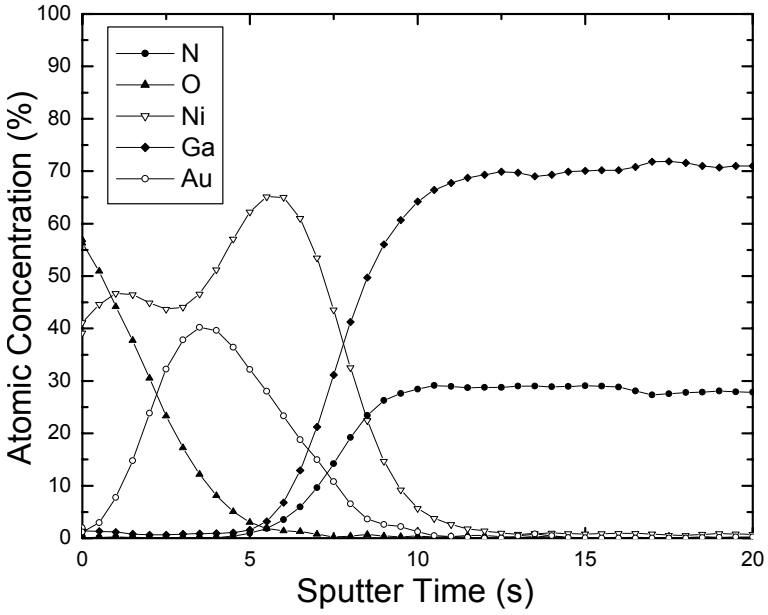

(b) 600 °C-1 min N_2-annealed Ni/Au to AQ surface-treated p-GaN.

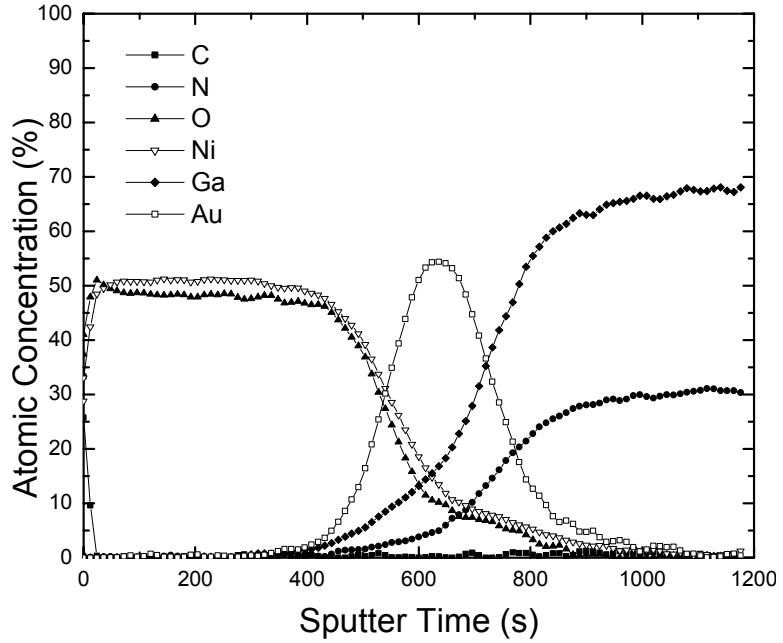

(c) 600 °C-1 min O_2-annealed Ni/Au to AQ surface-treated p-GaN.

Figure 4.9: AES depth profiles of Ni/Au contact to AQ surface-treated p-GaN for (a) As-deposited; (b) N_2 annealing and (c) O_2 annealing. Both N_2 and O_2 annealings were carried out at 600 °C for 1 min.

4.5.3 Ni/Au contact to Cl_2/N_2 plasma-treated p-GaN

In the case of the plasma-treated samples, the trend of O_2-annealed contacts yielding better electrical characteristics than the N_2-annealed contacts is not observed (see Figure 4.6, curves (c) and (d)). While both N_2 and O_2 annealings are found to improve the Cl_2/N_2 plasma-treated contacts with respect to the as-deposited contact, the improvement caused by the N_2 annealing is larger than that by the O_2 annealing. Here, we observe that the I-V characteristic obtained by the Cl_2N_2/N contact is almost identical to that obtained by the AQ/N contact. And since the as-deposited I-V characteristics for these samples are comparable, as shown in Figure 4.5, we can conclude that N_2 annealing has a similar effect on the Ni/Au contact for both the AQ and Cl_2/N_2 plasma surface-treated samples – it is not sensitive to the p-GaN surface. On the other hand, we see a distinctively large difference in the effect of O_2 annealing on these two surface-treated contacts. We shall seek to understand the reason for this.

Figure 4.10 shows the XRD spectra obtained for the O_2-annealed Ni/Au contact to Cl_2/N_2 plasma-treated p-GaN. The O_2 annealing was carried out at 600 °C for 0.5 min – the annealing condition which resulted in the best I-V characteristics for this contact. Comparing this with the XRD spectra obtained for the AQ surface-treated sample, the only observable difference is the presence of the Ni_3N (110) here which is absent in Figure 4.8 (b). The presence of Ni-N phases at the metal/semiconductor interface has been reported by Sheu *et. al.* [62] to be detrimental to p-GaN contact

formation due to their high Schottky barrier height, indicating that this is one possible cause for the much worse electrical characteristics observed for the O_2-annealed Cl_2/N_2 plasma-treated sample compared with the AQ-treated sample.

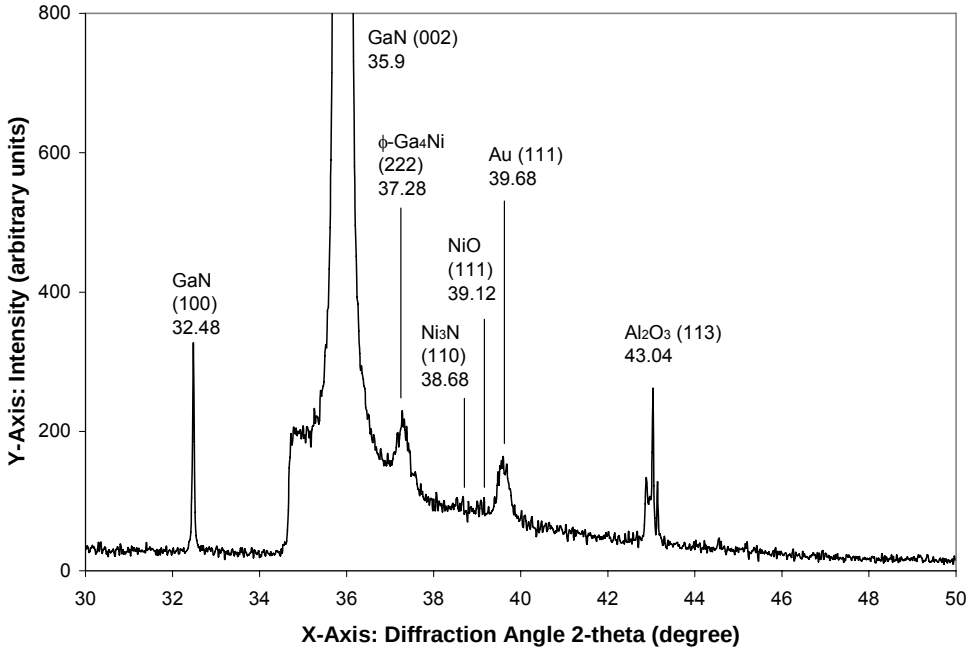

Figure 4.10: XRD spectra of O_2-annealed Ni/Au contact to Cl_2/N_2 plasma surface-treated p-GaN.

Figure 4.11 shows the AES depth profile that is obtained for the Ni/Au contact to Cl_2/N_2 plasma surface-treated p-GaN. Here, we observe the reversal of the Ni and Au layers upon O_2 annealing, which is similar to the profile obtained for the AQ-treated sample, as shown in Figure 4.9 (c). However, we also observe a slightly higher amount of inter-diffusion at the surface of p-GaN. This can be seen from the slightly

smaller peak of Au observed, indicating a higher percentage of other elements present at the surface. This slight increase in inter-diffusion of Ni, O, Ga and N indicates the possibility of interfacial compounds forming. Here, the formation of NiO appears to be complete as well, since the O profile is seen to coincide with that of Ni, similar to what was observed for the AQ treated sample. Hence, the only difference observed in the AES depth profiles of the AQ-treated sample and the Cl_2/N_2 plasma-treated sample is the increased amount of inter-diffusion at the p-GaN surface for the Cl_2/N_2 plasma-treated sample, which does not contradict the XRD results, where the Ni_3N (110) interfacial product has been found to have formed. This formation of Ni_3N upon O_2 annealing is likely the cause for the Cl_2/N_2 plasma-treated p-GaN sample not resulting in electrical characteristics that are as good as that of the AQ-treated sample.

Hence, we can conclude that the full oxidation of Ni and the occurrence of layer-reversal between the Ni and Ay layers are not sufficient in ensuring the positive effect of O_2 annealing on the Ni/Au contact. The surface treatment applied prior to metallization contributes to the products that will be formed upon O_2 annealing. In this case, the Ni_3N interfacial product was observed to have formed, resulting in worse electrical characteristics. On the other hand, such sensitivity was not observed for N_2 annealing.

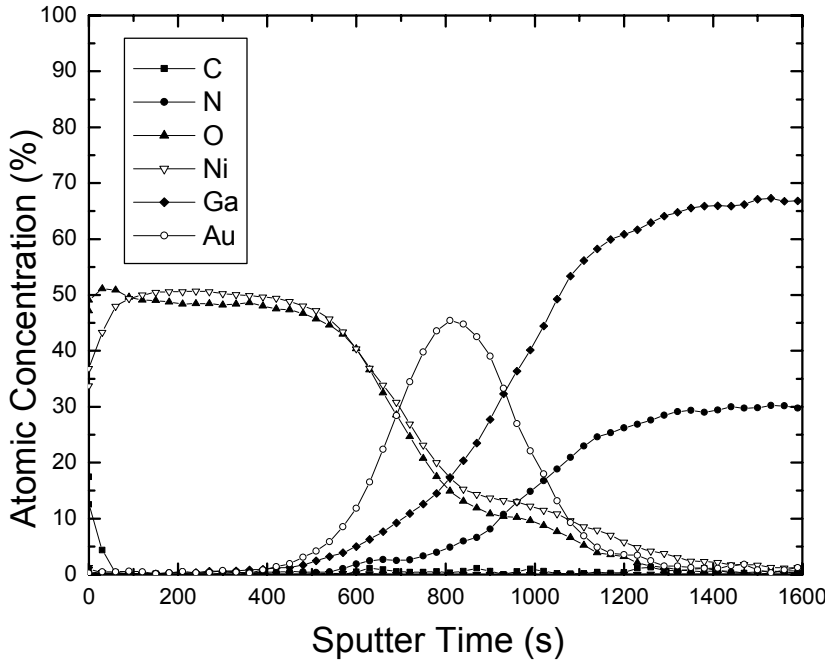

Figure 4.11: AES depth profile of O_2-annealed Ni/Au contact to Cl_2/N_2 plasma surface-treated p-GaN.

4.5.4 Ni/Au contact to O_2 plasma-treated p-GaN

For the O_2 plasma-treated contacts, we see that both N_2 and O_2 annealing yield comparable I-V characteristics, as shown by curves (e) and (f) in Figure 4.6. We also see that the O_2 plasma-treated contacts are not improved by either the N_2 or O_2 annealing, unlike the other samples surface-treated by either AQ or Cl_2/N_2 plasma. We shall now look at the XRD spectra and AES depth profiles to understand the reasons for this.

Figure 4.12 (a) and (b) show the XRD profiles of the as-deposited and O_2-annealed (600 ^oC-1 min) Ni/Au contacts to O_2 plasma surface-treated p-GaN. The XRD

profile for the O_2-annealed sample shown in Figure 4.12 (b) is observed to be similar to that obtained for the O_2-annealed Cl_2/N_2 plasma-treated sample shown in Figure 4.10. Comparing this to the spectra obtained for the as-deposited sample in Figure 4.12 (a), the appearance of the NiO peak indicates that oxidation of Ni has taken place during O_2 annealing. We also see that the undesired Ni_3N interfacial product has formed upon O_2 annealing. Similar to the Cl_2/N_2 plasma-treated sample, this is possibly the cause for O_2 annealing not resulting in better I-V characteristics for the O_2 plasma-treated contact. Nonetheless, its I-V curve is observed to be much worse than that obtained by the O_2-annealed Cl_2/N_2 plasma-treated sample even though its XRD results are similar to those of the Cl_2/N_2 plasma-treated sample.

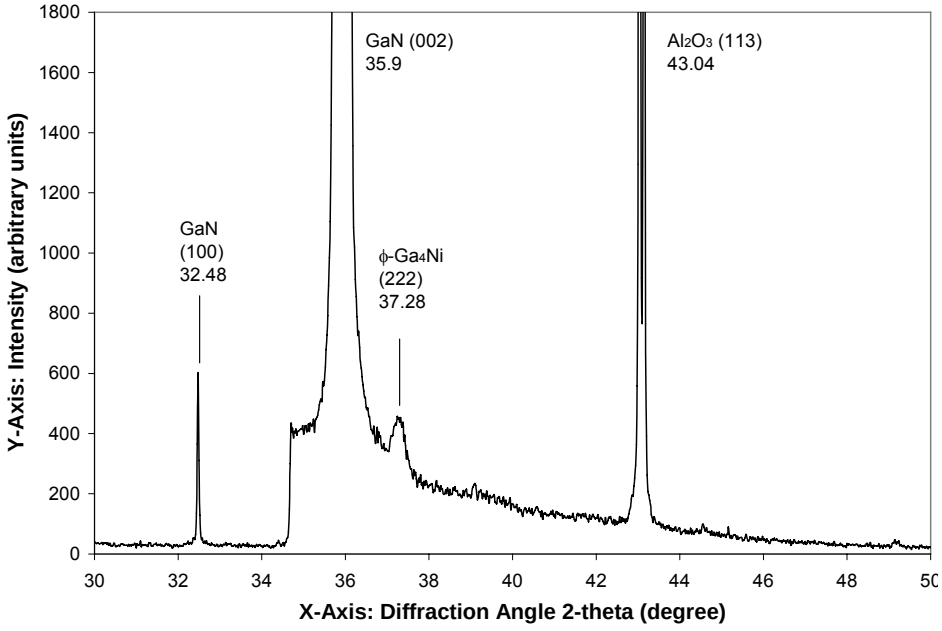

(a) As-deposited Ni/Au to O_2 plasma surface-treated p-GaN.

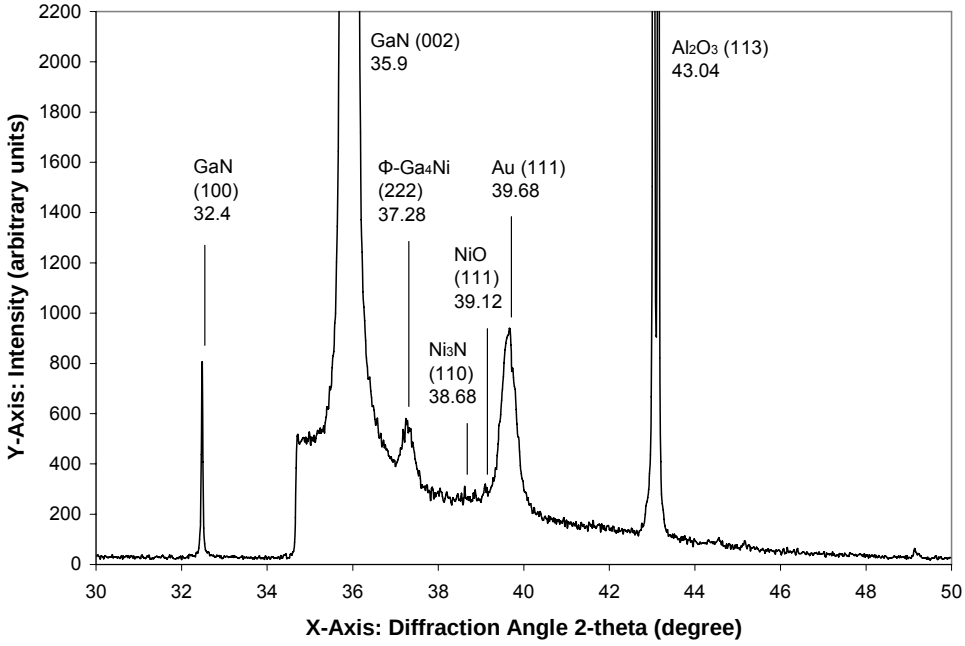

(b) 600 ^{o}C-1 min O_2-annealed Ni/Au to O_2 plasma surface-treated p-GaN.

Figure 4.12: XRD spectra of the Ni/Au contact to O_2 plasma surface-treated p-GaN for (a) as-deposited and (b) O_2 annealing (600 ^{o}C-1 min).

Figure 4.13 (a) and (b) show the AES depth profiles of the Ni/Au contact to O_2 plasma-treated p-GaN for the as-deposited state and after O_2 annealing, respectively. Comparing the profile for the as-deposited sample in Figure 4.13 (a) with that of the AQ-treated sample (see Figure 4.9 (a)), we notice the presence of O at the p-GaN surface for the O_2 plasma-treated sample but not for the AQ-treated sample. This is a strong indication of the inadequacy of the subsequent 1 min AQ in removing the oxide layer that has been formed during O_2 plasma treatment. This concurs with the

AES results (refer to Table 4.2) where the O/Ga ratio for the O_2_AQ1 sample is considerably higher than those of the Pure_AQ and Cl_2/N_2 _AQ1 samples.

Upon O_2 annealing, we observe a similar profile to those obtained by the O_2-annealed AQ and O_2 plasma-treated samples as shown in Figures 4.9 (c) and 4.11 respectively. We observe in Figure 4.13 (b) the reversal of the Ni and Au layers upon O_2 annealing as well as the complete oxidation of Ni, since the O and Ni profiles coincide in the same way as in the other 2 samples (see Figures 4.9 (c) and 4.11). This is congruent with what has been observed from the XRD spectra, where the NiO peak is observed to appear and the Ni peak disappears upon O_2 annealing. The only observable differences here is the amount of inter-diffusion that has taken place at the p-GaN surface and the slightly increased amount of C at the surface of p-GaN compared to those obtained by the AQ and Cl_2/N_2 plasma-treated samples (Figures 4.9 (c) and 4.11). Even so, the interfacial products detected by the XRD have been recognized to be the same compound, Ni_3N that has formed for the Cl_2/N_2-treated sample. Thus, the only difference between the O_2 plasma and Cl_2/N_2 plasma-treated samples causing the difference in their I-V characteristics herein lies in the surface condition of these samples, which we will discuss with reference to the AES and XPS surface analyses.

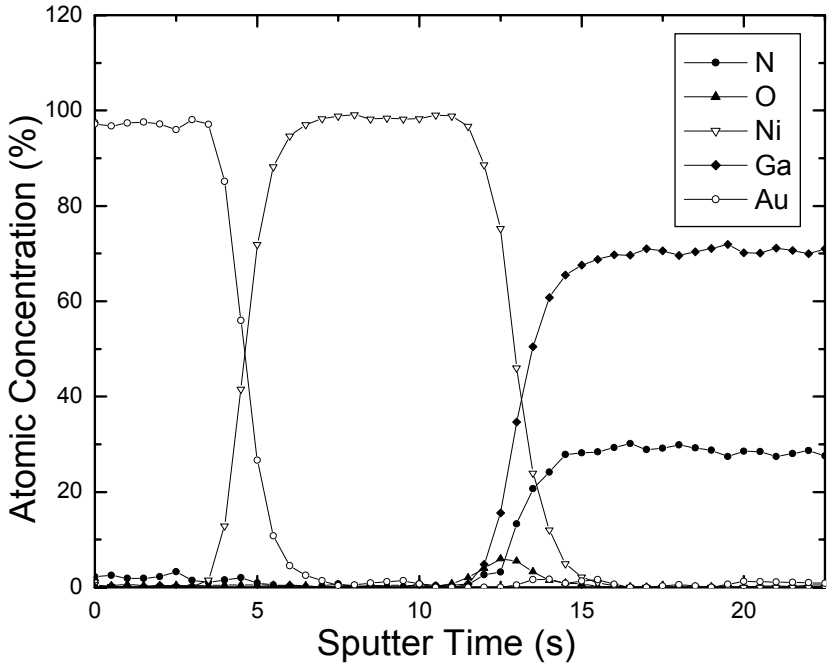

(a) As-deposited Ni/Au to O_2 plasma surface-treated p-GaN.

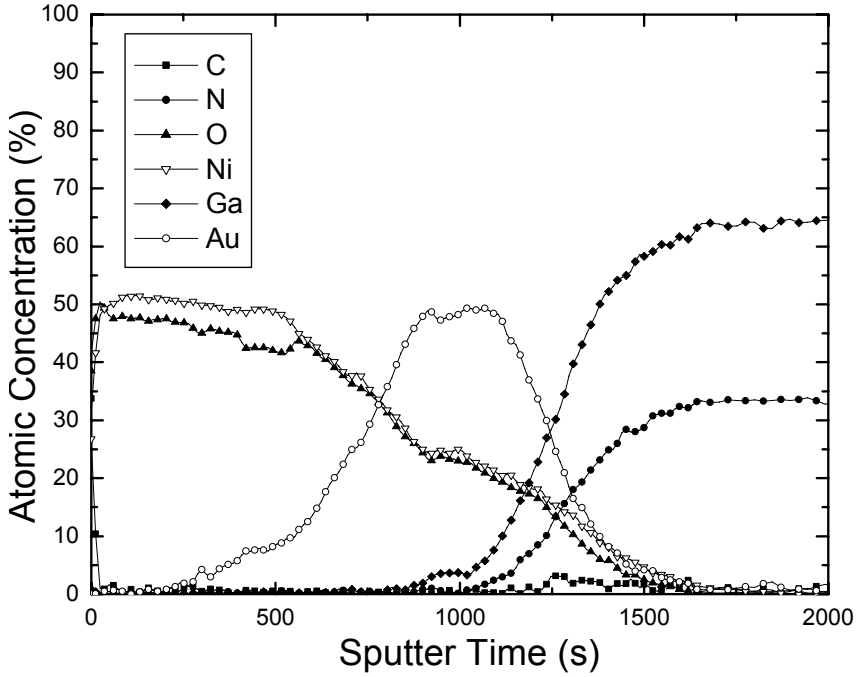

(b) 600 ^{o}C-1 min O_2-annealed Ni/Au to O_2 plasma surface-treated p-GaN.

Figure 4.13: AES depth profiles of Ni/Au contact to O_2 plasma surface-treated p-GaN for (a) As-deposited and (b) O_2 annealing (600 ^{o}C-1 min).

From Table 4.3, the most distinct dissimilarity of the O_2-AQ1 sample from the Cl_2/N_2-AQ1 sample is its high O/Ga ratio. While we have argued earlier that its high O/Ga ratio is balanced out by its low Ga/N ratio as supported by the similar I-V characteristics obtained for all three surface-treated, as-deposited samples in **Section 4.4.2**, there may be a change in the effect of the Ga/N and O/Ga ratios on the contact upon O_2 annealing. We recall that the O_2-annealed samples for all three chemical surface treatments resulted in similar I-V characteristics and this phenomenon was explained by the contribution of the surface oxides to the oxidation of Ni during O_2 annealing. In view of this, we postulate that the amount of surface oxides present for the O_2 plasma treated sample exceeds the utilizable amount for the oxidation of Ni and hence, cannot be fully depleted in a similar manner to the other O_2-annealed samples. Coupled with the formation of the undesirable Ni_3N interfacial compound, this explains the electrical characteristics of the O_2 plasma-treated sample not improving upon O_2 annealing and resulting in a much worse I-V than that of the Cl_2/N_2 plasma-treated sample.

In the attempt to reduce the surface oxides formed during O_2 plasma treatment, a subsequent 5 min AQ treatment (O_2-AQ5) was carried out. The surface was then studied via AES and the Ga/N and O/Ga ratios were extracted and presented in Table 4.3. Here, we see that even though the O/Ga ratio has decreased for the O_2-AQ5 compared to the O_2-AQ1 sample, we observe an atypical increase in the Ga/N ratio

for the O_2-AQ5 sample. Nonetheless, this increase is slight and falls well within the 20% error margin expected of the AES.

The following are postulates based on the trend of the Ga/N ratios obtained for the O_2 plasma treated samples: For the O_2-no_AQ sample, the high Ga/N ratio of 10.767 is due to the significant out-diffusion of N that had occurred during the O_2 plasma treatment. We then see a decrease in the Ga/N ratio for the O_2-AQ1 sample, which has been attributed to the stripping away of the top layer of GaO_x, thus removing a fair amount of Ga with it. (This is supported by the drastic drop observed in the O/Ga ratios). This is desirable for contact formation to p-GaN as discussed in **Section 1.2.2**.

Next, we see a decrease in the O/Ga ratio concurrently with a slight increase in the Ga/N ratio for the O_2-AQ5 sample. The XPS narrow scan will be employed to aid in understanding this peculiar phenomenon observed. From the narrow scan results, we can find out the compounds which a particular element exists in. In understanding this, we can better explain the trends of the Ga/N and O/Ga ratios observed from the AES surface analysis results. This is done by de-convoluting the narrow scan peaks into sub-peaks. These sub-peaks are then identified from a database of energy peaks as the compound in which the element exists in. The areas under these sub-peaks represent the relative percentage of the element which exists in the respective compounds. The energy peaks that were analyzed for this work include the Ga-3d

and O-1s peaks. Table 4.5 summarizes the energy peaks of these elements and their related compounds as reported in the literature [63]-[67].

Table 4.5: Energy peaks of elements and the associated compounds as reported in the literature for the Ga-3d, O-1s and the C-1s peaks. All data are obtained from reference [63] unless otherwise indicated.

Ga-3d peak		**O-1s** peak	
Elemental Compound	Associated Binding Energy (eV)	Elemental Compound	Associated Binding Energy (eV)
Ga	18.7	O	530.0 [65]
GaN	19.7	Ga_2O_3	531.1 [66]
Ga_2O_3	21.2 [64]	O-C*	532.6 [67]

** due to atmospheric contamination*

Table 4.6 summarizes the XPS results of the de-convoluted Ga-3d peaks for the O_2 plasma-treated p-GaN samples (O_2-no_AQ, O_2-AQ1 and O_2-AQ5), literature results of elemental compounds with their associated binding energies and proposed compound responsible for each energy peak.

Figure 4.14 shows the schematic of the lattice structure of Ga_2O_3, where each Ga atom (yellow) is bonded to 6 O atoms (red) and each O atom is bonded to 4 Ga atoms. Figure 4.15 shows the possible Ga bonding configurations corresponding to the various XPS energy peaks, shown along a Ga 3d energy spectrum.

Table 4.6: Summary of XPS results of the de-convoluted Ga-3d peaks for the O_2 plasma-treated p-GaN samples, literature results of elemental compounds with their associated binding energies and proposed compound responsible for each energy peak. References for literature data are indicated.

Sample	**XPS results**		**Literature results**		**Proposed elemental compound**
	De-convoluted sub-peaks (eV)	% of total Ga	Elemental Compound	Associated Binding Energy (eV)	
O_2-no_AQ	20.00	68.8	GaN	19.7	GaN
	21.14	31.20	Ga_2O_3	21.2	Ga_2O_3
O_2-AQ1	20.07	47.07	GaN	19.7	GaN
	20.41	52.93	GaN / Ga_2O_3	19.7 / 21.2	N-Ga-O_x
O_2-AQ5	20.17	44.17	GaN	19.7	GaN
	20.48	55.83	GaN / Ga_2O_3	19.7 / 21.2	N-Ga-O_x

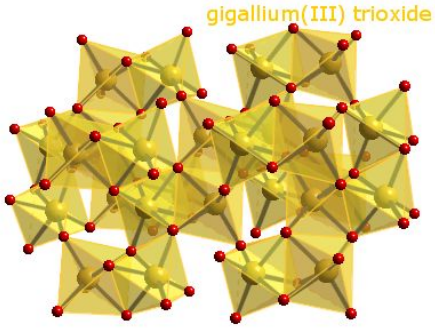

Figure 4.14: Schematic showing the Ga_2O_3 lattice structure.

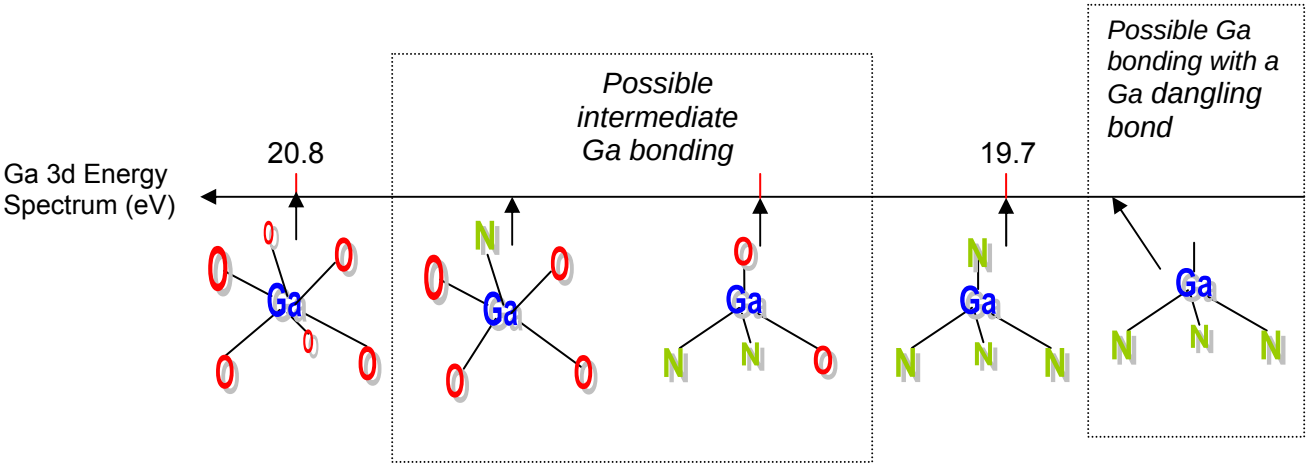

Figure 4.15: Ga bonding configurations corresponding to the various XPS energy peaks, shown along a Ga 3d energy spectrum.

Generally, high binding energies are associated with elements being bonded to another highly electronegative element; the higher the binding energy, the more electronegative is the element. In this case, illustrated in Figure 4.15, we see that the higher binding energy of 20.8 eV corresponds to Ga being bonded to O, as compared to the lower binding energy of 19.7 eV corresponding to Ga being bonded to N. N is a less electronegative element compared to O. Some other intermediate Ga bondings have been postulated in Figure 4.15, prompted by the XPS results of the de-convoluted Ga-3d peaks obtained which have shown some Ga binding energies to be between those of Ga_2O_3 and GaN. The intermediate states between Ga_2O_3 and GaN can be viewed as a transition stage between the Ga being originally bonded to N to its reacting with O on the surface to form Ga_2O_3. We will refer to this complex as N-Ga-O_x with its binding energies ranging from 19.7 to 21.2 eV.

From Table 4.6, we see that this N-Ga-O_x complex was found on the surface of the O_2-AQ1 and O_2-AQ5 samples, as opposed to Ga_2O_3 which was observed for the O_2-no_AQ sample. This suggests the formation of a bi-layer of oxide that could have occurred during O_2 plasma treatment, where the bottom layer is an intermediary compound, N-Ga-O_x and the top layer is GaO_x. The N-Ga-O_x layer is exposed upon 1 min of AQ treatment after O_2 plasma treatment. 5 min of AQ treatment further reduces the oxide, as seen from the decrease of the O/Ga ratio, but the presence of the N-Ga-O_x complex seemingly remains.

Table 4.7 summarizes the XPS results of the de-convoluted O-1s peaks for the AQ, Cl_2/N_2 plasma, Cl_2/N_2 plasma + 1min AQ, O_2 plasma, O_2 plasma + 1min AQ and O_2 plasma + 5min AQ samples, literature results of elemental compounds with their associated binding energies and proposed compound responsible for each energy peak.

Table 4.7: XPS results of the de-convoluted O-1s peaks for p-GaN samples with the following surface treatments: Aqua Regia (AQ), Cl_2/N_2 plasma, Cl_2/N_2 plasma + 1min AQ, O_2 plasma, O_2 plasma + 1min AQ and O_2 plasma + 5min AQ, literature results of elemental compounds with their associated binding energies and proposed compound responsible for each energy peak.

Sample	**XPS results**		**Literature results**		**Proposed elemental compound**
	De-convoluted sub-peaks (eV)	% of total O	Associated Binding Energy (eV)	Elemental Compound	
Pure_AQ	531.33	61.09	531.1	Ga_2O_3	Ga_2O_3
	532.60	38.91	532.6	O-C	O-C
Cl_2/N_2-no_AQ	531.73	63.97	531.1	Ga_2O_3	Ga_2O_3
	532.87	36.03	532.6	O-C	O-C
Cl_2/N_2-AQ1	531.11	32.20	531.1	Ga_2O_3	Ga_2O_3
	532.63	67.80	532.6	O-C	O-C
O_2-no_AQ	531.06	77.24	531.1	Ga_2O_3	Ga_2O_3
	532.48	22.76	532.6	O-C	O-C
O_2-AQ1	530.47	25.52	530.0 / 531.1	O / Ga_2O_3	GaO_x
	531.78	74.48	531.1 / 532.6	Ga_2O_3 / O-C	Ga-O_x-C
O_2-AQ5	530.99	31.85	530.0 / 531.1	O / Ga_2O_3	GaO_x
	532.05	68.15	531.1 / 532.6	Ga_2O_3 / O-C	Ga-O_x-C

From Table 4.7, we once again observe Ga_2O_3 at the surface of the O_2-no_AQ sample but not for the O_2-AQ1 and O_2-AQ5 samples. Instead, we observe two complexes that have formed for the O_2-AQ1 and O_2-AQ5 samples – GaO_x and Ga-O_x-C. At this point, it is noteworthy that these complexes are not observed to have

formed for any of the other samples (Pure_AQ, Cl_2/N_2-no_AQ and Cl_2/N_2-AQ1). Furthermore, this observation for the formation of Ga-O_x-C complexes concur with the AES depth profile obtained in Figure 4.13 where a higher C profile was observed at the p-GaN surface compared to the AQ and Cl_2/N_2 plasma-treated contacts. Hence, the proposed formation of the oxide bi-layer can be illustrated in a simplified schematic shown in Figure 4.16, where we see the possible two oxide layers formed. However, in practice, the two oxide layers are unlikely to be distinct and continuous. We conclude here that complexes, specifically N-Ga-O_x and Ga-O_x-C, have formed at the surface of p-GaN as a result of O_2 plasma treatment and cannot be removed by subsequent AQ treatment.

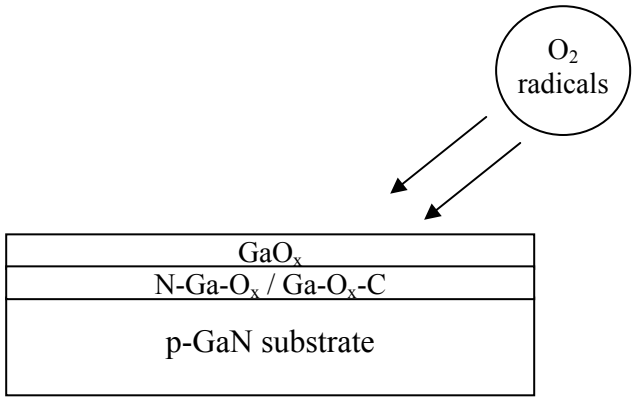

Figure 4.16 Simplified schematic showing the possible formation of a bi-layer oxide during O_2 plasma treatment.

While we observe a decrease in the O/Ga ratio for the O_2-AQ5 sample compared to the O_2-AQ1 sample, indicating the O_2-AQ5 sample may result in better electrical characteristics, we postulate that even if it improves, it will not be as good as the

AQ-treated sample. The reason for this is because of the formation of Ni_3N that is observed for both plasma-treated (Cl_2/N_2 and O_2) samples. While the application of plasma treatment and subsequent AQ may aid in improving the Ga/N and O/Ga ratio at the surface of GaN, it not necessarily guarantees a good contact, as seen from the results obtained for the Cl_2/N_2 plasma-treated sample, where the worse I-V characteristic obtained has been attributed to the formation of Ni_3N. Application of plasma treatment is thus postulated to be responsible for this, by altering the surface conditions of GaN, making it vulnerable to the formation of complexes. In this case, the complexes formed were undesirable.

4.6 SUMMARY

Firstly, we have found that the AQ, $HCl:H_2O$ and $HF:HCl:H_2O$ surface treatments do not yield significantly different I-V characteristics but AQ results in the best adhesion of contacts to GaN and was employed for this work.

Secondly, we optimized the RIE powers of the Cl_2/N_2 and O_2 plasma treatments and have found that a low RIE power of 100 W is good for both plasma treatments.

Next, we studied the effect of the AQ, Cl_2/N_2 plasma and O_2 plasma treatments on the as-deposited Ni/Au contact to p-GaN via electrical characterizations and AES surface characterizations and were found to result in similar I-V characteristics for

all, which has been attributed to the small difference observed for the Ga/N and O/Ga ratios for all the samples.

Thereafter, the effects of N_2 and O_2 annealing on the Ni/Au contact to p-GaN with the AQ, Cl_2/N_2 plasma and O_2 plasma surface treatments were studied via electrical characterizations, XRD analysis, AES depth profiling and XPS analysis.

For the AQ-treated samples, O_2 annealing gave a better I-V curve than N_2 annealing. This has been attributed to the successful formation of NiO as well as the layer-reversal that has taken place upon O_2 annealing. Ni-Au solid solutions that were formed upon N_2 annealing but not O_2 annealing are suspected to be detrimental to p-GaN and the reason for N_2 annealing resulting in worse electrical characteristics.

For the Cl_2/N_2 plasma-treated samples, the I-V characteristic of the N_2-annealed sample is similar to the AQ-treated sample. However, O_2 annealing resulted in a much worse I-V curve compared to the AQ-treated sample, which has been attributed to the formation of the Ni_3N compounds. The formation of NiO and the layer-reversal were both observed in this sample. We conclude that the effect of O_2 annealing is more sensitive to the surface conditions of p-GaN than N_2 annealing.

For the O_2 plasma-treated samples, N_2 and O_2 annealing did not improve its electrical characteristics and both gave comparable I-V curves. This has been

attributed to the formation of the N-Ga-O_x and Ga-O_x-C complexes during O_2 plasma treatment which cannot be removed by subsequent AQ.

Overall, the AQ-treated sample resulted in the best electrical characteristics. We conclude from this work that while plasma treatment and subsequent AQ improves the Ga/N and O/Ga ratio at the GaN surface, it not necessarily guarantees a good contact. Application of plasma treatment alters the surface conditions of GaN, making it vulnerable to the formation of complexes. In the case of Cl_2/N_2 and O_2 plasma treatments, the complexes formed were undesirable.

CHAPTER 5

Rh-BASED CONTACTS TO p-GaN

5.1 INTRODUCTION

In this chapter, the investigations conducted on Rhodium (Rh) based contacts to p-GaN will be reported. Firstly, the preliminary work carried out on the optimization of the annealing temperature range and of the contact thicknesses to be used will be presented.

Next, we will study the effects of N_2 and O_2 annealings on the following Rh-based contacts: Rh, Rh/Ni/Au, Rh/Au and Rh/Ni. This will be done via electrical characterizations and the I-V curves obtained will be presented. The Rh-based contact which gives the best I-V characteristics, in this case the Rh/Ni contact, will be further studied via X-ray Diffraction (XRD) and Auger Electron Spectroscopy (AES) depth profiling. Transmission Electron Microscopy (TEM) will also be employed.

Finally, in seeking to obtain a contact with better electrical characteristics than the best obtained by the Rh/Ni contact to AQ surface-treated p-GaN, two possible means will be presented. They are: using an alternative surface treatment, HCl, and inverting the metal layers by fabricating the Ni/Rh contact.

The hole concentration of p-GaN samples used in this work is 3.52×10^{17} cm^{-3}, as determined by Hall measurements. All contacts were fabricated according to the experimental procedure shown in Figure 3.2. The AQ surface treatment was employed for all samples unless otherwise stated.

5.2 PRELIMINARY STUDIES

5.2.1 Optimization of Annealing Temperature Range

Before any proper work was carried out on the Rh-based contacts, we fabricated an initial set of samples according to the experimental procedure shown in Figure 3.2 to find out the temperature range in which annealing should be carried out in the main study on the effect of annealing on these Rh-based contacts. This initial set of samples comprised Rh (40 nm), Rh/Ni (20/20 nm) and Rh/Ni/Au (20/20/20 nm).

We annealed the samples in N_2 and O_2 at 550, 600 and 650 °C for varying durations. The temperatures were chosen based on the typical annealing temperature range of 500-600 °C observed from Table 1.1 for reported contacts to p-GaN in the literature [7]-[23]. Since the O_2-annealed Ni/Au contact has been optimized in our work to be at 600 °C instead of 500 °C, as reported in the literature [8] (the annealing furnace was used in our work while the rapid thermal annealing system was used in the literature), a slightly higher temperature range was chosen here. The best I-V characteristic determined for each annealing temperature will be presented for each

contact and the respective I-V curves obtained by varying the annealing time for each annealing temperature can be found in **Appendix III**. As was defined in **Section 4.3**, "best I-V characteristic" in this work refers to the steepest and most linear I-V curve obtained by an annealed sample at a particular annealing temperature (to be specified).

(a) Rh contact

Figure 5.1 shows the best I-V characteristics of the Rh (40 nm) contact for (a) as-deposited, (b) N_2 annealing at 550 ˚C for 1 min, (c) N_2 annealing at 600 ˚C for 1 min, (d) N_2 annealing at 650 ˚C for 1 min, (e) O_2 annealing at 550 ˚C for 1 min, (f) O_2 annealing at 600 ˚C for 1 min, and (g) O_2 annealing at 650 ˚C for 1 min.

From Figure 5.1, both N_2 and O_2 annealings have shown to degrade the I-V curve of the Rh contact at all three temperatures used, indicating that the Rh contact yields the best I-V characteristics when it is as-deposited. In fact, the longer the annealing time, the worse is the I-V characteristic obtained (refer to **Appendix III-a** to **f**) and an annealing time of 1 min is seen to give the best result for every annealing temperature. For N_2 annealing, it can be seen from Figure 5.1 that all three temperatures give comparable I-V characteristics. In contrast, a lower temperature annealing is observed to result in better I-V characteristics for O_2 annealing, where the 550 ˚C annealed sample gives the best I-V curve, while the 650 ˚C annealed sample yields the worst I-V curve. Hence, it seems possible that annealing the Rh

contact in O_2 at lower temperatures may result in better I-V characteristics, which will be explored in the main study.

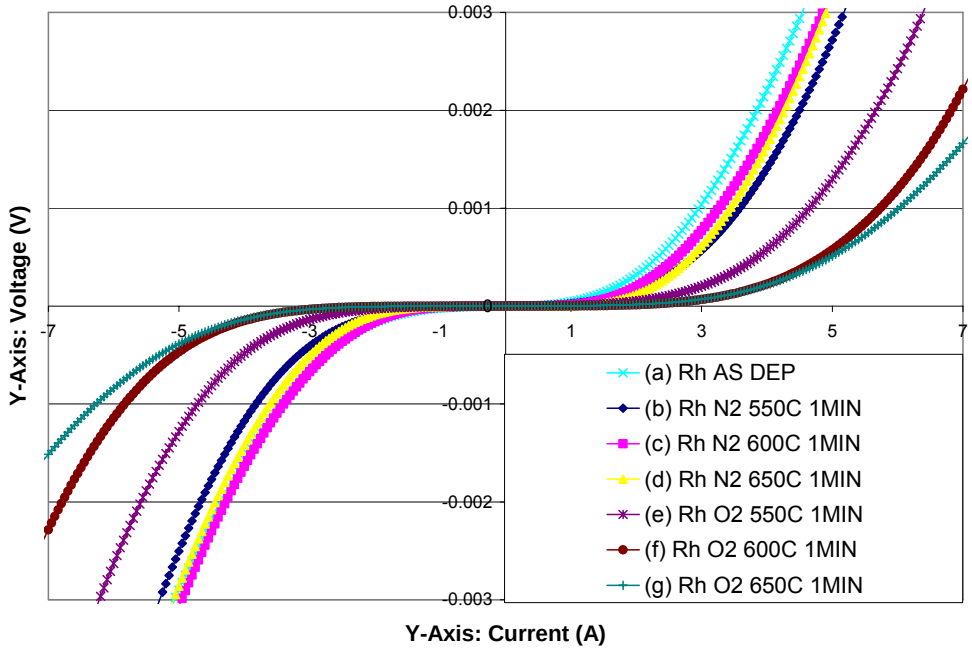

Figure 5.1 I-V characteristics of the Rh (40 nm) contact to p-GaN for: (a) as-deposited, (b) N_2 annealing at 550 ˚C for 1 min, (c) N_2 annealing at 600 ˚C for 1 min, (d) N_2 annealing at 650 ˚C for 1 min, (e) O_2 annealing at 550 ˚C for 1 min, (f) O_2 annealing at 600 ˚C for 1 min, and (g) O_2 annealing at 650 ˚C for 1 min.

(b) Rh/Ni contact

Figure 5.2 shows the best I-V characteristics of the Rh/Ni (20/20 nm) contact for (a) as-deposited, (b) N_2 annealing at 550 ˚C for 1 min, (c) N_2 annealing at 600 ˚C for 1 min, (d) N_2 annealing at 650 ˚C for 1 min, (e) O_2 annealing at 550 ˚C for 1 min, (f) O_2 annealing at 600 ˚C for 1 min, and (g) O_2 annealing at 650 ˚C for 1 min.

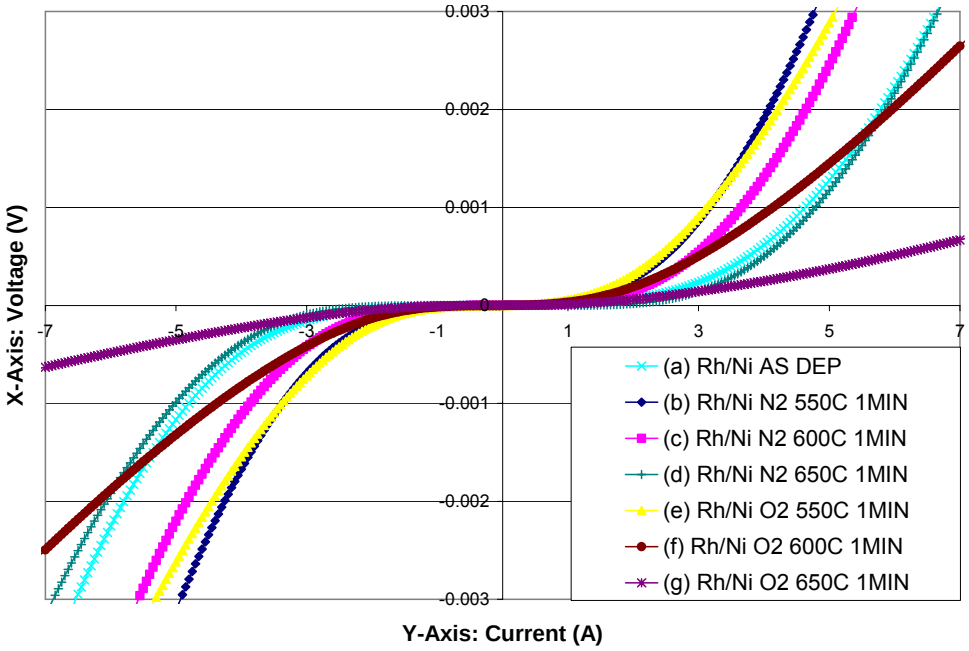

Figure 5.2 I-V characteristics of the Rh/Ni (20/20 nm) contact to p-GaN for: (a) as-deposited, (b) N_2 annealing at 550 ˚C for 1 min, (c) N_2 annealing at 600 ˚C for 1 min, (d) N_2 annealing at 650 ˚C for 1 min, (e) O_2 annealing at 550 ˚C for 1 min, (f) O_2 annealing at 600 ˚C for 1 min, and (g) O_2 annealing at 650 ˚C for 1 min.

From Figure 5.2, we see that both N_2 and O_2 annealings improve the Rh/Ni contact only for temperatures of 550 and 600 ˚C; annealing at 650 ˚C results in worse I-V characteristics. The most significant improvement is observed at 550 ˚C, where both N_2 and O_2 annealings result in similar I-V characteristics. Increasing the annealing time is not seen to improve the electrical characteristics, and the best I-V characteristics are obtained at 1 min for all temperatures for N_2 and O_2 annealings (see results presented in **Appendix III-g** to **l**). In summary, too high a temperature and too long an annealing time are seen to lead to adverse effects on the Rh/Ni contact. This gives us good reason to suspect that annealing this contact at lower

temperatures with a short annealing time can potentially result in even better I-V characteristics. This will be explored in the main study.

(c) Rh/Ni/Au contact

Figure 5.3 shows the best I-V characteristics of the Rh/Ni/Au (20/20/20 nm) contact for (a) as-deposited, (b) N_2 annealing at 550 ˚C for 1 min, (c) N_2 annealing at 600 ˚C for 1 min, (d) N_2 annealing at 650 ˚C for 1 min, (e) O_2 annealing at 550 ˚C for 1 min, (f) O_2 annealing at 600 ˚C for 1 min, and (g) O_2 annealing at 650 ˚C for 1 min.

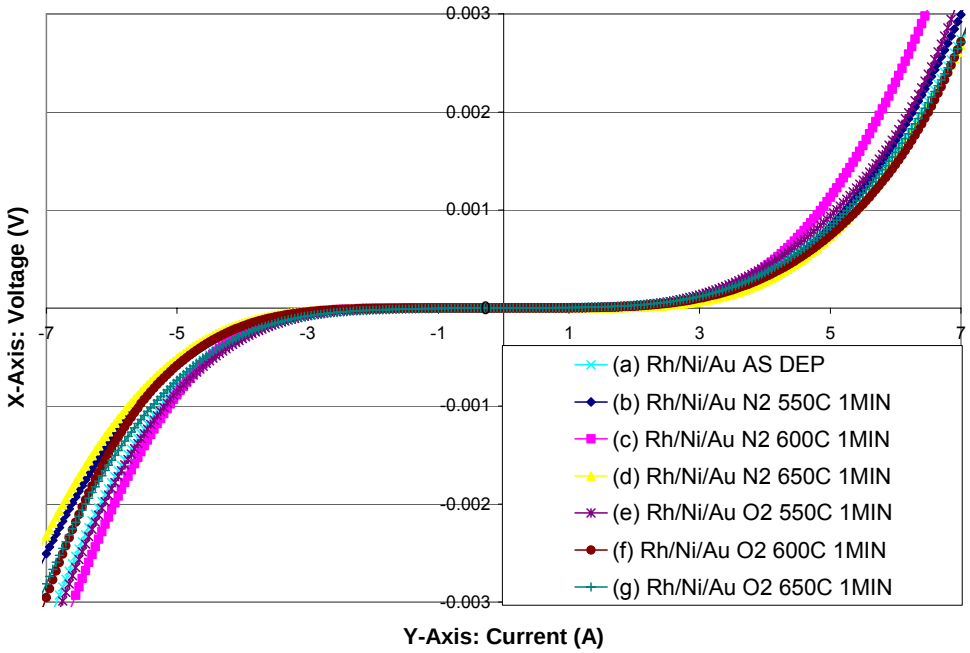

Figure 5.3 I-V characteristics of the Rh/Ni/Au (20/20/20 nm) contact to p-GaN for: (a) as-deposited, (b) N_2 annealing at 550 ˚C for 1 min, (c) N_2 annealing at 600 ˚C for 1 min, (d) N_2 annealing at 650 ˚C for 1 min, (e) O_2 annealing at 550 ˚C for 1 min, (f) O_2 annealing at 600 ˚C for 1 min, and (g) O_2 annealing at 650 ˚C for 1 min.

From Figure 5.3, we observe that both N_2 and O_2 annealings generally have insignificant effect on the Rh/Ni/Au contact. The only exception is the N_2 annealing at 600 ^oC, which results in some improvement. The effect of N_2 annealing at either 550 or 600 ˚C does not change with the annealing time (see **Appendix III-m** and **n**). Similar to the Rh/Ni contact, annealing at 650 ˚C is observed to degrade the Rh/Ni/Au contact beyond 1 minute of annealing time (see **Appendix III-o**); no change is observed for the first minute of annealing.

Just like N_2 annealing, O_2 annealing does not lead to much change in the I-V characteristics for all annealing temperatures used (see **Appendix III-p** to **r**); the I-V characteristics remain almost exactly the same as that of the as-deposited contact, indicating that the O_2 annealing has insignificant effect on the Rh/Ni/Au contact. While we cannot deduce a better annealing temperature range for the study of annealing on this contact, we can safely conclude that annealing it at lower temperatures may not be the likely solution to improving this contact. In the following sections, we will explore if thinner contact could help to improve the I-V characteristic.

5.2.2 Optimization of Contact Thicknesses

In a simple experiment to find out the effect of metal thickness on the electrical characteristics of Rh-based contacts to p-GaN, a second set of contacts were

fabricated according to the experimental procedure shown in Figure 3.2, comprising of Rh (20 nm), Rh/Ni (10/10 nm) and Rh/Ni/Au (10/10/10 nm). The I-V characteristics of these contacts will be compared to those obtained from **Section 5.2.1**, where the total thicknesses of the afore-mentioned samples are twice as thick. Figure 5.4 shows the I-V characteristics of both these sets of as-deposited contacts, namely, (a) Rh (40 nm); (b) Rh (20 nm); (c) Rh/Ni (20/20 nm); (d) Rh/Ni (10/10 nm); (e) Rh/Ni/Au (20/20/20 nm) and (f) Rh/Ni/Au (10/10/10 nm) contact to p-GaN.

From Figure 5.4, we clearly observe the trend of thinner metal layers resulting in significantly better I-V characteristics for every Rh-based contact. The degree of improvement is also observed to differ for each contact, with the Rh/Ni contact showing the most significant improvement when its thickness is halved, suggesting that the electrical characteristics of the Rh/Ni contact is highly sensitive to its metal thicknesses. It is also noteworthy that the trend of the electrical characteristics of these contacts is preserved through the change in contact thickness, with the Rh contact giving the best I-V and Rh/Ni/Au giving the worst.

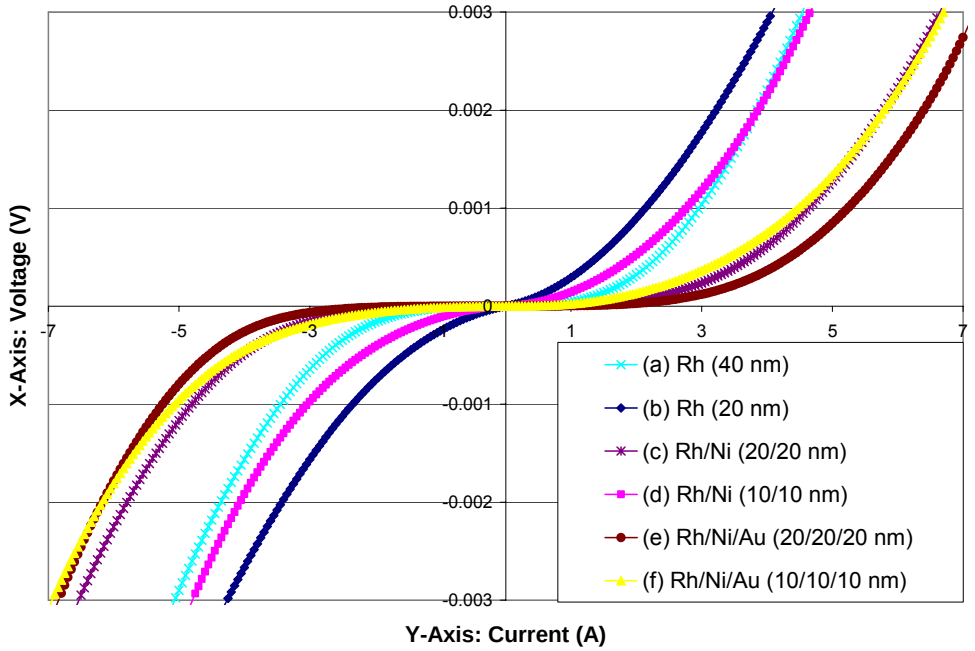

Figure 5.4: I-V characteristics of as-deposited (a) Rh (40 nm); (b) Rh (20 nm); (c) Rh/Ni (20/20 nm); (d) Rh/Ni (10/10 nm); (e) Rh/Ni/Au (20/20/20 nm) and (f) Rh/Ni/Au (10/10/10 nm) contact to p-GaN.

In summary, we conclude that thinner contact layers are beneficial for Rh-based contact formation to p-GaN and hence will be employed in the main study of this work.

5.3 EFFECT OF ANNEALING ON Rh-BASED CONTACTS TO p-GaN

In this main study on the effect of annealing on the Rh-based contacts to p-GaN, the following contacts were fabricated according to the experimental procedure shown in Figure 3.2: Rh (20 nm), Rh/Ni (10/10 nm), Rh/Au (10/10 nm) and Rh/Ni/Au (10/10/10 nm).

5.3.1 Electrical Characterizations

(a) As-deposited Contacts

Figure 5.5 shows the I-V characteristics of the as-deposited (a) Rh; (b) Rh/Ni/Au; (c) Rh/Au and (d) Rh/Ni contacts that have been fabricated. The best I-V characteristic obtained for the Ni/Au (20/20 nm) contact (O_2 annealing at 600 °C for 1 min), reported in Chapter 4, is added for comparison and is shown as curve (e) in Figure 5.5.

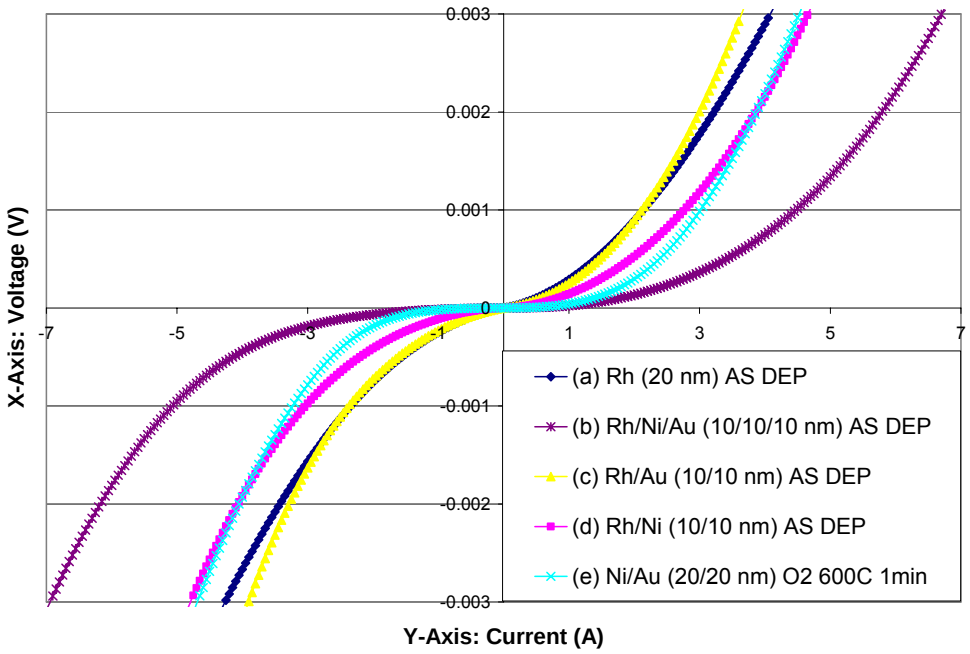

Figure 5.5: I-V characteristics of the following as-deposited contacts to p-GaN: (a) Rh; (b) Rh/Ni/Au; (c) Rh/Au and (d) Rh/Ni. The best I-V characteristic obtained for the (e) Ni/Au contact (O_2 annealing at 600 °C for 1 min) is added for comparison.

From Figure 5.5, the as-deposited Rh/Au contact is shown to give the best I-V characteristics, with the Rh contact yielding a highly comparable I-V curve at low voltage. This is in agreement with that reported in the literature [10], where the as-deposited Rh/Au contact yielded the lowest ρ_c of 9.3×10^{-6} Ω cm^2 and Rh giving a very similar ρ_c of 1.7×10^{-5} Ω cm^2. The hole concentration of p-GaN used in the literature was 4×10^{17} cm^{-3}. We also observe that the I-V characteristic of the Rh/Ni contact is not as good as the Rh and Rh/Au contacts. This is possibly for the simple reason that the electrical conductivity of Ni, 0.143×10^6 (cm-Ω)$^{-1}$ [68], is lower than those for Rh, 0.211×10^6 (cm-Ω)$^{-1}$ [69] and Au, 0.452×10^6 (cm-Ω)$^{-1}$ [70].

In Figure 5.5, we also observe that the best I-V obtained for the Ni/Au (20/20 nm) contact is comparable to that of the as-deposited Rh/Ni (10/10 nm) contact. Moreover, the as-deposited Rh (20 nm) and Rh/Au (10/10 nm) contacts give better I-V curves. This is noteworthy as these Rh-based contacts have not yet been annealed, whereas the best Ni/Au has been annealed. Hence, we will seek to find out if annealing can improve the I-V characteristics of these as-deposited Rh-based contacts and make their superior I-V characteristics ever better compared to that of the Ni/Au contact.

Several samples were prepared for each Rh-based contact to facilitate the study of the effect of annealing on its electrical characteristics. These samples were annealed in either N_2 or O_2 ambient for a range of temperatures (which will be specified) for

varying durations in order to determine the conditions for the best I-V curve that can be achieved by annealing.

(b) Rh contact

Figure 5.6 shows the I-V characteristics of the Rh contact for: (a) as-deposited; (b) N_2 annealing, 300 °C; (c) N_2 annealing, 400 °C; (d) N_2 annealing, 500 °C; (e) O_2 annealing, 300 °C; (f) O_2 annealing, 400 °C and (g) O_2 annealing, 500 °C. Note that the annealing temperatures used are lower than those used in the preliminary studies (550 ^oC and higher), where it was seen that annealing temperature lower than 550 ^oC may lead to better contact properties for Rh-based contacts.

From Figure 5.6, N_2 annealing is observed to have insignificant effect on the Rh contact at temperatures lower than 500 ˚C, regardless of annealing time (see **Appendix III-s**, **t**) and it starts to degrade slightly at 500 ˚C (see **Appendix III-u**). At no annealing temperature is the N_2 annealing observed to improve the electrical characteristics of the Rh contact. The same can be said for the O_2 annealing, where annealing at temperatures lower than 500 ˚C has insignificant effect on the electrical characteristics of the contact while annealing at 500 ˚C results in worse electrical characteristics (see **Appendix III-v** to **x**). This seems to tally well with the trend observed in the preliminary work, where the electrical characteristics of the thicker Rh contact were seen to worsen with higher temperature annealing.

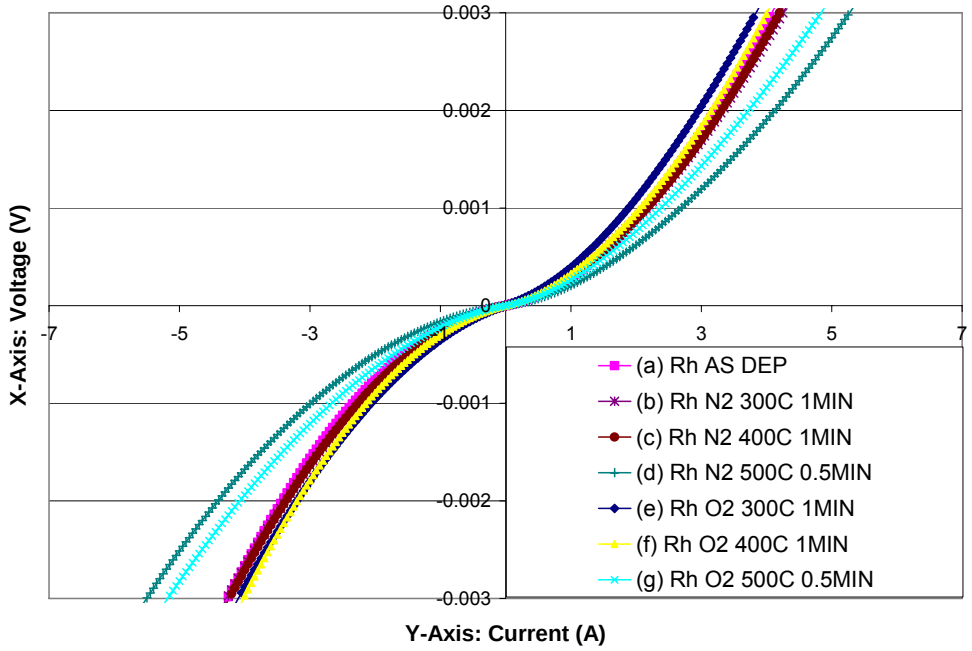

Figure 5.6 I-V characteristics of the Rh contact to p-GaN for: (a) as-deposited; (b) N_2 annealing, 300 °C; (c) N_2 annealing, 400 °C; (d) N_2 annealing, 500 °C; (e) O_2 annealing, 300 °C; (f) O_2 annealing, 400 °C and (g) O_2 annealing, 500 °C.

As reported by Song *et. al.* [10], the mechanism responsible for good contact formation of Rh to p-GaN is due to the formation of Rh-gallides at room temperature. Hence, the worsening of electrical characteristics observed for the annealed Rh contacts could hint at the possibility of the breakdown of these Rh-gallides at 500 ˚C and/or the formation of undesirable compounds between Rh and GaN at their interface.

Here, we conclude that the best electrical characteristic of the Rh contact to p-GaN occurs in its as-deposited state and cannot be improved by N_2 or O_2 annealing. N_2

and O_2 annealings are also observed to have a similar effect on the Rh contact, indicating that Rh is not reactive with O_2.

(c) Rh/Ni/Au contact

From the preliminary studies presented earlier in **Section 5.2.1**, we have seen that both N_2 and O_2 annealings generally have insignificant effect on the Rh/Ni/Au contact except for the 650 ˚C N_2 annealing, which degraded the contact. Hence, we will attempt to anneal the thinner contact in N_2 ambient at a lower temperature of 300 and 400 ˚C to see if this will have a positive effect on the contact. Figure 5.7 shows the I-V characteristics of the Rh/Ni/Au contact for: (a) as-deposited; (b) N_2 annealing, 300 °C; (c) N_2 annealing, 400 °C; (d) O_2 annealing, 400 °C; (e) O_2 annealing, 500 °C and (f) O_2 annealing, 600 °C. (We employed higher annealing temperatures for the O_2 annealing since there was no sign of significant effect - positive or negative - after O_2 annealing of the thicker contact up to 650 ˚C, as shown in Figure 5.3).

Similar to the results obtained for the Rh/Ni/Au (20/20/20 nm) contact annealed at temperatures of 550, 600 and 650 ˚C in N_2 ambient (as shown in Figure 5.3), we observe in Figure 5.7 that the Rh/Ni/Au (10/10/10 nm) contact gives worse I-V characteristic even for annealing at a lower temperature of 300 and 400 ˚C in N_2. Hence, we can conclude that this contact cannot be improved by N_2 annealing. On the other hand, the Rh/Ni/Au (10/10/10 nm) contact in this experiment shows an

improvement for all three temperatures of O_2 annealing, as shown in Figure 5.7. While all three temperatures of the O_2 annealing give better I-V characteristics compared to the as-deposited contact, the best I-V is achieved at 500 ˚C for 1 min. A higher annealing temperature of 600 ˚C gives a slightly worse contact. Thus, we can conclude that O_2 annealing can have a positive effect on the Rh/Ni/Au contact with the condition that the total thickness of metals used be reasonably thin.

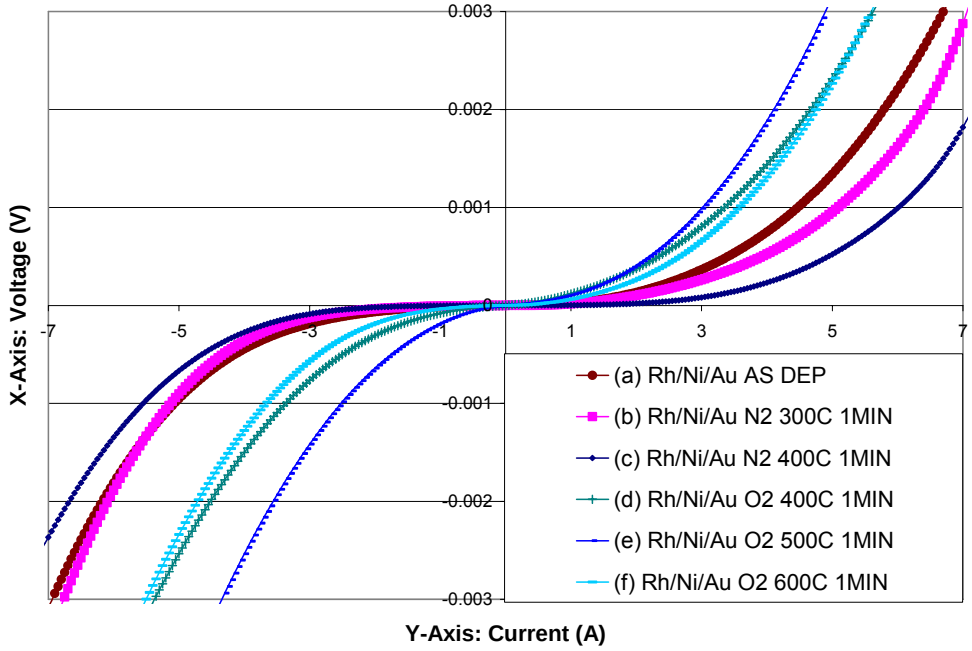

Figure 5.7 I-V characteristics of the Rh/Ni/Au contact to p-GaN for: (a) as-deposited; (b) N_2 annealing, 300 °C; (c) N_2 annealing, 400 °C; (d) O_2 annealing, 400 °C; (e) O_2 annealing, 500 °C and (f) O_2 annealing, 600 °C.

(d) Rh/Au contact

Figure 5.8 shows the I-V characteristics of the Rh/Au contact for: (a) as-deposited; (b) N_2 annealing, 300 °C; (c) N_2 annealing, 400 °C; (d) N_2 annealing, 500 °C; (e) O_2 annealing, 300 °C; (f) O_2 annealing, 400 °C and (g) O_2 annealing, 500 °C.

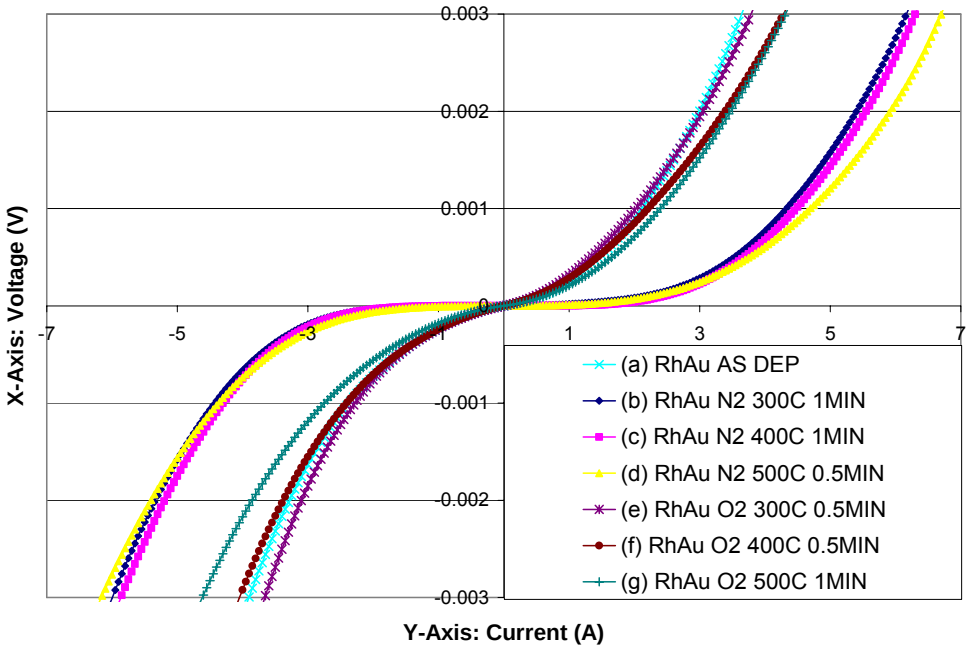

Figure 5.8 I-V characteristics of the Rh/Au contact to p-GaN for: (a) as-deposited; (b) N_2 annealing, 300 °C; (c) N_2 annealing, 400 °C; (d) N_2 annealing, 500 °C; (e) O_2 annealing, 300 °C; (f) O_2 annealing, 400 °C and (g) O_2 annealing, 500 °C.

From Figure 5.8, we observe a similar trend to that of the Rh contact, where neither N_2 nor O_2 annealing is found to improve the electrical characteristics of the Rh/Au contact. While O_2 annealing results in a slight worsening of the I-V characteristic –

arguably insignificant, N_2 annealing is observed to degrade the contact considerably – the higher the annealing temperature, the worse its electrical characteristics. The as-deposited Rh/Au contact remains the state that gives the best electrical characteristics to p-GaN. Thus, as the Rh/Au as-deposited contact has been observed to give the best I-V characteristic (see Figure 5.5) and that it cannot be improved by N_2 or O_2 annealing, it will not be pursued further.

(e) Rh/Ni contact

Figure 5.9 shows the I-V characteristics of the Rh/Ni contact for: (a) as-deposited; (b) N_2 annealing, 300 °C; (c) N_2 annealing, 400 °C; (d) N_2 annealing, 500 °C; (e) O_2 annealing, 300 °C / 350 °C; (f) O_2 annealing, 380 °C; (g) O_2 annealing, 400 °C; (h) O_2 annealing, 450 °C and (i) O_2 annealing, 500 °C.

From Figure 5.9, N_2 annealing is seen to improve the I-V characteristics of the Rh/Ni contact slightly for all three temperatures of 300, 400 and 500 ˚C, with the 300 and 400 ˚C annealings giving similar characteristics and the 500 ˚C giving slightly worse characteristics. In the preliminary work, N_2 annealing was shown to improve the Rh/Ni contact for annealing temperatures of 550 and 600 ˚C, beyond which the electrical characteristics was observed to worsen. The collective results suggest that N_2 annealing improves the electrical characteristics of the Rh/Ni contact at annealing temperatures lower than 650 ˚C, with the lowest temperature resulting in the best electrical contact.

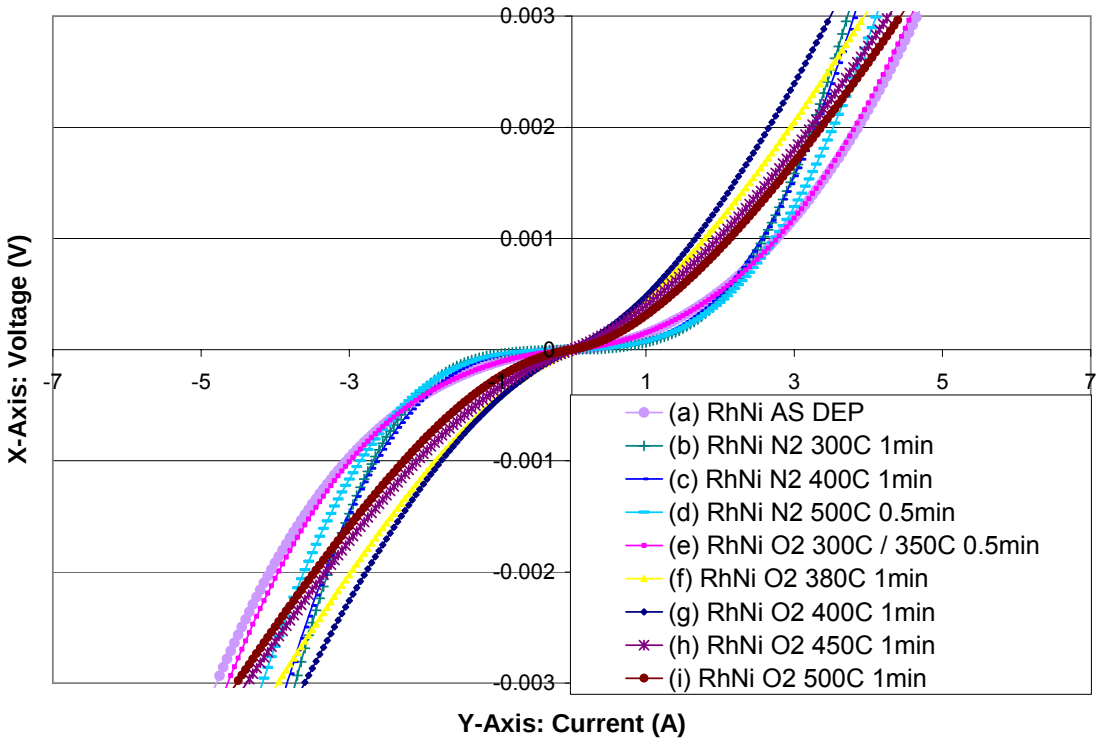

Figure 5.9 I-V characteristics of the Rh/Ni contact to p-GaN for: (a) as-deposited; (b) N_2 annealing, 300 °C; (c) N_2 annealing, 400 °C; (d) N_2 annealing, 500 °C; (e) O_2 annealing, 300 °C / 350 °C; (f) O_2 annealing, 380 °C; (g) O_2 annealing, 400 °C; (h) O_2 annealing, 450 °C and (i) O_2 annealing, 500 °C.

Similar to N_2 annealing, O_2 annealing is also seen to improve the Rh/Ni contact. However, O_2 annealing requires a minimum temperature of 380 ˚C for a positive effect to be observed on the Rh/Ni contact, as seen in Figure 5.9. Additional annealing is carried out at temperatures of 350, 380 and 450 ˚C for this sample as the I-V curve shows potential to become linear. The 300 and 350 ˚C annealings result in the same I-V curve, having no effect on the as-deposited Rh/Ni contact. The most

significant improvement in the I-V characteristic is observed at 400 ˚C for 1 minute where an almost-linear I-V characteristic is exhibited. Beyond this temperature, the improvement in the I-V becomes less significant. Increased annealing time also cannot improve the 400 ˚C-annealed Rh/Ni contact.

We shall now compare the best I-V characteristics obtained for N_2 and O_2 annealings of all the Rh-based contacts that have been fabricated to identify the contact which has been improved by the furthest extent by annealing.

(f) Best I-V characteristics of Rh-based contacts

Figure 5.10 shows the as-deposited I-V characteristics and the best annealed I-V characteristics that were achieved for each Rh-based contact, namely: I-V characteristics of the following contacts: (a) Rh, as-deposited / N_2 annealed / O_2-annealed; (b) Rh/Ni/Au, as-deposited; (c) Rh/Ni/Au, O_2-annealed; (d) Rh/Au, as-deposited / O_2-annealed; (e) Rh/Ni, as-deposited; (f) Rh/Ni, O_2-annealed and (g) Ni/Au, O_2-annealed. The Rh as-deposited, N_2-annealed and O_2-annealed contacts are combined (as they are similar) and shown as curve (a) in Figure 5.10 for the purpose of clarity in the presentation of these curves in a single graph. Similarly, the Rh/Au as-deposited and O_2-annealed contacts are combined and shown as curve (d) in Figure 5.10. The best I-V characteristic obtained for the Ni/Au contact in the previous chapter was included for comparison and is shown as curve (g) in Figure 5.10.

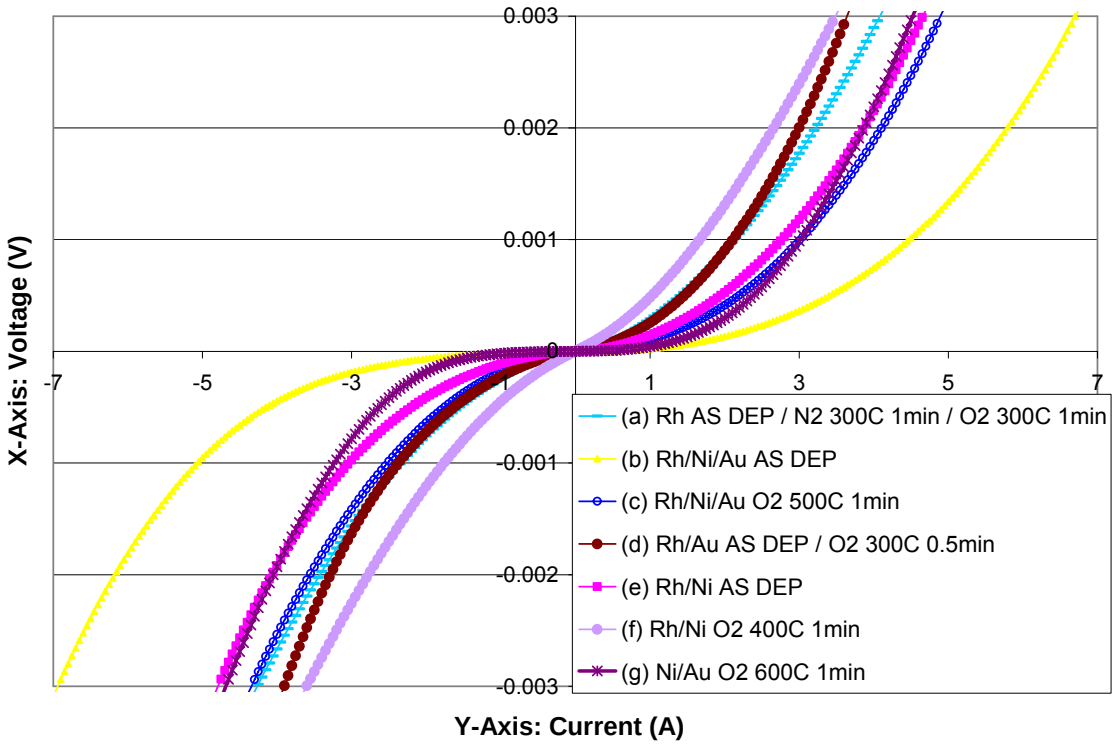

Figure 5.10 I-V characteristics of the following contacts: (a) Rh, as-deposited / N_2 annealed / O_2-annealed; (b) Rh/Ni/Au, as-deposited; (c) Rh/Ni/Au, O_2-annealed; (d) Rh/Au, as-deposited / O_2-annealed; (e) Rh/Ni, as-deposited; (f) Rh/Ni, O_2-annealed and (g) Ni/Au, O_2-annealed.

From Figure 5.10, the I-V characteristic of the Rh/Ni upon O_2 annealing is observed to be better than that of the as-deposited Rh/Au contact, as shown by curves (d) and (f), indicating that O_2 annealing has successfully improved the previously best I-V curve obtained by the Rh-based contacts. The Rh/Ni/Au contact has also seen an improvement in its I-V characteristics by O_2-annealing. However, it is far short of that of the Rh/Ni contact and hence will not be pursued further.

From the I-V characteristics obtained for all the N_2- and O_2-annealed Rh-based contacts that have been fabricated for this work, we observe that the Rh/Ni is the only contact which is improved by both N_2 and O_2 annealings. It is also apparent from Figure 5.10 that the Rh/Ni contact annealed in O_2 has resulted in the overall best I-V characteristic. It is noteworthy that this I-V curve obtained is significantly better than the best I-V curve obtained by the Ni/Au contact (see Figure 5.10, curves (f) and (g)). Since the difference in hole concentrations of the p-GaN samples used for the fabrication of these two contacts is negligibly small (3.38×10^{17} cm^{-3} for the Ni/Au contact and 3.52×10^{17} cm^{-3} for the Rh/Ni contact), we can safely conclude, based on the electrical characteristics, that the O_2-annealed Rh/Ni contact is better than the O_2-annealed Ni/Au contact. We shall now seek to study the effect of annealing (O_2 annealing in particular) on the Rh/Ni contact by using other measurement techniques.

5.3.2 XRD AND AES CHARACTERIZATIONS OF Rh/Ni CONTACT

X-ray Diffraction (XRD) and Auger Electron Spectroscopy (AES) analyses were carried out for the as-deposited, N_2-annealed and O_2-annealed Rh/Ni (10/10 nm) samples. The N_2 and O_2 annealings were carried out at 400 ˚C for 1 min, which was shown in **Section 5.3.1** to give the best electrical characteristics for their respective annealing ambients. The XRD spectra and AES depth profiles obtained by these samples are shown in Figure 5.11 (a) to (c) and Figure 5.12 (a) to (c), respectively.

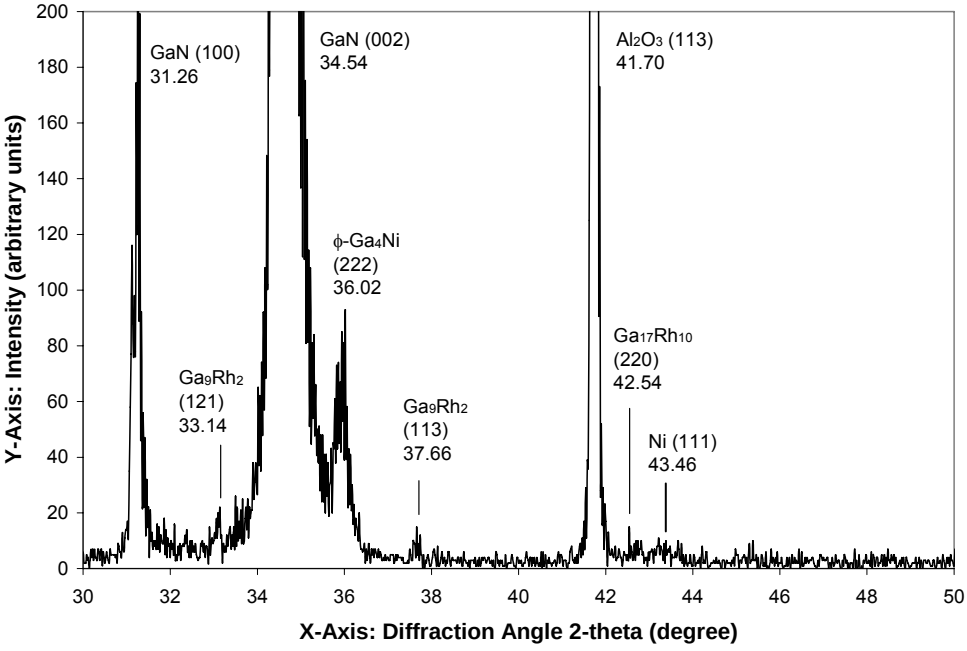

(a) As-deposited Rh/Ni to p-GaN

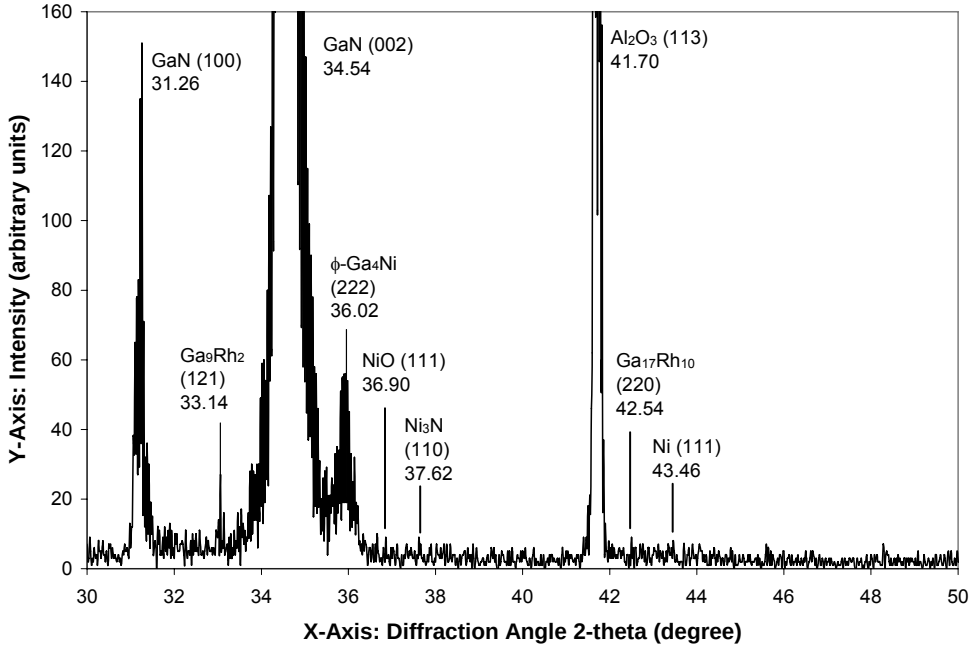

(b) 400 ^{o}C-1 min N_2-annealed Rh/Ni to p-GaN

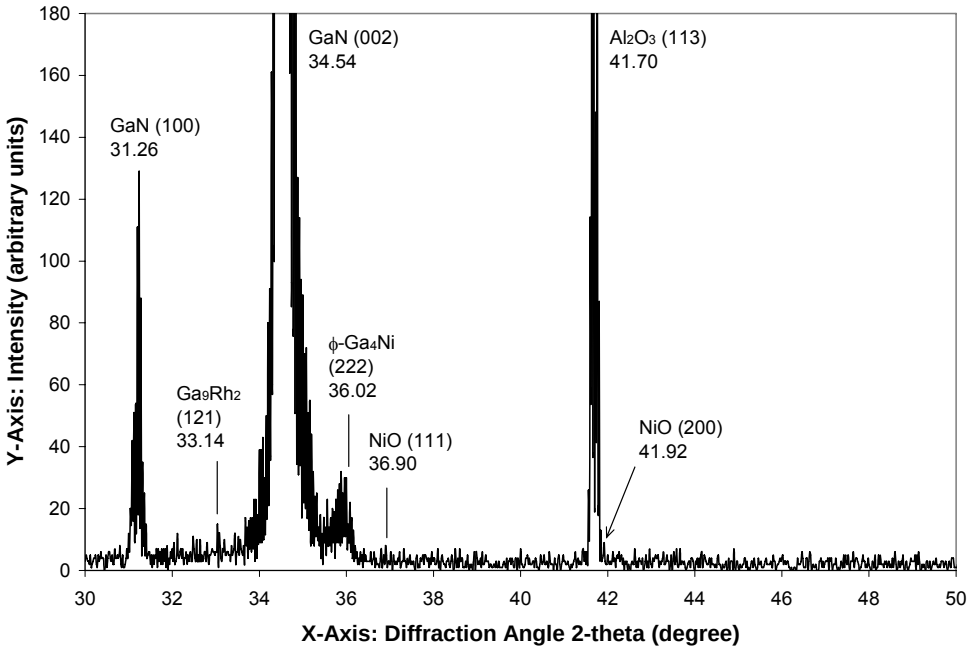

(c) 400 ^{o}C-1 min O_2-annealed Rh/Ni to p-GaN

Figure 5.11 XRD spectra of the Rh/Ni (10 nm/10 nm) contact to p-GaN for (a) as-deposited; (b) 400 ^{o}C-1 min N_2 annealing and (c) 400 ^{o}C-1 min O_2 annealing.

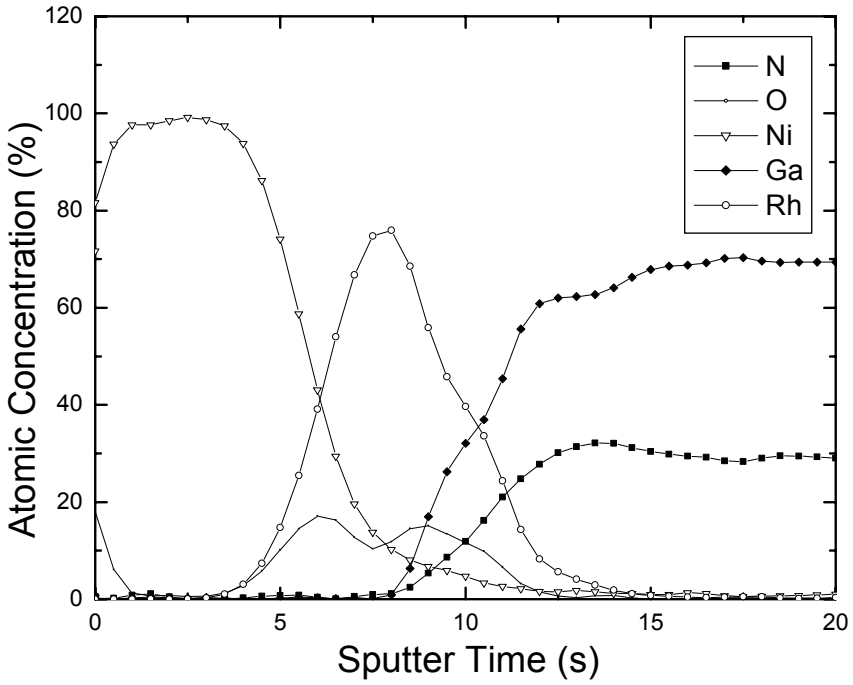

(a) As-deposited Rh/Ni to p-GaN

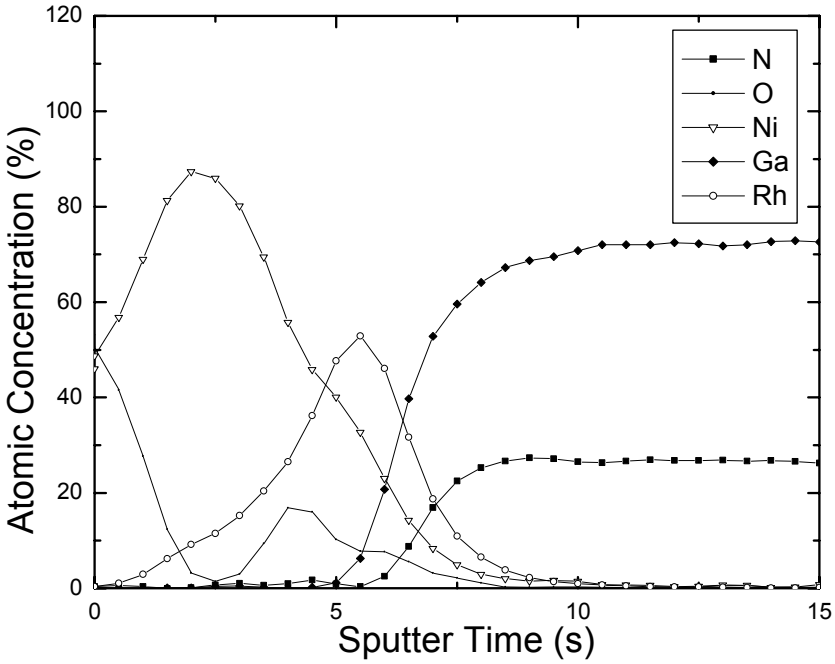

(b) 400 ^{o}C-1 min N_2-annealed Rh/Ni to p-GaN

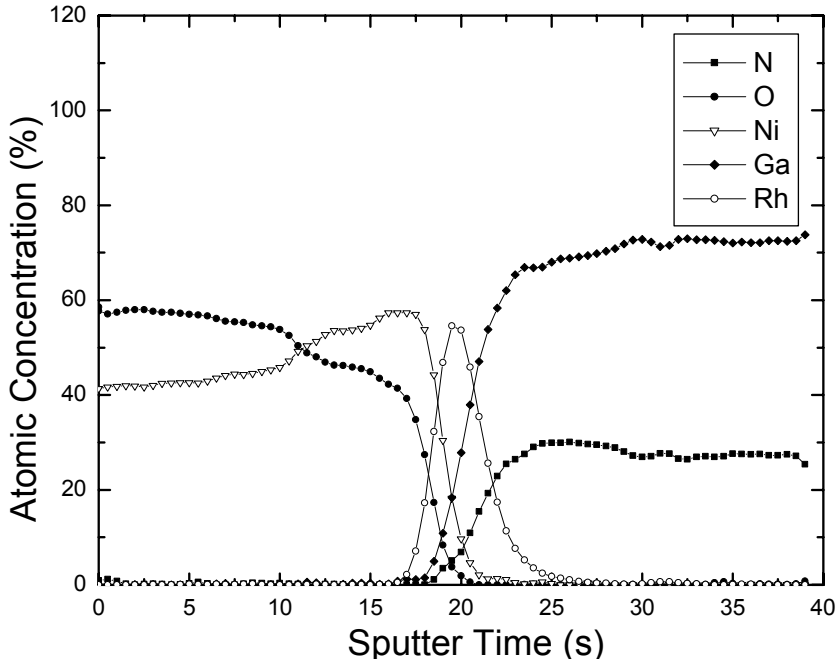

(c) 400 ^{o}C-1 min O_2-annealed Rh/Ni to p-GaN

Figure 5.12 AES depth profiles of the Rh/Ni (10 nm/10 nm) contact to p-GaN for (a) as-deposited; (b) 400 ^{o}C-1 min N_2 annealing and (c) 400 ^{o}C-1 min O_2 annealing.

From Figure 5.11 (a), we confirm the formation of Rh-gallides in the as-deposited state of Rh/Ni, as reported by Song *et. al.* [10]. Here, the gallides observed to have formed are Ga_9Rh_2 (121), Ga_9Rh_2 (113) and $Ga_{17}Rh_{10}$ (220). These gallides are reportedly beneficial for ohmic contact formation to p-GaN as they cause Ga vacancies (V_{Ga}'s) to form at the surface, which subsequently result in an increase in the effective hole concentration at the p-GaN surface, as explained in **Section 2.2.3**. This also concurs with the AES depth profile obtained for this sample, as shown in Figure 5.12 (a), where we observe some overlapping of the Rh and Ga profiles,

indicating the possibility of the formation of these Rh-gallides at the surface of p-GaN.

Upon N_2 annealing, one of the Rh-gallides peaks, Ga_9Rh_2 (113), which was present in the as-deposited sample, is not observed in Figure 5.11 (b). In addition, we observe the presence of Ni_3N (110) upon N_2 annealing in Figure 5.11 (b). As discussed in **Section 4.5.3**, this Ni-N phase is reportedly undesirable to p-GaN contact formation [60]. This agrees with the AES depth profile obtained for this sample shown in Figure 5.12 (b), where more Ni is observed to have in-diffused to the p-GaN surface compared to the as-deposited sample (see Figure 5.12 (a)), hinting at the possibility of the formation of Ni-N compounds.

Hence, at this point in time, the worsening of the N_2-annealed Rh/Ni contact at low voltages (as shown in Figure 5.9, curves (a) to (d) could either be due to the absence of Ga_9Rh_2 (113) or the formation of the undesirable Ni_3N compound, or both. Here, we seek to understand the implications of each possibility and decide if it is one or both of these reasons which the worsening of the contact for N_2 annealing is attributed to. We recall from **Section 5.3.1 (b)** that N_2 annealing at 400 ˚C for 1 min has no effect on the Rh as-deposited contact. It is reasonable to assume that Ga_9Rh_2 (113) would also disappear in a Rh contact upon N_2 annealing at 400 ˚C for 1 min, just like the Rh/Ni contact. Hence, we could conclude that the absence of Ga_9Rh_2 (113) is probably not the main reason for the worsening of the I-V characteristic

observed for the N_2-annealed Rh/Ni contact. Moreover, the slight worsening is observed at low voltages (less than 3 V). Due to the understanding that conductivity at low voltages is affected by the interface conditions of the metal and semiconductor, the in-diffusion of Ni to the surface of p-GaN resulting in the formation of the undesirable Ni_3N compounds may be a more likely reason for the slight worsening of the N_2-annealed Rh/Ni sample observed.

Some oxidation of Ni might also have taken place during N_2 annealing due to the possible introduction of some O_2 into the annealing furnace, as was the case for the Ni/Au contact. However, the extent of this oxidation is small for the N_2-annealed contact, as compared to that observed for the O_2-annealed sample, as can be seen from Figures 5.12 (b) and (c). Moreover, Ni is seen to be present in the N_2-annealed but not O_2-annealed samples, as shown in Figures 5.11 (b) and (c), indicating that Ni was not completely oxidized during N_2 annealing as opposed to O_2 annealing. Recalling that the N_2-annealed Rh/Ni contact does not result in better I-V characteristic than the O_2-annealed Rh/Ni contact, this result agrees with the study on the Ni/Au contacts, where the complete oxidation of Ni is seen to be required for the formation of NiO to have a positive effect on the contact electrical characteristics.

For the O_2-annealed Rh/Ni contact, we observe the disappearance of the Ga_9Rh_2 (113) and $Ga_{17}Rh_{10}$ (220) peaks. Similarly, we assert that this does not have a significant effect on the electrical characteristics of the contact as the O_2-annealed

Rh contact (400 ˚C for 1 min) is observed to be no different from that of the as-deposited Rh contact (see Figure 5.6). Nonetheless, we observed that the Ga_9Rh_2 (121) peak remains in all three samples in Figures 5.11 (a) to (c), indicating that at least one form of crystalline Rh-gallides is present in all these samples. This is important to note since this study on Rh-based contacts is based on the formation of Rh-gallides upon deposition to p-GaN and its positive effect on the electrical characteristics of these contacts.

From Figure 5.11 (c), we also note the formation of NiO. Unlike the case for the O_2-annealed Ni/Au contacts where only NiO (111) was detected (see Figures 4.8 (b), 4.10 and 4.12 (b)), we identify both NiO (111) and NiO (200) here, indicating the formation of polycrystalline NiO.

From Figure 5.12 (c), we see a very different profile for the O_2-annealed Rh/Ni contact. Here, Ni is clearly seen to have reacted with O to form NiO_x, from the large amount of in-diffusion of O into the Ni layer. The O profile is also observed to tail off when Ni tails off, in the Rh layer, indicating that Rh does not react with O. This also confirms what was discussed earlier in **Section 5.3.1 (b)**, where Rh was seen not to be reactive to O_2 as the N_2 and O_2 annealings were seen to have similar effects on the Rh contact.

From Figure 5.12 (c), we also observe a large amount of inter-diffusion that has taken place, particularly at the p-GaN surface, which we will seek to better understand from the TEM images that will be presented in the section that follows.

5.3.3 TEM IMAGES OF O_2-ANNEALED Rh/Ni CONTACT

Figure 5.13 shows the Transmission Electron Microscopy (TEM) images obtained for the cross-section of Rh/Ni contact to p-GaN O_2-annealed at 400 ˚C for 1 minute. Four layers have been identified, labeled A - D. The thickness of each layer is shown on the image.

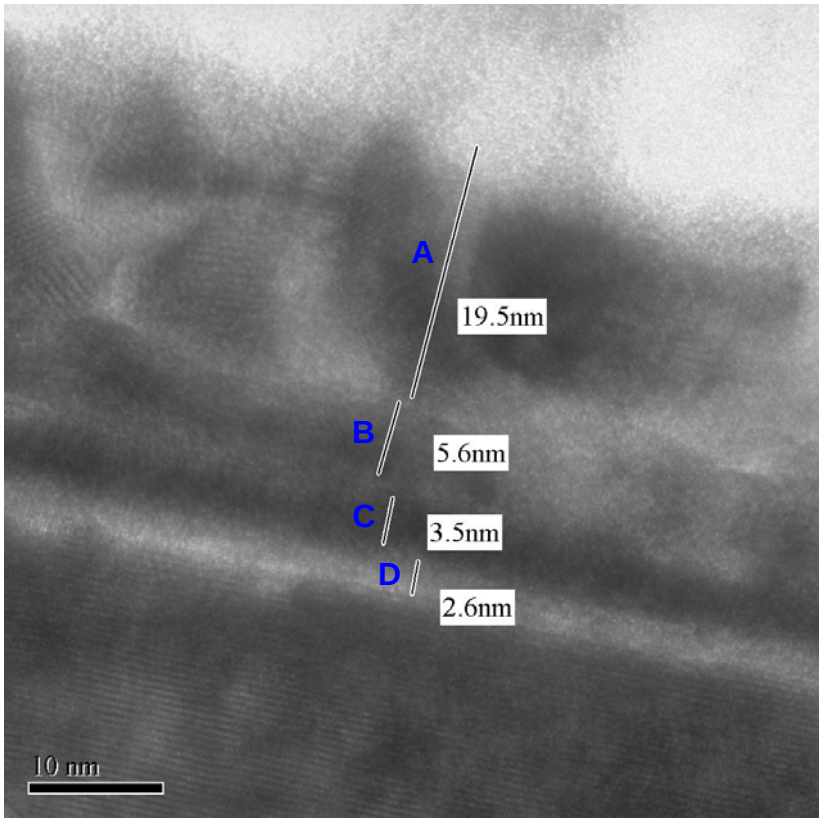

Figure 5.13: TEM image of the Rh/Ni (10 nm/10 nm) contact O_2-annealed at 400 ˚C for 1 minute.

Figure 5.14 shows another TEM image of the same O_2-annealed Rh/Ni contact at a lower magnification so that we can observe the continuity of each layer and any inter-diffusion between the layers. Energy Dispersive X-ray (EDX) analysis results obtained for each region is summarized in Table 5.1. The details of these results as well as a brief explanation of the EDX method can be found in **Appendix IV**. For the purpose of this study, it suffices to focus on the qualitative aspect of analyzing the EDX results obtained. The results agree with the AES depth profile in Figure 5.12 (c) where other than the top-most NiO layer, the GaN surface was observed to consist of all the elements listed: Ni, O, Rh, Ga and N. The percentages of these elements are not included in the Table because they vary with location within each layer. Hence, we will seek to understand these results qualitatively.

From the TEM image shown in Figure 5.13, the top-most layer, Region 'A', is identified to be polycrystalline from the numerous crystal grains observed. This concurs with the XRD results for this sample where NiO with two crystalline orientations, NiO (111) and NiO (200), have been identified (see Figure 5.11 (c)). The EDX results obtained in Table 5.1 also show the layer to consist only of Ni and O.

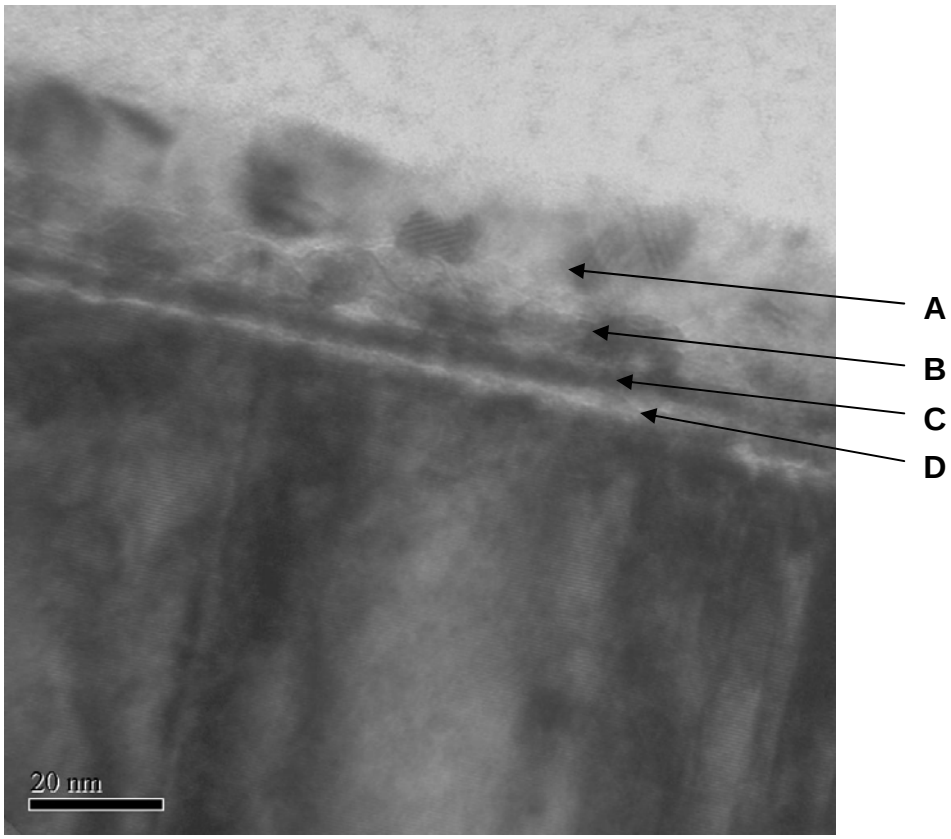

Figure 5.14: Lower magnification TEM image of the Rh/Ni contact O_2-annealed at 400 ˚C for 1 minute.

Table 5.1 Summary of the EDX results obtained for the identification of the elements present in each of the regions, A-C, as identified in Figure 5.13.

Region:	**A**	**B**	**C**
Elements identified:	Ni	Ni	Ni
	O	O	O
		Rh	Rh
		Ga	Ga
			N

In Region 'B', we observe some penetration of the polycrystalline NiO from region 'A'. Here, we observe that this layer appears like an interface between Regions 'A' and 'C', where islands of NiO seem to form thus creating a non-distinct, non-uniform layer, unlike Regions 'C' and 'D' which are observed in Figure 5.14 to be distinct layers. EDX results showing the presence of Ni, O, Rh and Ga in Region 'B' confirms this.

In Region 'C', we observe the presence of the same elements that have been identified in Region 'B' with the addition of N. We also observe a distinct change in the appearance of the layer compared to Region 'B', indicating the change in the elemental composition of the layer and also possibly a change in the compounds that have been formed. Unfortunately, we are unable to detect how each element reacts with the others and the detection of the formation of compounds is left entirely to the XRD (which can only detect crystalline elements or compounds). Nonetheless, we postulate that Region 'C' consists mainly of Rh-gallides with the presence of some NiO and N, and Region 'B', being the interface between Region 'A' (the NiO layer) and Region 'C', consists of a discontinuous layer of Rh-gallides with islets of NiO. Region 'D' is merely a thin interfacial layer that has formed on the GaN surface, probably a result of the AQ surface treatment that has been carried out prior to metal deposition.

The in-diffusion of NiO into the Rh-gallides layer as well as p-GaN surface that is observed from the TEM images has important implications, since several postulations have been made with regard to the role of NiO in the good electrical characteristics observed for the oxidized Ni/Au contact to p-GaN, as discussed in **Section 1.2.2**. One of the claims made was that the layer reversal observed between Ni and Au is vital in obtaining good Ni/Au contacts to p-GaN due to the optimal distribution of NiO into the Au lower layer [24], [25], with some NiO still in direct contact with p-GaN. While the layer reversal is not observed for the O_2-annealed Rh/Ni contact since Ni is already the upper layer, the in-diffusion of the NiO to the surface of GaN is apparent from the TEM images and AES depth profiles obtained. This suggests that the final structure of the oxidized Rh/Ni is similar to that of the oxidized Ni/Au, with islands of NiO observed to have formed in the Rh-Ga layer at the surface of GaN. The difference between these contacts lies in the Rh layer serving the additional function of forming gallides, known to be beneficial to p-GaN contact formation and hence resulting in even better electrical characteristics than the Ni/Au contact.

5.4 ALTERNATIVES TO Rh/Ni CONTACT TO AQ-TREATED p-GaN

We shall now look at two ways which have been explored in the quest to further improve the electrical characteristics obtained by the Rh/Ni contact to p-GaN.

5.4.1 HCl surface treatment

Recalling that the HCl ($HCl:H_2O = 1:1$) surface treatment has shown to give slightly better electrical characteristics than the AQ treatment for the case of the as-deposited and N_2-annealed Ni/Au contacts at low voltages, as shown in Figure 4.1, we will attempt to fabricate the Rh/Ni contact using this alternative surface treatment in seeking to improve it in a like manner. Rh/Ni contacts with AQ and HCl surface treatments were fabricated according to the experimental procedure shown in Figure 3.2.

Figure 5.15 shows the I-V characteristics of the (a) as-deposited; (b) N_2-annealed; (c) O_2-annealed Rh/Ni contacts to AQ-treated p-GaN and the (d) as-deposited; (e) N_2-annealed; (f) O_2-annealed Rh/Ni contacts to HCl-treated p-GaN. Both N_2 and O_2 anneals were carried out at 400˚C for 1 min, optimized from experiments carried out in **Section 5.3.1**. From the Rh/Ni as-deposited contacts, we observe that the AQ-treated sample gives significantly better I-V characteristics than the HCl-treated sample, suggesting that the AQ treatment has resulted in a better p-GaN surface for contact formation.

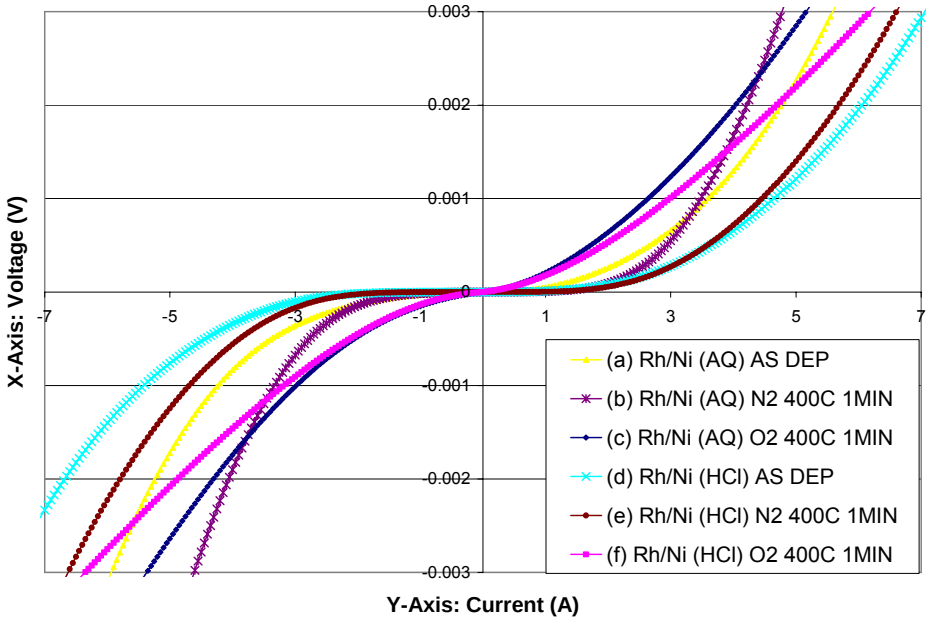

Figure 5.15: I-V characteristics of (a) as-deposited; (b) N_2-annealed; (c) O_2-annealed Rh/Ni contacts to AQ-treated p-GaN and (d) as-deposited; (e) N_2-annealed; (f) O_2-annealed Rh/Ni contacts to HCl-treated p-GaN. Both N_2 and O_2 anneals were carried out at 400˚C for 1 min.

The same trend is observed upon N_2 annealing, even though the I-V curves for both contacts were observed to improve slightly. O_2 annealing, on the other hand, resulted in a significant improvement for both surface-treated contacts and comparable I-V curves for the O_2-annealed samples. We recall that for the Ni/Au contact, while the as-deposited contacts showed the same trend as the Rh/Ni contact, O_2 anneal was also seen to result in identical I-V curves for both surface-treated contacts (see Figure 4.1). This has been attributed to the behavioral role of Ni in O_2 anneal, where it oxidizes to form NiO. The recurrence of this observation in the Rh/Ni contact confirms our earlier postulation on surface oxides contributing to the oxidation of Ni during O_2 annealing, hence depleting itself to a large extent.

In summary, we see that the Rh/Ni contact to p-GaN cannot be improved by using the HCl surface treatment. Instead, the AQ surface treatment resulted in better electrical characteristics for the Rh/Ni contact.

5.4.2 Ni/Rh contact

In seeking to obtain an I-V characteristic better than that obtained by the oxidized Rh/Ni contact, the Ni/Rh contact was attempted. The motivation behind this is the most widely-reported O_2-annealed contact to p-GaN - the Ni/Au contact, which involves Ni being the immediate layer in contact with GaN. This Ni participates in a layer-reversal during O_2 anneal, widely recognized as a major reason for it resulting in good electrical characteristics. Thus, taking into consideration the Rh/Ni contact has shown to give promising electrical characteristics when annealed in O_2, and even possibly resulting in a similar final structure as the O_2-annealed Ni/Au as shown in **Section 5.3.3**, it is worth exploring the effect of changing the sequence of metal deposition (depositing Ni first, similar to Ni/Au) and determine if the change will result in better electrical characteristics.

The Ni/Rh (10 nm/10 nm) contact was fabricated according to the experimental procedure shown in Figure 3.2. Several samples were prepared and each was annealed in O_2 at 400, 450, 500 and 600 ˚C for 1 min each. The resultant I-V

characteristics are plotted in Figure 5.16 along with the Rh/Ni contact for as-deposited and its best I-V obtained for O_2 annealing at 400 ˚C, 1 min.

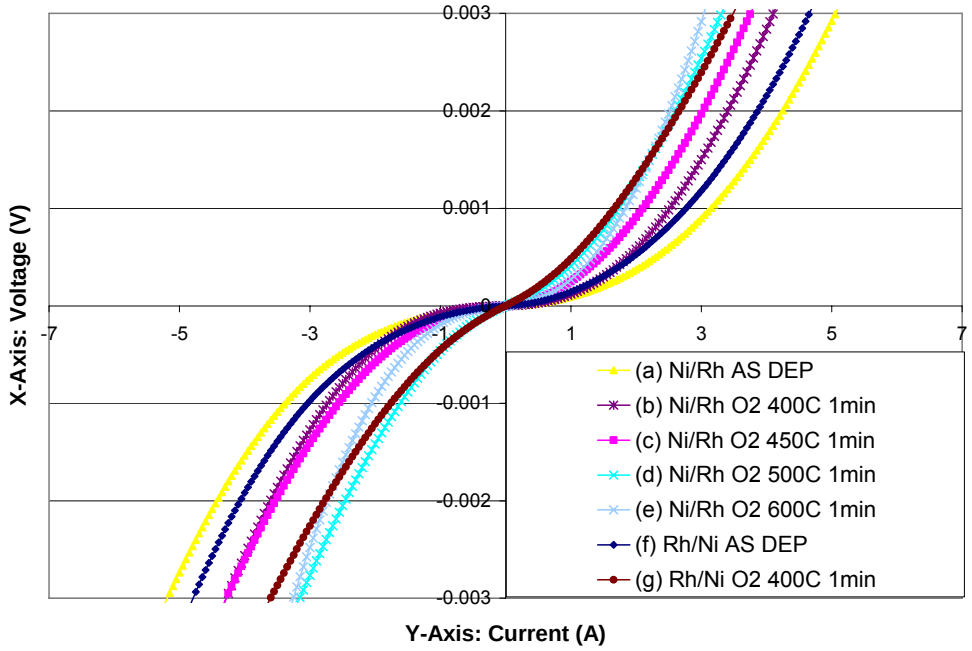

Figure 5.16: I-V characteristics of the Ni/Rh contact for (a) as-deposited; (b) O_2 annealing, 400 ˚C; (c) O_2 annealing, 450 ˚C; (d) O_2 annealing, 500 ˚C; (e) O_2 annealing, 600 ˚C and of the Rh/Ni contact for (f) as-deposited and (g) O_2 annealing, 400 ˚C.

From Figure 5.16, we see that the best I-V characteristic for the Ni/Rh contact is obtained for O_2 annealing at 500 ˚C for 1 minute. While the I-V curve obtained for the 600 ˚C annealing appears better at high voltages, it is much worse at voltages less than 3 V and is much less linear than the I-V curve obtained for the 500 annealing. The I-V characteristic obtained for the 500 ˚C annealing is not improved by

increasing its annealing time, as shown in Figure 5.17, where the contact has been annealed in 500 ˚C up to 5 min; the best I-V characteristic is obtained at 1 min.

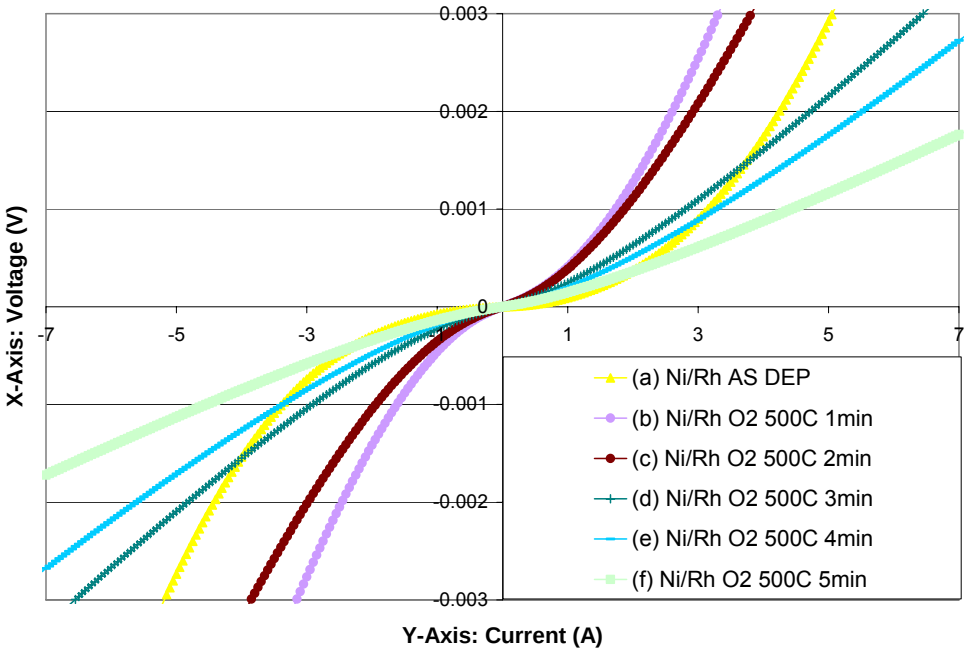

Figure 5.17: I-V characteristics of the Ni/Rh contact for (a) as-deposited and O_2 annealing at 500 ˚C for (b) 1 min; (c) 2 min; (d) 3 min; (e) 4 min and (f) 5 min.

From Figure 5.16, the best I-V characteristics obtained for the Rh/Ni and Ni/Rh contacts are observed to be similar. The annealed Ni/Rh contact is not observed to be better than the annealed Rh/Ni contact and does not seem to improve with increased annealing temperature nor annealing time. Nonetheless, optimization of its thickness can be done in seeking to improve its electrical characteristics, given that the metal contact thicknesses used has been shown to have a considerable effect on its resultant

I-V characteristics. On the same note, further optimization of the Rh/Ni contact thickness can also be done in seeking to improve its electrical characteristics.

5.5 SUMMARY

In summary, we see that a lower temperature annealing range (300 to 500 ˚C) as well as a short annealing time of about 1 min is good for N_2 and O_2 annealings of the Rh-based contacts. Thinner contact thicknesses used for the Rh-based contacts also correspond to better I-V characteristics.

For annealing of the contacts, both N_2 and O_2 annealings are seen to be unlikely to improve the electrical characteristics of the Rh and Rh/Au contacts. N_2 annealing was only observed to improve the Rh/Ni contact while O_2 annealing improved both the Rh/Ni and Rh/Ni/Au contacts. However, taking into consideration that the improvement seen in the N_2-annealed Rh/Ni contact is not very significant, we can conclude that in general, N_2 annealing is unable to improve Rh-based contacts to p-GaN. From these results, it can also be seen that any positive effect of annealing was only observed for the Rh-based contacts consisting of a Ni layer, and this is particularly true for the O_2 annealing. This strongly hints at the role NiO has to play in improving contact to p-GaN, which is in agreement with the wave of recent reports on the positive effect of the O_2 annealing on the Ni/Au contact to p-GaN [8], [24]-[27].

From the AES depth profiles and TEM images obtained for the O_2-annealed Rh/Ni sample, we confirm the complete oxidation of Ni to form NiO upon O_2 annealing. Some NiO has also been observed to in-diffuse to the GaN surface, while much of the Rh is still in direct contact with p-GaN, hinting that the final structure of the oxidized Rh/Ni contact might be similar to the oxidized Ni/Au contact. The difference lies in the role of Rh, which is known to form gallides, resulting in a Ga-deficient GaN surface and consequently, a good contact to p-GaN.

CHAPTER 6

CONCLUSION AND FUTURE WORKS

In this work, the effects of N_2 and O_2 annealing (600 ˚C-1 min) on the Ni/Au (20/20 nm) contact to AQ, Cl_2/N_2 plasma and O_2 plasma surface-treated p-GaN has been studied. We have found that O_2 annealing is beneficial only to the AQ surface-treated contacts even though the formation of NiO and the layer-reversal of Ni/Au have been observed for all three surface-treated contacts. This has been attributed to the formation of the N-Ga-O_x and Ga-O_x-C complexes during O_2 plasma treatment and undesirable Ni_3N compounds during O_2 annealing for both Cl_2/N_2 and O_2 plasma treatments. The complexes formed during O_2 plasma treatment cannot be removed by subsequent AQ and is recognized to be the cause for N_2 and O_2 annealing proving detrimental to the O_2 plasma-treated contacts.

N_2 annealing, on the other hand, has been found to have the same effect on the AQ and N_2/Cl_2 plasma-treated contacts and we conclude that it is less sensitive to the surface conditions compared to O_2 annealing.

Hence, we can conclude from this work that plasma treatment is generally not beneficial for O_2 annealing of Ni/Au contact formation to p-GaN. Other than the Ga/N and O/Ga ratios, the modification of the surface conditions has also been seen

to play an important role in determining the electrical characteristics of the contact. A possible future study could be on the surface conditions, such as the surface roughness, resulting from various surface treatments and its effect on the O_2-annealed Ni/Au contact to determine the reason behind the negative effects observed here.

The effects of N_2 and O_2 annealings on the following Rh-based contacts to p-GaN: Rh (20 nm), Rh/Ni/Au (10/10/10 nm), Rh/Au (10/10 nm) and Rh/Ni (10/10 nm) have also been successfully studied. We have found that both N_2 and O_2 annealings are seen to be unlikely to improve the electrical characteristics of the Rh and Rh/Au contacts.

N_2 annealing has seen to improve only the Rh/Ni contact, although not significantly, and we conclude that N_2 annealing is generally unable to improve Rh-based contacts to p-GaN. O_2 annealing, on the other hand, can improve both the Rh/Ni and Rh/Ni/Au contacts, both of which consist of a Ni layer and therefore strongly hinting at the role NiO has to play in improving the contact to p-GaN, which is in agreement with the wave of recent reports on the positive effect of the O_2 annealing on the Ni/Au contact to p-GaN [8], [24]-[27].

The best Rh-based contact to p-GaN obtained has been identified to be the 400 ˚C-1 min O_2-annealed Rh/Ni contact. The complete oxidation of Ni to NiO upon O_2

annealing has been observed from AES depth profiles and TEM images. Some NiO has also been observed to in-diffuse to the GaN surface, while much of the Rh remains in direct contact with p-GaN, hinting that the final structure of the oxidized Rh/Ni contact might be similar to the oxidized Ni/Au contact. The difference lies in the role of Rh, which is known to form gallides, resulting in a Ga-deficient GaN surface and hence resulting in a good contact to p-GaN.

The best I-V characteristic for the Ni/Rh (10/10 nm) contact, obtained at 500 ˚C-1 min O_2 annealing, has been found to be comparable to the best I-V characteristic obtained by the O_2-annealed Rh/Ni contact. In view of metal contact thicknesses having shown to have a considerable effect on resultant I-V characteristics of a contact, it would be interesting to attempt an optimization of the thickness of Ni/Rh used, in seeking to improve its electrical characteristics. On the same note, further optimization of the Rh/Ni contact thickness can also be done in seeking to improve its electrical characteristics.

REFERENCES

[1] S. Nakamura, M. Senoh, N. Iwasa, S. Nagahama, *"High-Brightness InGaN Blue, Green and Yellow Light-Emitting Diodes with Quantum Well Structures",* Jpn. J. Appl. Phys., Part 2 Vol.34, P.L797 (1995).

[2] M. Asif Khan, J. N. Kuznia, A. R. Bhattarai, D. T. Olson, *"Metal semiconductor field effect transistor based on single crystal GaN",* Appl. Phys. Lett. Vol.62 P.1786 (1993).

[3] M. Asif Khan, A. R. Bhattarai, J. N. Kuznia, D. T. Olson, "*High electron mobility transistor based on a GaN-*AI_x Ga_{1-x} *N heterojunction",* Appl. Phys. Lett. Vol.63 P.1214 (1993).

[4] S. Nakamura, M. Senoh, N. Iwasa, T. Yamada, T. Matsushita, H. Kiyoku, Y. Sugimoto, *"InGaN Multi-Quantum-Well-Structure Laser Diodes with Cleaved Mirror Cavity Facets",* Jpn. J. Appl. Phys., Part 2 Vol.35, P.L217 (1996).

[5] M. Asif Khan, J. N. Kuznia, D. T. Olson, J. M. Van Hove, M. Blasingame, L. F. Reitz, *"High-responsivity photoconductive ultraviolet sensors based on insulating single-crystal GaN epilayers",* Appl. Phys. Lett. Vol.60, P.2917 (1992).

[6] J. Pankove, S.S. Chang, H.C. Lee, R.J. Molnar, T.D. Moustakes, B.V. Zeghbroeck, *"High-Temperature GaN/SiC Heterojunction Bipolar Transistor with High Gain",* IEDM, P.389 (1994).

[7] J-S Jang, S-J Park, and T-Y Seong, "*Metallization scheme for highly low-resistance, transparent,and thermally stable ohmic contacts to p-GaN*," Appl. Phys. Lett., Vol.76, P.2898 (2000).

[8] L-C Chen, J-K Ho, C-S Jong, C.C. Chiu, K-K Shih, F-R Chen, J-J Kai, L. Chang, "*Oxidised Ni/Pt and Ni/Au ohmic contacts to p-type GaN",* Appl. Phys. Lett., Vol.76, P.3073 (2000).

[9] J.O. Song, K-K Kim, S-J Park, T-Y Seong, *"Highly low resistance and transparent Ni/ZnO ohmic contacts to p-type GaN"*, Appl. Phys. Lett., Vol.83, P.479 (2003).

[10] J.O. Song and D-S Leem, J.S. Kwak, O.H. Nam, Y. Park, T-Y Seong, "*High-quality nonalloyed rhodium-based ohmic contacts to p-type GaN*", Appl. Phys. Lett., Vol.83, P.2372 (2003).

[11] J. Narayana, H. Wang, T-H Oh, H.K. Choi, J.C.C. Fan, *"Formation of epitaxial Au/Ni/Au ohmic contacts to p-GaN",* Appl. Phys. Lett., Vol.81, P.3978 (2002).

[12] W.J. Ho, J-L Lee, "*Transparent Ohmic contacts of oxidized Ru and Ir on p-type GaN",* J. Appl. Phys., Vol.93, P.5416 (2003).

[13] L. Zhou, W. Lanford, A. T. Ping, I. Adesida, J. W. Yang, A. Khan, "*Low resistance Ti/Pt/Au ohmic contacts to p-type GaN",* Appl. Phys. Lett., Vol.76, P.3451 (2000).

[14] W.J. Ho, W. Urbanek, M.C. Yoo, J-L Lee, *"Low-resistant and high-transparent Ru/Ni ohmic contact on p-type GaN",* Appl. Phys. Lett., Vol.80, P.2937 (2002).

[15] H.W. Jang, K.H. Kim, J.K. Kim, S-W Hwang, J.J. Yang, K.J.Lee, S-J Son, J-L Lee, *"Low-resistance and thermally stable ohmic contact on p-type GaN using Pd/Ni metallization",* Appl. Phys. Lett., Vol.79, P.1822 (2001).

[16] C-F Chu, C.C Yu, Y.K Wang, J.Y. Tsai, F.I. Lai, S.C.Wang, "*Low-resistance ohmic contacts on p-type GaN using Ni/Pd/Au metallization",* Appl. Phys. Lett., Vol.77, P.3423 (2000).

[17] L-C Chen, F-R Chen, J-J Kai, L. Chang, J-K Ho, C-S Jong, C.C. Chiu, K-K Shih, C-N Huang, C-Y Chen, "*Microstructural investigation of oxidized Ni/Au ohmic contact to p-GaN",* J. Appl. Phys., Vol.86, P.3826 (1999).

[18] D. Zhang, *"Ohmic contacts to compound semiconductors: Gallium Arsenide and Gallium Nitride",* Degree of Master of Engineering thesis, National University of Singapore (2000).

[19] J-S Jang, I-S Chang, H-K Kim, T-Y Seong, S. Lee, S-J Park, "*Low-resistance Pt/Ni/Au ohmic contacts to p-type GaN",* Appl. Phys. Lett., Vol.74, P.70 (1999).

[20] R-H Horng, D-S Wuu, Y-C Lien, W-H Lan, "*Low-resistance and high-transparency Ni/Indium Tin Oxide ohmic contacts to p-type GaN",* Appl. Phys. Lett., Vol.79, P.2925 (2001).

[21] T. Arai, H. Sueyoshi, Y. Koide, M. Moriyama, M. Marakami, "*Development of Pt-based ohmic materials for p-type GaN",* J. Appl. Phys., Vol.89, P.2826 (2001).

[22] B. Liu, M.H. Ahonen, P.H. Holloway, "*A thermodynamic approach to Ohmic contact formation to p-GaN",* MRS Symp. W (1999).

[23] D.J. King, L. Zhang, J.C. Ramer, S.D. Hersee, L.F. Lester, "*Temperature behaviour of ohmic contacts to p-GaN",* MRS Symp. Procs., Vol.468, P.421 (1997).

[24] J-K Ho, C-S Jong, C.C Chiu, C-N Huang. K.K. Shih, L.C. Chen, F.R. Chen, J.J. Kai, *"Low-resistance ohmic contacts to p-type GaN achieved by the oxidation of Ni/Au films",* J. Appl. Phys., Vol.86, P.4491 (1999).

[25] L-C Chen, F-R Chen, J-J Kai, L. Chang, J-K Ho, C-S Jong, C.C. Chiu, K-K Shih, C-N Huang, C-Y Chen, "*Microstructural investigation of oxidized Ni/Au ohmic contact to p-type GaN",* J. Appl. Phys., Vol.86, P.3826 (1999).

[26] D. Qiao, L. S. Yu, S. S. Lau, J. Y. Lin, H. X. Jiang, T. E. Haynes, *"A study of the Au/Ni ohmic contact on p-GaN***",** J. Appl. Phys., Vol. 88, P.71 (2000).

[27] W.J. Ho, Y.K. Soo, J-L Lee, *"Mechanism for Ohmic contact formation of oxidized Ni/Au on p-type GaN",* J. Appl. Phys., Vol.94, P.1748 (2003).

[28] J-S Jang, S-J Park, T-Y Seong, *"Ultrahigh transparency of Ni/Au ohmic contacts to surface-treated p-type GaN"*, J. Appl. Phys., Vol.88, P.5490 (2000).

[29] Y. Koide, T. Maeda, T. Kawakami, S. Fujita, T. Uemura, N. Shibata, M. Murakami, "*Effects of Annealing in an Oxygen Ambient on Electrical Properties of Ohmic Contacts to p-Type GaN*", J. Electron. Mater., Vol.28, P.341 (1999).

[30] B.A. Hull, S.E. Mohney, H.S. Venugopalan, J.C. Ramer, *"Influence of oxygen on the activation of p-type GaN",* Appl. Phys. Lett., Vol.76, P.2271(2000).

[31] S. Nakamura, N. Iwasa, M. Senoh, T. Mukai, "*Hole Compensation Mechanism of P-Type GaN Films*" Jpn. J. Appl. Phys., Vol.31, P.1258 (1992).

[32] J. A. van Vechten, J. D. Zook, R. D. Hornig, B. Goldenberg, "*Defeating Compensation in Wide Gap Semiconductors by Growing in H that is Removed by Low Temperature De-Ionizing Radiation*", Jpn. J. Appl. Phys., Vol.31, P.3662 (1992).

[33] W. Gotz, N. M. Johnson, J. Walker, D. P. Bour, H. Amano, I. Akasaki, "*Hydrogen passivation of Mg acceptors in GaN grown by metalorganic chemical vapor deposition",* Appl. Phys. Lett. Vol.67, P.2666 (1995).

[34] D-H Youn, M. Lachab, M. Hao, T. Sugahara, H. Takenaka, Y. Naoi, S. Sakai, *"Investigation on the p-type activation mechanism in Mg-doped GaN films grown by metalorganic chemical vapor deposition",* Jpn. J. Appl. Phys., Vol.38, P.631 (1999).

[35] T-C Wen, S-C Lee, W-I Lee, T-Y Chen, S-H Chan, J-S Tsang, *"Activation of p-type GaN in a pure oxygen ambient",* Jpn. J. Appl. Phys., Vol.40, P.495 (2001).

[36] T. Mori, T. Kozawa, T. Ohwaki, and Y. Taga, S. Nagai, S. Yamasaki, S. Asami, N. Shibata, and M. Koike *"Schottky barriers and contact resistances on p-type GaN"*, Appl. Phys. Lett., Vol.69, P.3537 (1996).

[37] L.L. Smith, R.F. Davis, M.J. Kim, R.W. Carpenter, and Y. Huang, *"Microstructure, electrical properties, and thermal stability of Au-based ohmic contacts to p-GaN"*, J. Mater. Res. Vol.12, P.2249 (1997).

[38] K. M. Yu, W. Walukiewicz, J. M. Jaklevic, E. E. Haller, *"Effects of interface reactions on electrical characteristics of metal-GaAs contacts"*, Appl. Phys. Lett., Vol.51, P.189 (1987).

[39] T. Sands, V. G. Keramidas, K. M. Yu, J. Washburn, K. Krishnan, *"A comparative study of phase stability and film morphology in thin-film M/GaAs systems (M=Co, Rh, Ir, Ni, Pd, and Pt)"*, J. Appl. Phys., Vol.62, P.2070 (1987).

[40] J-K Ho, C-S Jong, C.C Chiu, C-N Huang, C-Y Chen, K-K Shih, *"Low-resistance ohmic contacts to p-type GaN",* Appl. Phys. Lett., Vol.74, P.1275 (1999).

[41] T. Maeda, Y. Koide, M. Murakami, "*Effects of NiO on electrical properties of NiAu-based ohmic contacts for p-type GaN*", Appl. Phys. Lett. Vol.75, P.4145 (1999).

[42] C.L. Lee, *"Investigations on ohmic contact to p-doped Gallium Nitride",* Degree of Master of Engineering thesis, National University of Singapore (2003).

[43] E. H. Rhoderick and R. H. Williams, "*Metal-Semiconductor Contacts*", 2nd Edition, Clarendon, Oxford, P. 11-28 (1998).

[44] S. M. Sze, "*Physics of Semiconductor Devices*", John Wiley & Sons, 2nd Edition (1981).

[45] J. W. Mayer and S. S. Lau, "*Electronic Materials Science: For Integrated Circuits in Si and GaAs*", Macmillan Publishing, New York (1990)..

[46] J. Bardeen, "*Surface States and Rectification at a Metal Semiconductor Contact*", Phys. Rev., Vol. 71, P.717 (1947).

[47] http://matlb.kjist.ac.kr/~tflab/MEM_2.pdf

[48] J. S. Foresi, T. D. Moustakas, *"Metal contacts to Gallium Nitride"*, Appl. Phys. Lett., Vol. 62, P.2859 (1993).

[49] A. T. Ping, M. A. Khan, I. Adesaida, *"Ohmic Contacts to n-type GaN using Pd/Al metallization"*, J. Electron Materials, Vol. 25, P.819 (1996).

[50] H. Ishikawa, S. Kobayashi, Y. Koide, S. Yamasaki, S. Nagai, J. Umezaki, M. Koide, M. Murakami, *"Effects of surface treatment and metal work functions on electrical properties at p-GaN/metal interface"*, J. Appl. Phys., Vol. 81,P.1315 (1997).

[51] T. Yamamoto, H. Katayama-Yoshida, "*Materials Design for the Fabrication of Low-Resistivity p-Type GaN Using a Codoping Method*", Jpn. J. Appl. Phys., Vol.36, P.180 (1997).

[52] K. K. Jong, "*Microstructural Investigation of Ni/Au Ohmic contact on p-type GaN"*, J. Electrochem. Soc., Vol.147(12), P.4645 (2000).

[53] C. J. Bernard, "*Ohmic contacts to compound semiconductors"*, Ph.D. Thesis, Auburn University (1992).

[54] W. G. Bickley, "*Bessel Functions"*, University Press, Cambridge (1960).

[55] V. Adivarahan, A. Lunev, M. Asif Khan, J. Yang, G. Simin, M. S. Shur and R. Gaska, "*Very-low-specific-resistance Pd/Ag/Au/Ti/Au alloyed ohmic contact to p-GaN for high devices*," Appl. Phys. Lett., Vol.78, P.2781 (2001).

[56] J. Lim, E. F. Chor, L. S. Tan, *"Metal Contacts to GaN-based Compound Semiconductor"*, Degree of Bachelor of Engineering thesis, National University of Singapore (2003).

[57] K. K. Jong, K-J Kim, B. Kim, J. N. Kim, J. S. Kwak, Y. J. Park, J-L Lee, *"Effects of Surface Treatment Using Aqua Regia Solution on the Change of Surface Band Bending of p-type GaN"*, J. Elect. Mat., Vol.30, P.129 (2001).

[58] K. K. Jong, J-L Lee, W. L. Jae, E. S. Hyun, J. P. Yong, T. Kim, *"Low resistance Pd/Au ohmic contacts to p-type GaN using surface treatment",* Appl. Phys. Lett., Vol.73, P.2953 (1998).

[59] K.K. Jong, C.K. Chong, S.C. Tae, H.J. Jung, S.K. Joon, J.P. Yong, J-L Lee, *"Effects of Surface treatments on the Electrical and the Microstructural changes of Pd contact on p-type GaN"*, J. Elect. Mat., Vol.30, P.170 (2001).

[60] S. Ruvimov, Z. Liliental-Weber, J. Washburn, K. J. Duxstad, E. E. Haller, Z.-F. Fan, S. N. Mohammad, W. Kim, A. E. Botchkarev, H. Morkoç, "*Microstructure of Ti/Al and Ti/Al/Ni/Au Ohmic contacts for n –GaN*", Appl. Phys. Lett., Vol.69, P.1556 (1996).

[61] J. Elsner, R. Jones, M. I. Heggie, P. K. Sitch, M. Haugk, Th. Frauenheim, S. Öberg, P. R. Briddon, "*Deep acceptors trapped at threading-edge dislocations in GaN*", Phys. Rev. B, Vol.58, P.12571 (1998).

[62] J. K. Sheu, Y. K. Su, G. C. Chi, W. C. Chen, C. Y. Chen, C. N. Huang, J. M. Hong, Y. C. Yu, C. W. Wang, E. K. Lin, *"The effect of thermal annealing on the Ni/Au contact to p-type GaN"*, J. Appl. Phys., Vol.83, P.3172 (1998).

[63] NIST X-ray Photoelectron Spectroscopy Database, National Institute of Standards and Technology, http://srdata.nist.gov/XPS/

[64] K. Prabhakaran, T. G. Andersson, K. Nowaza, *"Nature of native oxide on GaN surface and its reaction with Al"*, Appl. Phys. Lett., Vol.69, P.3212 (1996).

[65] A. S. Lim, A. Atrens, *"ESCA studies of Nitrogen-Containing Stainless Steels*", Appl. Phys. A, Vol.51, P.411 (1990).

[66] P. A. Zhdan, A. P. Shepelin, Z. G. Osipova, V. D. Sokolovskii, J. Catal. Vol.58, P.8 (1979).

[67] P. Y. Jouan, M. C. Peignon, C. H. Cardinaud, G. Lemperiere, *"Characterisation of TiN coatings and of the TiN/Si interface by x-ray photoelectron spectroscopy and Auger electron spectroscopy*", Appl. Surf. Science, Vol.68, P.595 (1993).

[68] http://environmentalchemistry.com/yogi/periodic/Ni.html

[69] http://environmentalchemistry.com/yogi/periodic/Rh.html

[70] http://environmentalchemistry.com/yogi/periodic/Au.html

APPENDIX I

PERIODIC TABLE EXTRACT

Legend:

Workfunction (eV)

Melting Point (°C)

Vapour Pressure at melting point (μmHg)

Electrical Resistivity (μΩ-cm)

		Ni 5.25 1455 1778 7.0	
Ru 4.71 2250 10.5 7.1	**Rh** 4.98 1966 4.75 4.3	**Pd** 5.11 1554 9.98 10	
		Pt 5.65 1769 0.234 10.6	**Au** 5.15 1065 0.0184 2.2

APPENDIX II

HALL MEASUREMENT RESULTS

Hall measurement was carried out on the p-GaN samples used in this project to determine the p-doping concentration. The Hall measurements for each p-GaN sample were taken via four indium dots deposited at the four corners of each 5 mm by 5 mm sized sample. The use of the HL 55WIN Hall system was employed, which gives the sheet concentration of the sample under test. The hole concentration of the p-GaN sample is calculated by dividing the sheet concentration by the thickness of the p+ GaN layer, i.e.,

Hole concentration = Sheet concentration / thickness of p+ GaN layer,

where thickness of p+ GaN layer = 1.0 μm.

Two p-GaN wafers were used in the course of this work and the hole concentration of these wafers were determined to be (1) 3.38×10^{17} cm^{-3} and (2) 3.52×10^{17} cm^{-3}. The sheet concentration for each p-GaN sample can be found in the details of the Hall measurement results shown in the figures below.

(1) p-GaN wafer with hole concentration = 3.38×10^{17} cm^{-3}

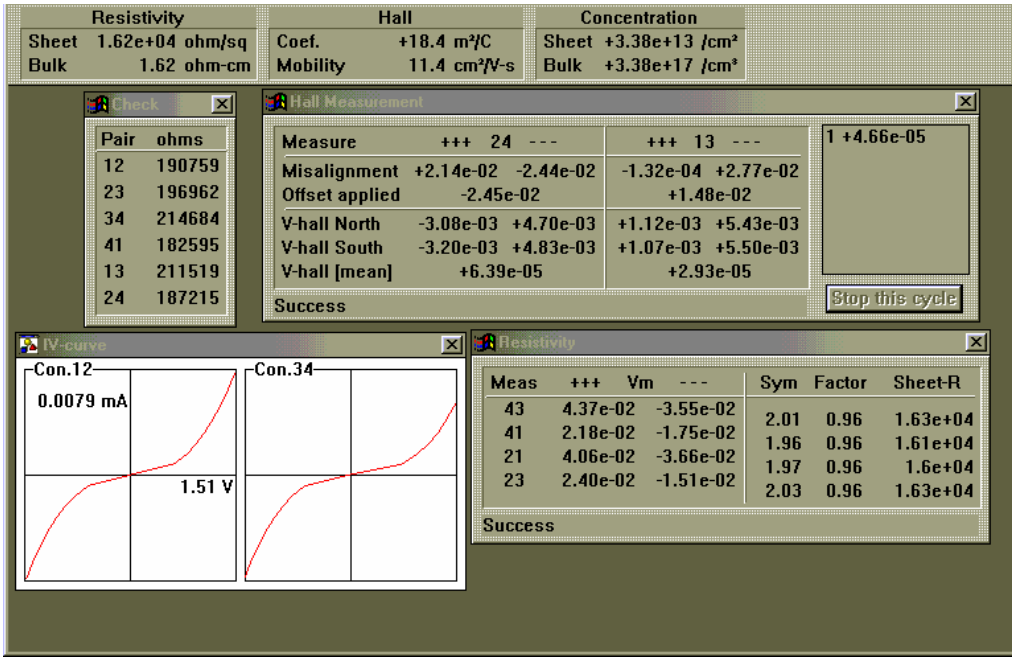

(2) p-GaN wafer with hole concentration = 3.52×10^{17} cm^{-3}

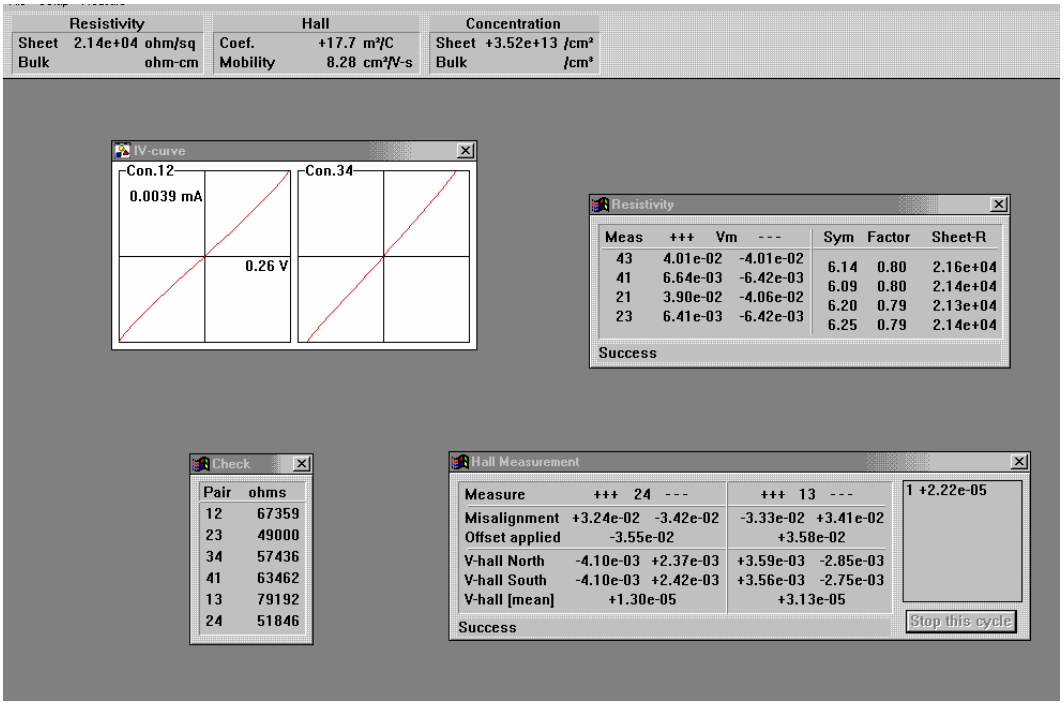

APPENDIX III

I-V GRAPHS FOR Rh-BASED CONTACTS TO p-GaN

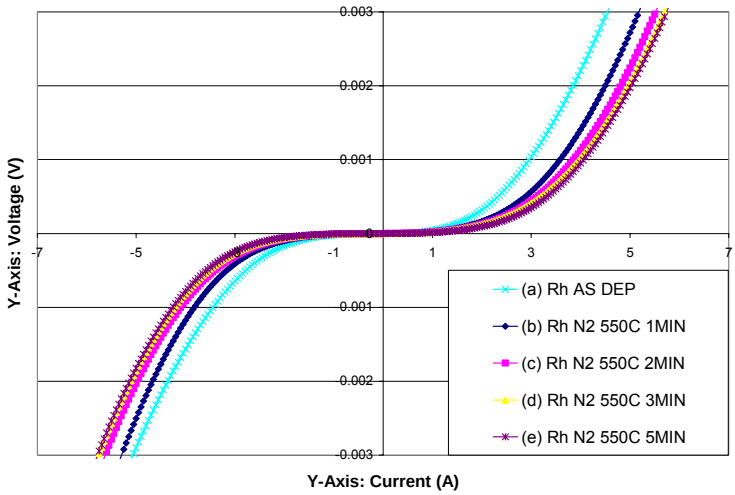

Figure III-a I-V characteristics of Rh (40 nm) contact to p-GaN for (a) as-deposited and annealed in N_2 at 550 ˚C for (b) 1 min (c) 2 min (d) 3 min and (e) 5 min.

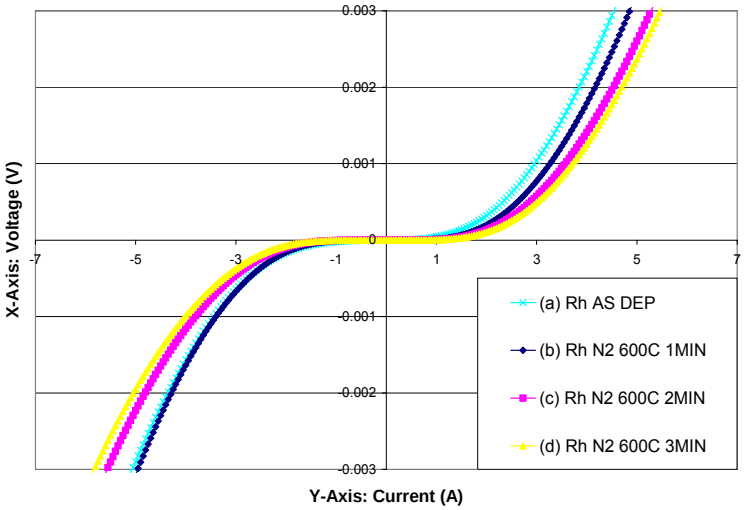

Figure III-b I-V characteristics of Rh (40 nm) contact to p-GaN for (a) as-deposited and annealed in N_2 at 600 ˚C for (b) 1 min (c) 2 min and (d) 3 min.

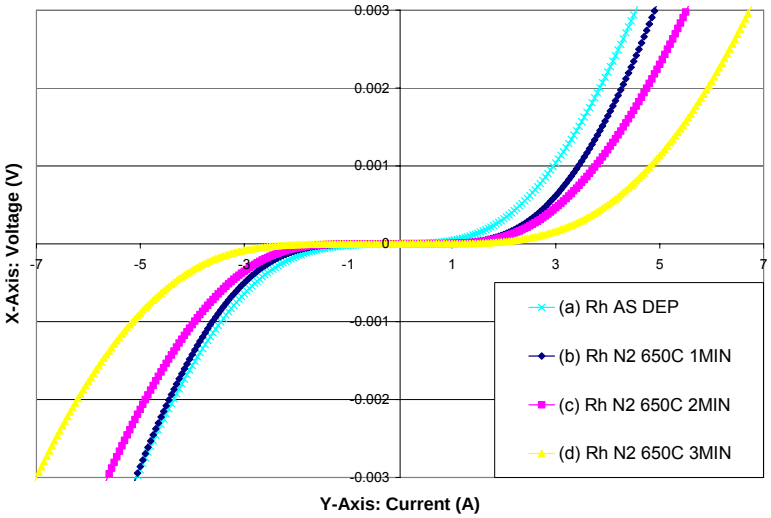

Figure III-c I-V characteristics of Rh (40 nm) contact to p-GaN for (a) as-deposited and annealed in N_2 at 650 ˚C for (b) 1 min (c) 2 min and (d) 3 min.

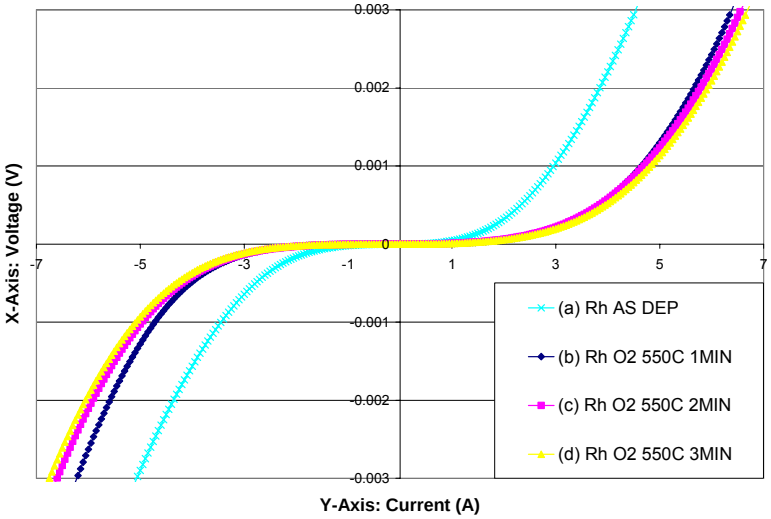

Figure III-d I-V characteristics of Rh (40 nm) contact to p-GaN for (a) as-deposited and annealed in O_2 at 550 ˚C for (b) 1 min (c) 2 min and (d) 3 min.

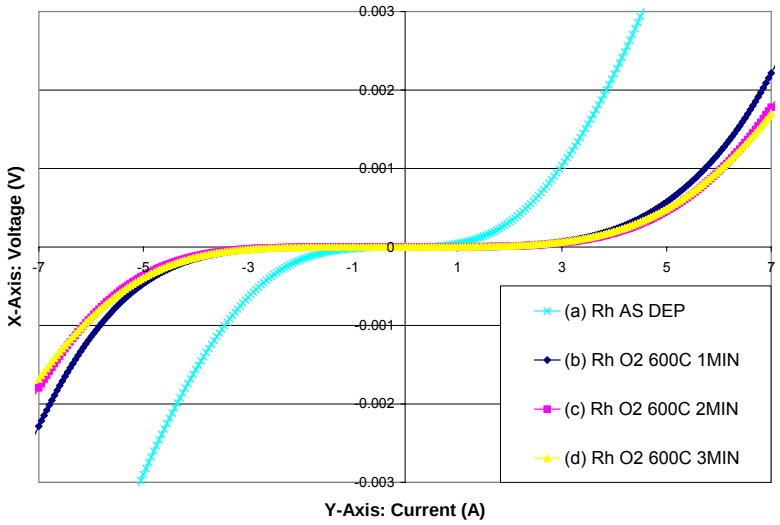

Figure III-e I-V characteristics of Rh (40 nm) contact to p-GaN for (a) as-deposited and annealed in O_2 at 600 ˚C for (b) 1 min (c) 2 min and (d) 3 min.

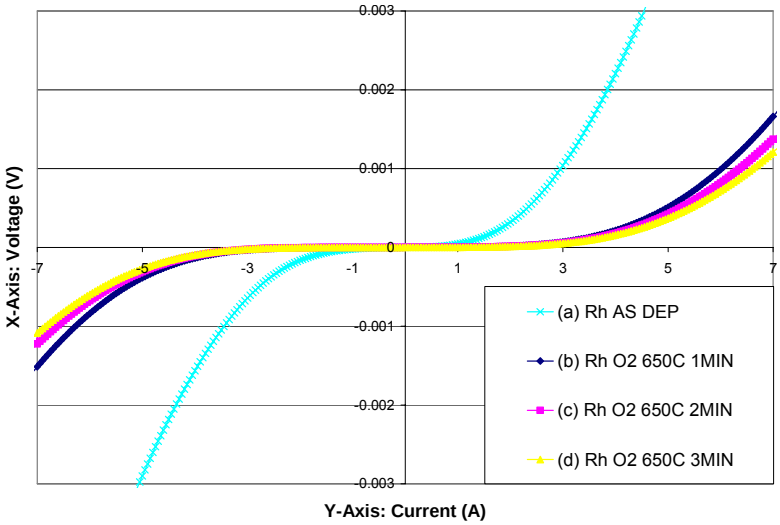

Figure III-f I-V characteristics of Rh (40 nm) contact to p-GaN for (a) as-deposited and annealed in O_2 at 650 ˚C for (b) 1 min (c) 2 min and (d) 3 min.

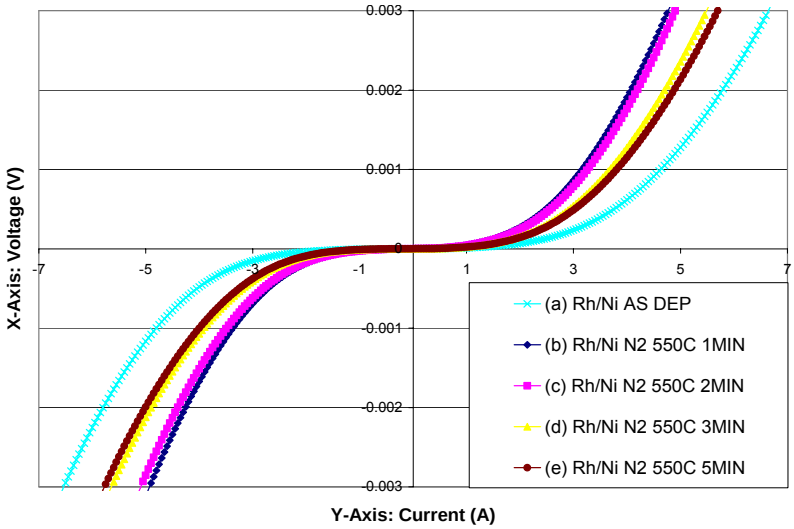

Figure III-g I-V characteristics of Rh/Ni (20 nm/20 nm) contact to p-GaN for (a) as-deposited and annealed in N_2 at 550 ˚C for (b) 1 min (c) 2 min (d) 3 min and (e) 5 min.

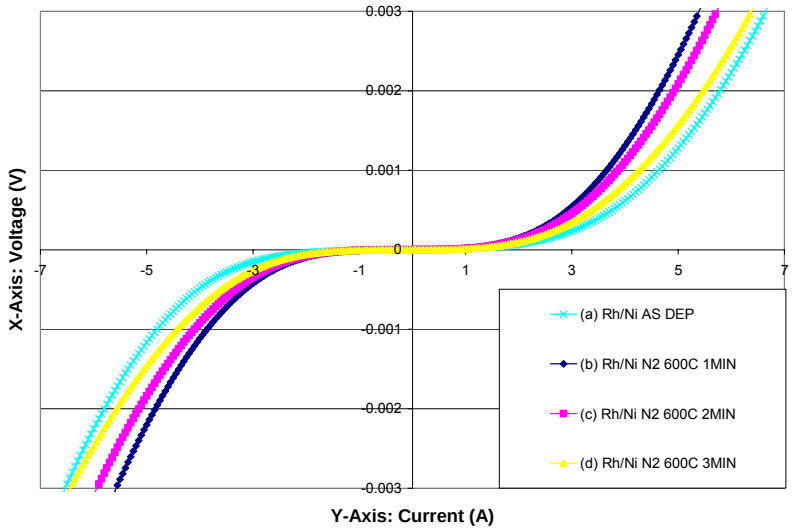

Figure III-h I-V characteristics of Rh/Ni (20 nm/20 nm) contact to p-GaN for (a) as-deposited and annealed in N_2 at 600 ˚C for (b) 1 min (c) 2 min and (d) 3 min.

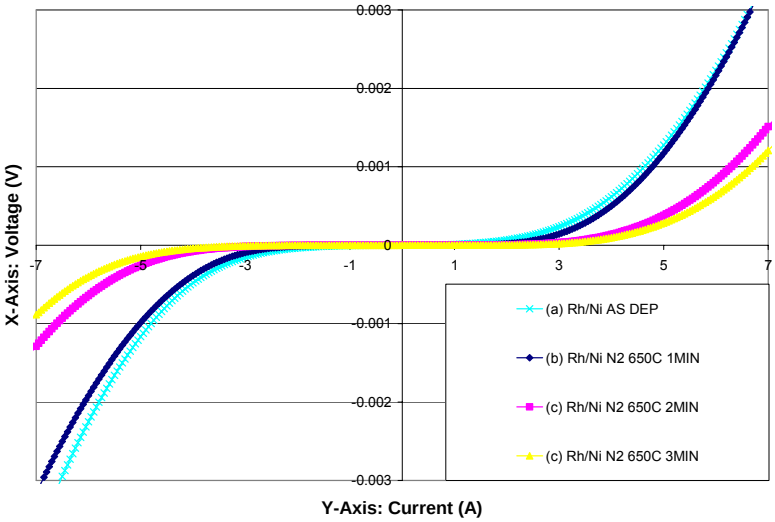

Figure III-i I-V characteristics of Rh/Ni (20 nm/20 nm) contact to p-GaN for (a) as-deposited and annealed in N_2 at 650 ˚C for (b) 1 min (c) 2 min and (d) 3 min.

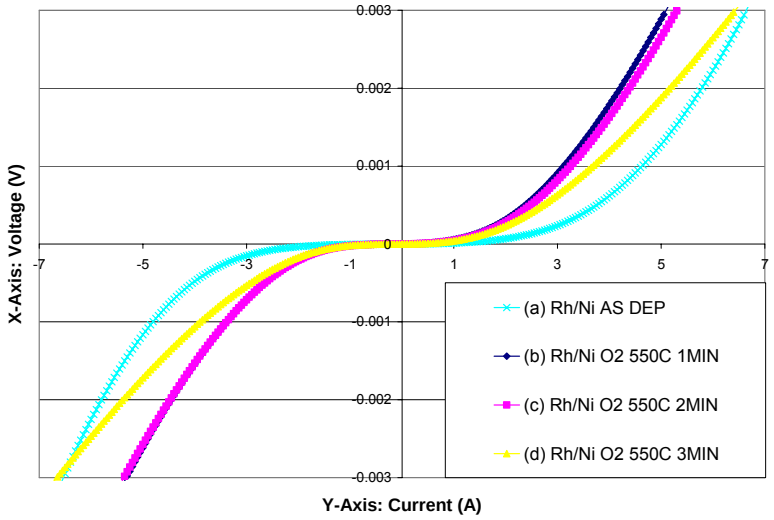

Figure III-j I-V characteristics of Rh/Ni (20 nm/20 nm) contact to p-GaN for (a) as-deposited and annealed in O_2 at 550 ˚C for (b) 1 min (c) 2 min and (d) 3 min.

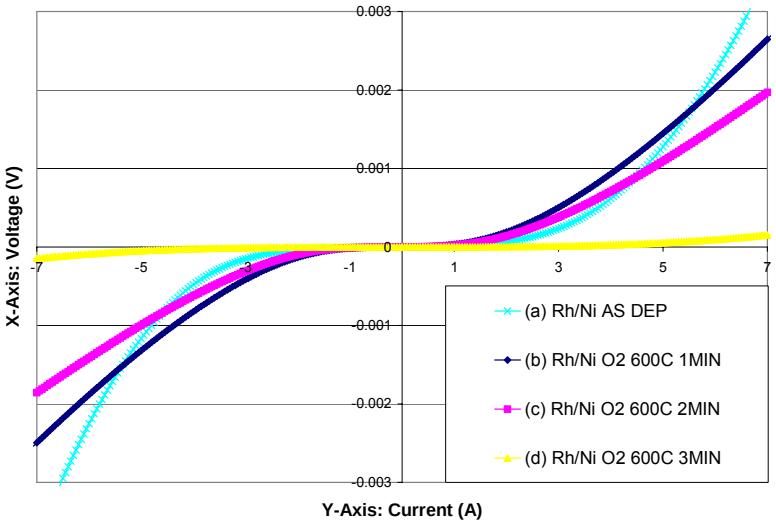

Figure III-k I-V characteristics of Rh/Ni (20 nm/20 nm) contact to p-GaN for (a) as-deposited and annealed in O_2 at 600 ˚C for (b) 1 min (c) 2 min and (d) 3 min.

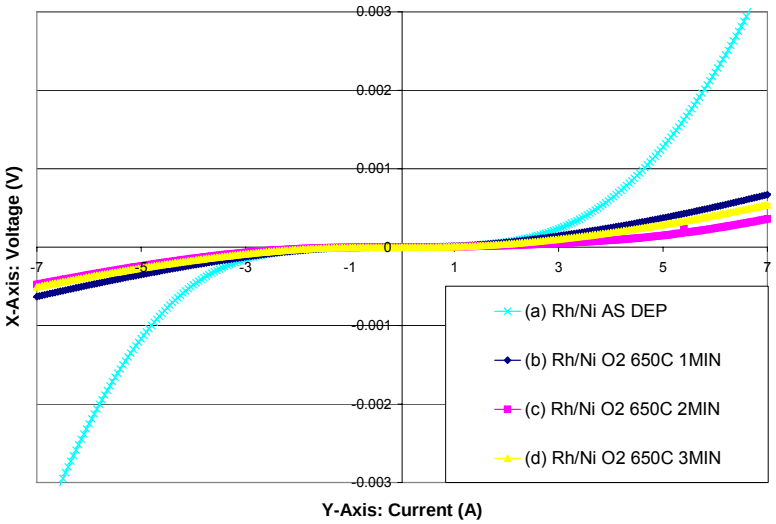

Figure III-l I-V characteristics of Rh/Ni (20 nm/20 nm) contact to p-GaN for (a) as-deposited and annealed in O_2 at 650 ˚C for (b) 1 min (c) 2 min and (d) 3 min.

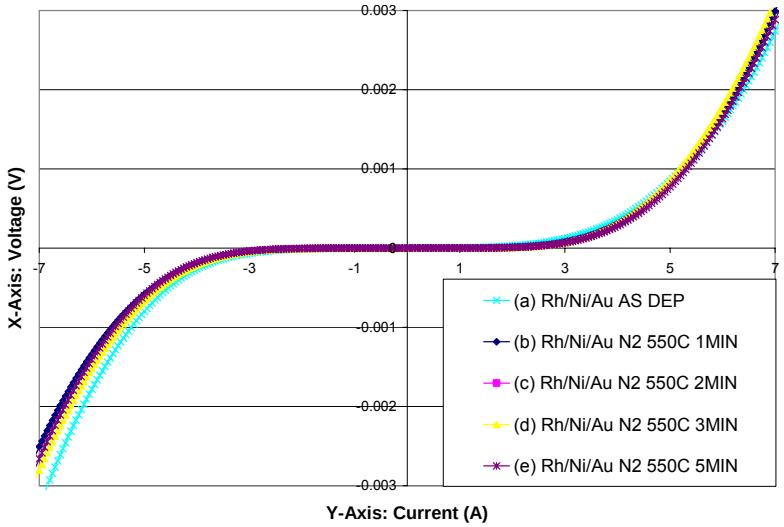

Figure III-m I-V characteristics of Rh/Ni/Au (20 nm/20 nm/20 nm) contact to p-GaN for (a) as-deposited and annealed in N_2 at 550 ˚C for (b) 1 min (c) 2 min (d) 3 min and (e) 5 min.

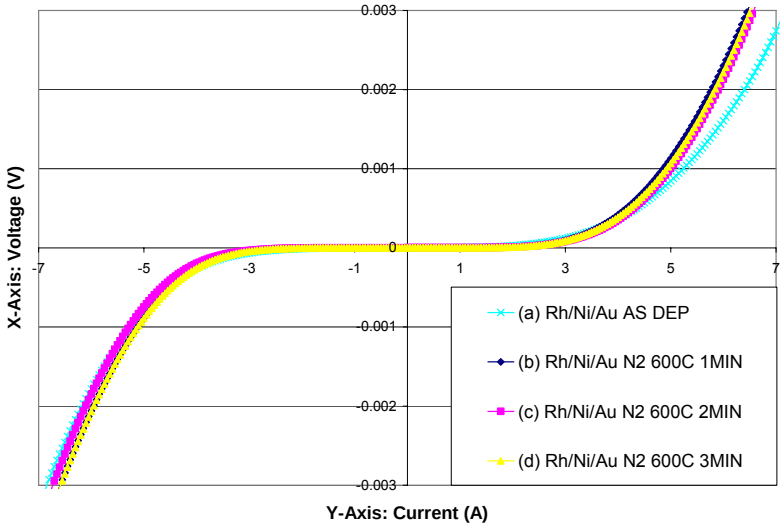

Figure III-n I-V characteristics of Rh/Ni/Au (20 nm/20 nm/20 nm) contact to p-GaN for (a) as-deposited and annealed in N_2 at 600 ˚C for (b) 1 min (c) 2 min and (d) 3 min.

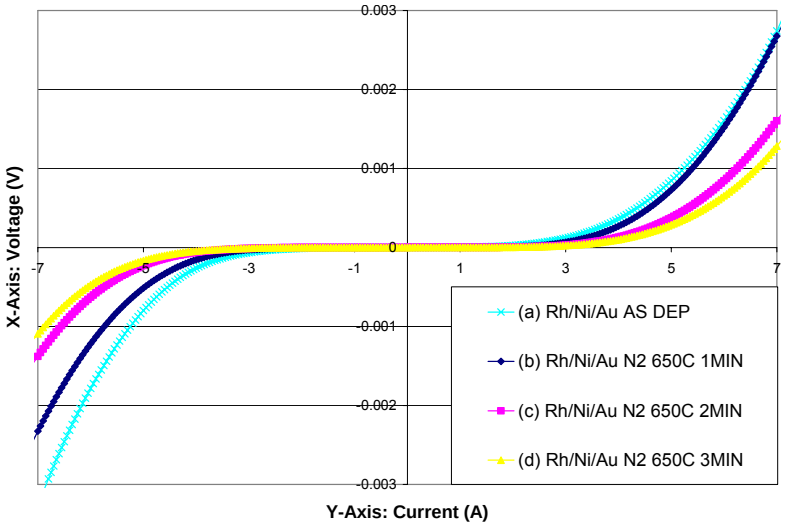

Figure III-o I-V characteristics of Rh/Ni/Au (20 nm/20 nm/20 nm) contact to p-GaN for (a) as-deposited and annealed in N_2 at 650 ˚C for (b) 1 min (c) 2 min and (d) 3 min.

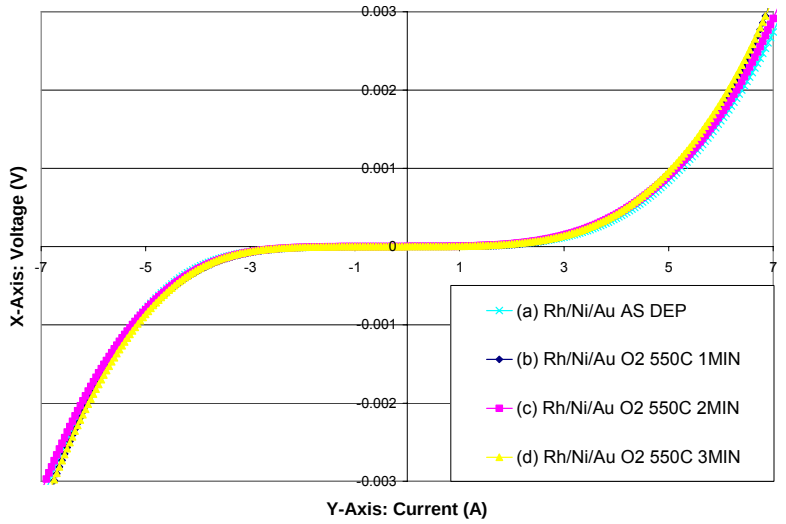

Figure III-p I-V characteristics of Rh/Ni/Au (20 nm/20 nm/20 nm) contact to p-GaN for (a) as-deposited and annealed in O_2 at 550 ˚C for (b) 1 min (c) 2 min and (d) 3 min.

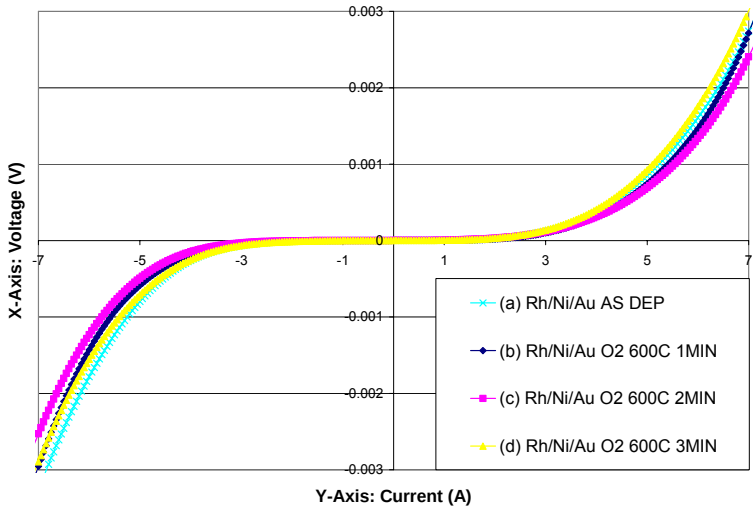

Figure III-q I-V characteristics of Rh/Ni/Au (20 nm/20 nm/20 nm) contact to p-GaN for (a) as-deposited and annealed in O_2 at 600 ˚C for (b) 1 min (c) 2 min and (d) 3 min.

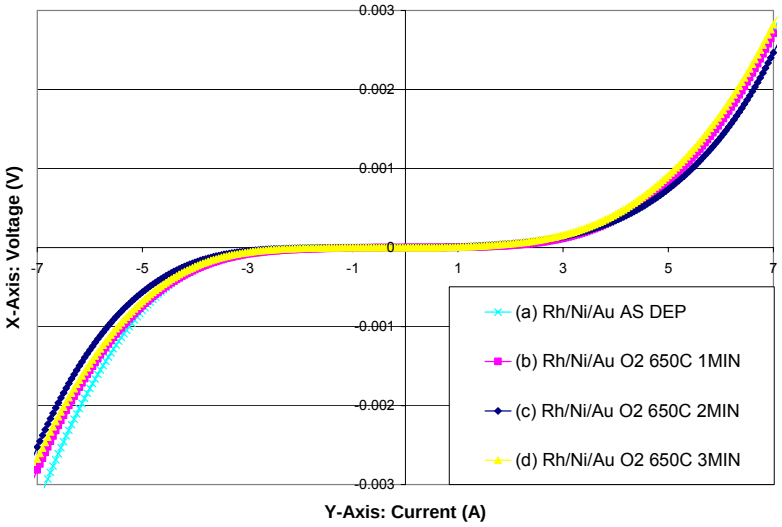

Figure III-r I-V characteristics of Rh/Ni/Au (20 nm/20 nm/20 nm) contact to p-GaN for (a) as-deposited and annealed in O_2 at 650 ˚C for (b) 1 min (c) 2 min and (d) 3 min.

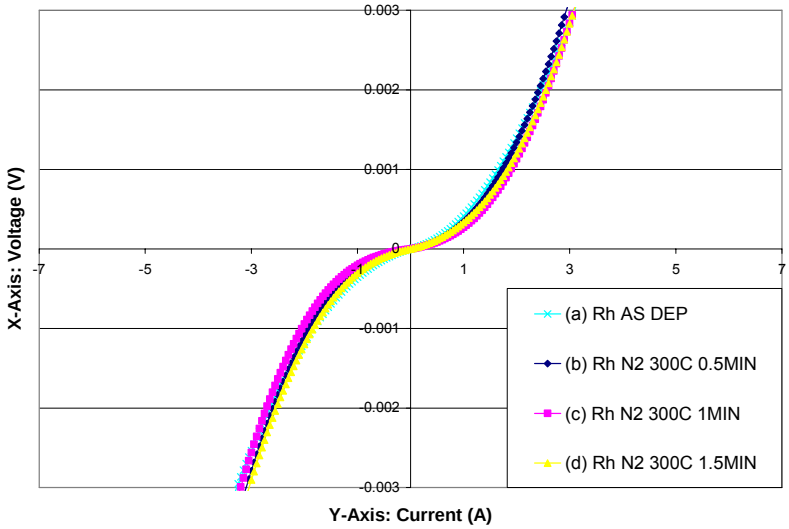

Figure III-s I-V characteristics of Rh (20 nm) contact to p-GaN for (a) as-deposited and annealed in N_2 at 300 ˚C for (b) 0.5 min (c) 1 min and (d) 1.5 min.

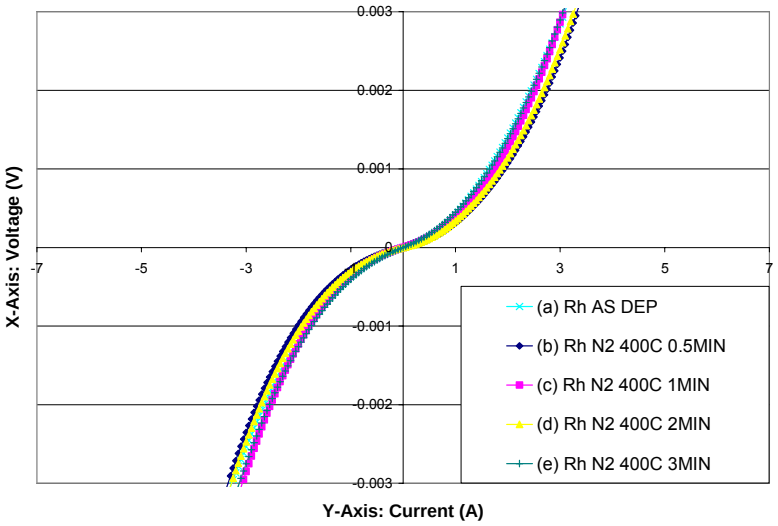

Figure III-t I-V characteristics of Rh (20 nm) contact to p-GaN for (a) as-deposited and annealed in N_2 at 400 ˚C for (b) 0.5 min (c) 1 min (d) 2 min and (e) 3 min.

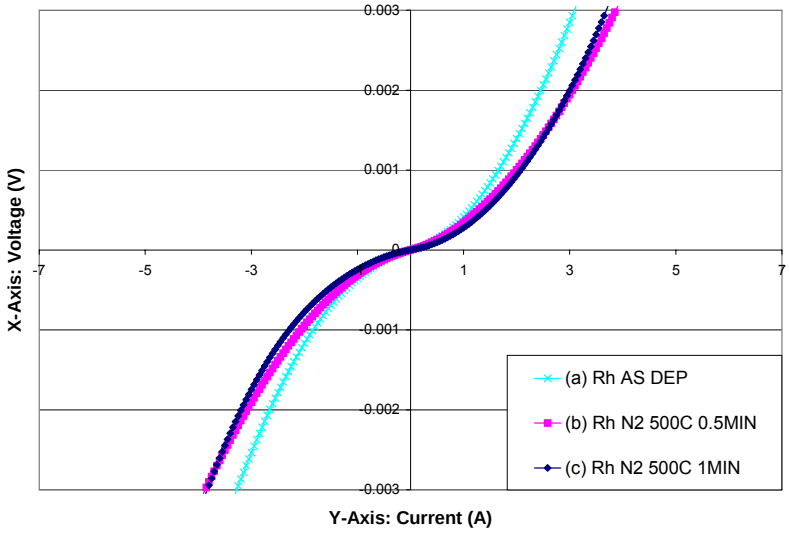

Figure III-u I-V characteristics of Rh (20 nm) contact to p-GaN for (a) as-deposited and annealed in N_2 at 500 ˚C for (b) 0.5 min and (c) 1 min.

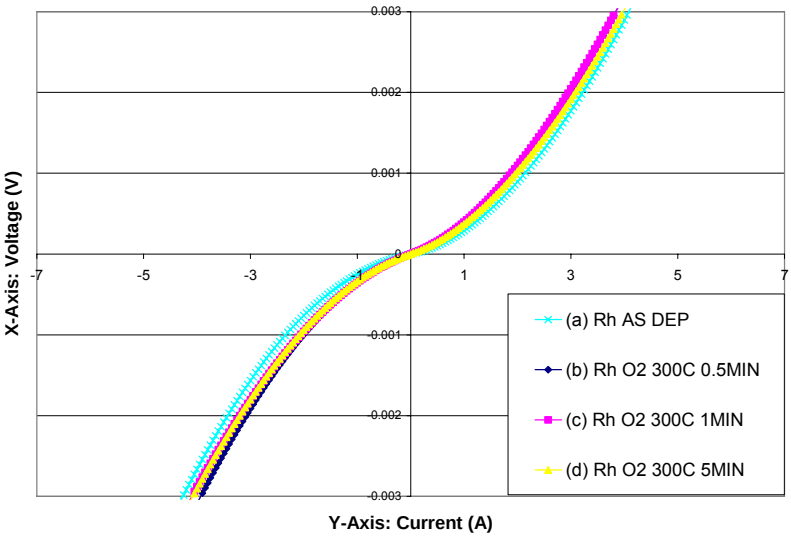

Figure III-v I-V characteristics of Rh (20 nm) contact to p-GaN for (a) as-deposited and annealed in O_2 at 300 ˚C for (b) 0.5 min (c) 1 min and (d) 5 min.

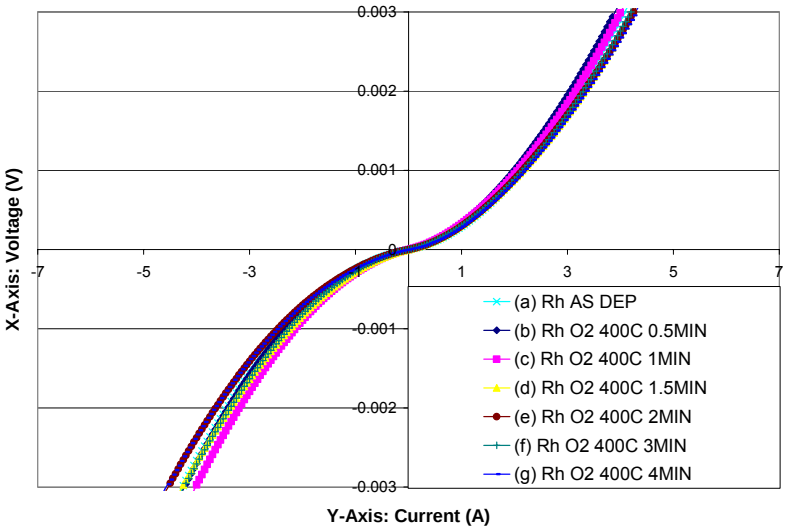

Figure III-w I-V characteristics of Rh (20 nm) contact to p-GaN for (a) as-deposited and annealed in O_2 at 400 ˚C for (b) 0.5 min (c) 1 min (d) 1.5 min (e) 2 min (f) 3 min and (g) 4 min.

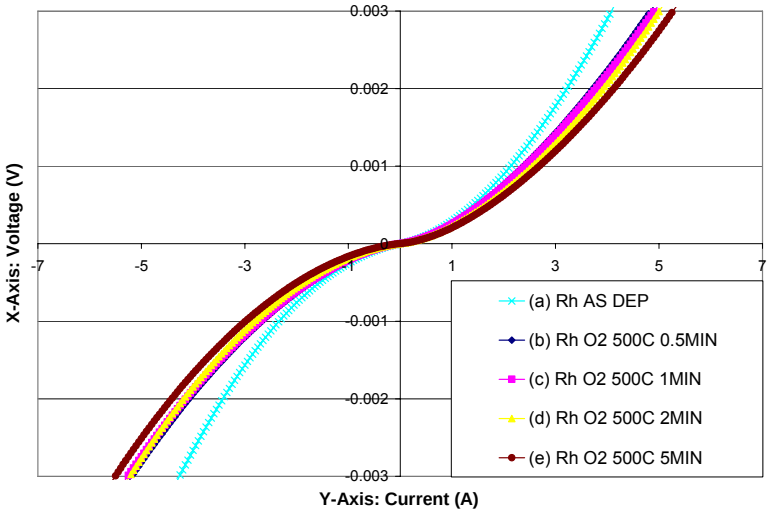

Figure III-x I-V characteristics of Rh (20 nm) contact to p-GaN for (a) as-deposited and annealed in O_2 at 500 ˚C for (b) 0.5 min (c) 1 min (d) 2 min and (e) 5 min.

APPENDIX IV

EDX RESULTS FOR O_2-ANNEALED Rh/Ni CONTACT TO p-GaN

Description of the EDX analysis

Energy Dispersive X-ray analysis (EDX) is a technique used for identifying the elemental composition of a specified area of the sample under test. It is an integrated feature of the Transmission Electron Microscope (TEM) that was employed in this work and cannot operate independently.

During EDX analysis, the sample is bombarded with an electron bean inside the TEM. The bombarding electrons collide with the sample atom's own electrons, knocking some of them off. Hence, vacant positions resulting from ejected inner shell electrons will eventually be filled by higher energy electrons from an outer shell. When this occurs, the outer shell electron releases some energy by emitting an X-ray with a particular energy. This energy is not only dependent on the shell from which the electron is from and the shell to which the electron is transferred to, it is also unique to each element. Hence, we are able to identify the element(s) present in the sample by measuring the energies released in the X-rays during the electron beam bombardment.

The output of an EDX analysis is an EDX spectrum, which is a plot of the frequency of X-rays detected for each energy level. Each of the peaks in the EDX spectrum is unique to an atom, and therefore corresponds to a single element. Quantitatively, the higher the peak is in a spectrum, the higher is the concentration of that particular element in the sample.

TEM image and EDX spectra obtained for Regions A-C defined in Figure 5.13

The TEM images and EDX spectra obtained for Regions A-C defined in Figure 5.13 are shown below.

(1) Region A

(a) TEM image of cross-section of Rh/Ni (10/10 nm) contact on p-GaN. "A" indicates the region of analysis (equivalent to Region A in Figure 5.13) (b) EDX spectra obtained for Region A.

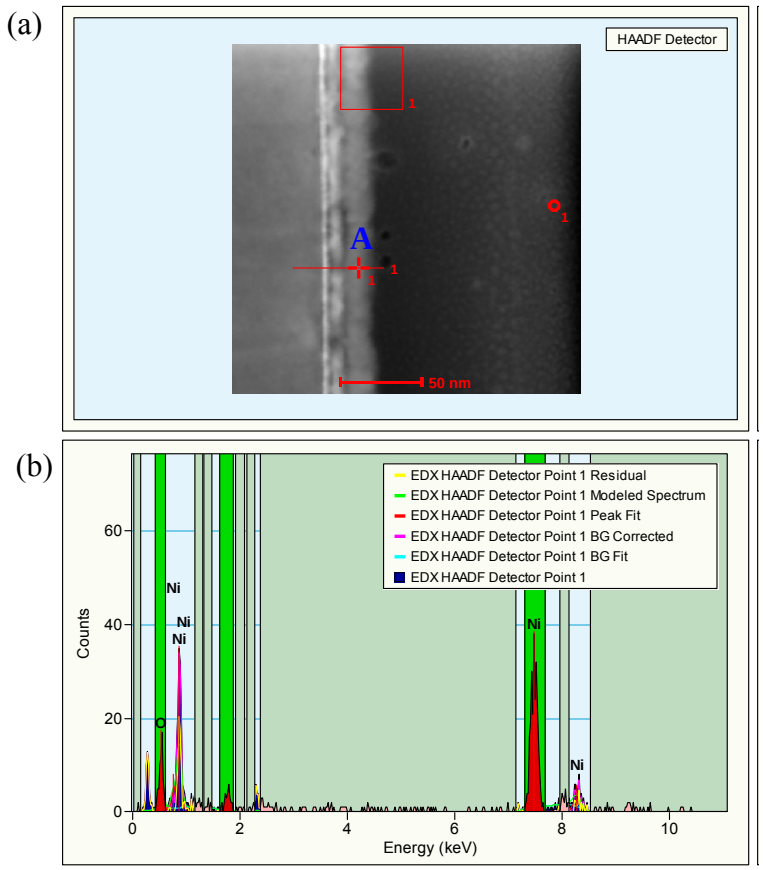

(2) Region B

(a) TEM image of cross-section of Rh/Ni (10/10 nm) contact on p-GaN. "B" indicates the region of analysis (equivalent to Region B in Figure 5.13) (b) EDX spectra obtained for Region B.

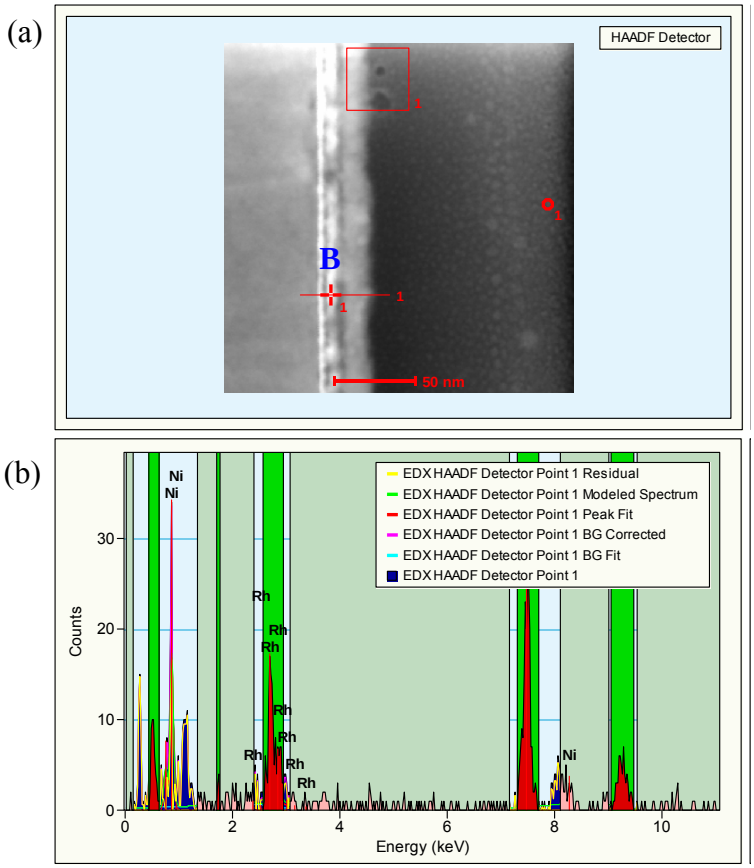

(3) Region C:

(a) TEM image of cross-section of Rh/Ni (10/10 nm) contact on p-GaN. "C" indicates the region of analysis (equivalent to Region C in Figure 5.13) (b) EDX spectra obtained for Region C.